| | |
|---|---|
| Title | Synthesis, mechanism and characterization of conjugated polymers and their applications for designing novel interface materials through surface functionalization |
| Author(s) | PHUNG, An |
| Citation | 高知工科大学, 博士論文. |
| Date of issue | 2018-03 |
| URL | http://hdl.handle.net/10173/1874 |
| Rights | |
| Text version | ETD |

**2018**

# Synthesis, mechanism and characterization of conjugated polymers and the designing novel interface materials through surface functionalization

Phung Hai Thien An
*Kochi University of Technology*

# Synthesis, mechanism and characterization of conjugated polymers and the designing novel interface materials through surface functionalization

**KOCHI UNIVERSITY OF TECHNOLOGY**

By
**PHUNG HAI THIEN AN**
**Student ID number: 1196015**

A dissertation submitted to the
Engineering Course, School of Environmental Science and Engineering
Department of Engineering,
Graduate School of Engineering,
Kochi University of Technology,
Kochi, Japan
In partial fulfillment of the requirements for the degree of Doctor of Engineering

Assessment Committee:

Supervisor: Prof. Ryuichi SUGIMOTO
Co-supervisor: Prof. Nagatoshi NISHIWAKI, School of Environmental Science and Engineering
Prof. Kazuya KOBIRO, School of Environmental Science and Engineering
Toshiyuki KAWAHARAMURA
Masataka OHTANI

March, 2018

**Abstract**

The development of conductive polymers has interested scientists from many fields including chemistry, physics and material science for decades due to their excellent properties such as high conductivity, light weight, flexibility, opto-electronic and electrochemical. Polythiophene and its derivatives are promising as candidates for conjugated polymers and have played important roles in many applications such as energy storage systems, organic thermoelectric device, organic light emitting diodes, organic field-effect transistor, biological target chemosensors, and organic electronic devices. A better understanding of the syntheses, properties and characterizations of thiophene is crucial and high priority for performance enhancement and improving new prospects for next-generation materials.

Although $FeCl_3$ oxidative polymerization is the simplest method for synthesis of poly(3-hexylthiophene), some issues concerning the previously proposed mechanism remain to be solved. In addition, enhancement of the polyolefin properties via conjugated polymers will allow for potential applications such as the use of solar energy as a heating source for desalination or preparation of capacitor electrodes. Furthermore, "green" electronic, a novel scientific term, has now emerged as a "hot" area of research aiming at the incorporation of natural compounds and conductive polymers. Research in this regard would open up easy and efficient routes for the production of novel materials with interesting and advantageous properties such as biodegradability, biocompatibility, and sustainability.

Therefore, the goal of this dissertation includes the following targets:

- To propose new insights into the mechanism of oxidative polymerization of 3-hexylthiophene
- To carry out catalytic oxidative polymerization of 3-hexylthiophene
- Synthesis of conjugated copolymers based on 3-hexylthiophene and the application of the obtained material for ionic detection and fluorescence control
- Modification of the polypropylene surface through grafting poly(3-hexylthiophene)
- Surface functionalization of biomaterials with poly(3-hexylthiophene)
- Photoluminescence control of the biomaterial through novel oxidative polymerization

All desired objectives were accomplished, the oxidative polymerization, a facile and efficient method for the preparation and build-up of a conducting layer on the surface of polypropylene as well as the biomaterials. This method has the advantages of simple manipulation, mild conditions, and ease for industrial-scale production.

## Author's Declaration

I hereby declare that the work in this dissertation was conducted under the Regulations of Kochi University of Technology, Kochi, Japan. This is my own original work and this thesis has not been presented and submitted in part or in whole to any university or institution for a degree. Fourteen papers of this dissertation have been published in some academic journals.

## Publications

Sections of this work described in this thesis have been reported in the following publications:

1) "*Synthesis and properties of stable 3-hexylthiophene and triphenylamine copolymers*", Takuya Nakashita, Ryuichi Sugimoto, and Thien An Phung Hai, **Bulletin of the Chemical Society of Japan**, vol.89, pp.1-5, 2016.
2) "*Conjugated carbazole-thiophene copolymer: Synthesis, characterization and applications*", Thien An Phung Hai and Ryuichi Sugimoto, **Synthetic Metals**, vol.220, pp.59-71, 2016.
3) "*Synthesis and characterization of copolymers composed of 3-hexylthiophene and fluorene via chemical oxidation with $FeCl_3$*", Thien An Phung Hai and Ryuichi Sugimoto, **Polymer Journal**, vol.48, pp.1115-1121, 2016.
4) "*Effect of molar ratio of oxidizer/3-hexylthiophene monomer in chemical oxidative polymerization of poly(3-hexylthiophene)*", Thien An Phung Hai and Ryuichi Sugimoto, **Journal of Molecular Structure**, vol.1146, pp.660-668, 2017.
5) "*The catalytic oxidative polymerization of 3-hexylthiophene by oxidation of $Fe^{2+}$ to $Fe^{3+}$*", Thien An Phung Hai and Ryuichi Sugimoto, **Catalysis Letters**, vol.147, pp.1955-1965, 2017.
6) "*Grafting poly(3-hexylthiophene) to the surface of polypropylene using oxidative polymerization*", Thien An Phung Hai, Hirotsugu Matsukuma and Ryuichi Sugimoto, **Polymer**, vol.121, pp.247-255, 2017.
7) "*Surface functionalization of cellulose with poly(3-hexylthiophene) via novel oxidative polymerization*", Thien An Phung Hai and Ryuichi Sugimoto, **Carbohydrate Polymers**, vol.179, pp.221-227, 2018.
8) "*Photoluminescence control of cellulose via surface functionalization using oxidative polymerization*", Thien An Phung Hai and Ryuichi Sugimoto, **Biomacromolecules**, vol.18, pp.4011-4021, 2017.
9) "*Surface modification of chitin and chitosan with poly(3-hexylthiophene) via oxidative polymerization*", Thien An Phung Hai and Ryuichi Sugimoto, **Applied Surface Science**, vol.434, pp. 188-197, 2018.
10) "*Surface modification of polypropylene with poly(3-hexylthiophene) via oxidative polymerization*", Thien An Phung Hai, Hirotsugu Matsukuma and Ryuichi Sugimoto, **Reactive and Functional Polymers,** vol.1146, pp. 660-668, 2017.
11) "*Chemical modification of polypropylene with thiophene*", Thien An Phung Hai, and Ryuichi Sugimoto, **Journal of the Society of Electrical Materials Engineering** vol.26, pp. 35-43, 2017.
12) "*Fluorescence control of chitin and chitosan fabricated surface functionalization using direct oxidative polymerization*", Thien An Phung Hai and Ryuichi Sugimoto, **RSC Advance**, vol.8, pp. 7005-7013, 2018.
13) "*Fabrication of multicolor fluorescent polyvinyl alcohol through surface modification with conjugated polymers by oxidative polymerization*", Thien An Phung Hai and Ryuichi Sugimoto, **Applied Surface Science,** vol. 443C, pp.1-10, 2018 (DOI: 10.1016/j.apsusc.2018.02.200)
14) "*Synthesis and characterization of poly(3-hexylthiophene)-grafted polyvinyl alcohol*", Thien An Phung Hai and Ryuichi Sugimoto, **Synthetic Metals**

**Acknowledgements**

I sincerely express my deep gratitude to the people who have guided and supported me throughout the past three years. I am appreciative of their kindness, encouragement, and heartening for my moral support. As I know I am not able to complete my thesis without them.

Sincere thanks must be offered to my supervisor, Prof. Sugimoto who gave me an opportunity to be a SSP student in Kochi University of Technology (KUT). His invaluable support, guidance, tolerance, and encouragement help me to develop myself as a scientist. Throughout the three years of Doctoral course, there were time in which I was depressed for looking for "light" or "hope" for my research, but he suggested the paths and solutions that inspire me to overcome these obstacles.

I would like to thank Prof. Asahara for instruction me how to measure HR-MS and HPLC MS. I am incredibly grateful to Prof. Kawaharamuara and Dr. Dang who gave me full support for PYS, TGA and Raman measurements. Special thanks to Prof. Ohtani for his instructions to analyze material through TEM, SEM and EDX techniques. Thanks to Prof. Ito for giving lessons to me about Quantum Yield and photoluminescence measurements. I wish to express my sincere thanks to my co-supervisors Prof. Kobiro and Prof. Nishiwaki for their valuable suggestions, comments, enthusiasms and inspirations.

Warm thanks are also sent to all my classmates for helping and supporting me during the past three years.

Finally yet importantly, I wish to express my deepest appreciations to my family for all their support, encouragement and helping during my Doctoral course as well as my life.

# Contents

# Chapter 1:

# New insights into the mechanism of oxidative polymerization of 3-hexylthiophene

## 1.1 Introduction

Thiophene and its derivatives are organic macromolecules with a system of delocalized π-electrons, provide novel properties that can be potential useful in the applications of molecular imaging [1], blue light emitting polymers [2], organic solar cells [3,4], chemical sensors [5], artificial muscles [6], memory devices [7], organic electronics and photovoltaic cells [8]. The three most frequently used strategies for synthesizing poly(3-hexylthiophene) (P3HT) including cross coupling polycondensation [9-11], oxidative polymerization [12,13] and electrochemical methods [14,15]. A number of mechanisms for P3HT synthesis have been proposed such as the radical mechanism [16], carbocation mechanism [17], and radical cation mechanism [18]. In case of oxidative polymerization, the oligomer with a chlorine end group was detected using Matrix-assisted laser desorption/ionization mass spectrometry (MALDI TOF MS)[19]. Furthermore, the MALDI TOF MS results indicated that the end-group of the poly(3-hexylthiophene) chains synthesized by the polycondensation method depend on the solvent used in reaction[20]. With the use of the flow method and bio-derived "green" solvent for Grignard metathesis (GRIM) polymerization, full conversion of P3HT could be obtained in less than one minute [21]. Recently, the step polymerization of thiophene using onium salts[22,23] and the initial photooxidation mechanism[24] confirmed the formation of radicals. The iron (III) chloride and hydrogen peroxide system is effective for the polymerization of thiophene in aqueous media[25]. The bronsted acids are effective for the initiation for cationic chain growth polymerization of thiophene derivatives [26]. In addition, the effect of solvents and temperatures on the yield and regioregularity of P3HT have been investigated [27,28], and among the solvents used, a mixture of dichloromethane and nitrobenzene gave higher yield, higher molecular weight and excellent reproducibility [28]. Furthermore, zeolite, halloysite nanotube, and metal organic framework, known as nanocavities, were applied for the solvent free oxidative polymerization of 3-hexylthiophene [29]. To meet green chemistry requirements, ionic liquids were also used as solvents for $FeCl_3$-catalyzed oxidative polymerization of 3-octylthiophene [30]. Although, ionic liquids can replace conventional solvents and produce polymers in very high yield of 99% [30], their cost is still too high. In comparison to ionic liquids, deep eutectic solvents, a mixture of ammonium or phosphonium salts, have remarkable advantages such as biodegradability, low cost, fast polymerization generation and high yields.[31]

Over the past two decades, there has always been a need of four-fold $FeCl_3$ concentration relative to 3-alkylthiophene monomer in the synthesis of poly(3-alkylthiophene) by oxidative polymerization, regardless of the solvents used,e.g., chloroform, hexane, dichloromethane, acetonitrile [9-13,16,27,32-34], ionic liquids [30], and deep eutectic solvents [31].

In this chapter, we discuss a series of oxidative polymerization employing various ratios of $FeCl_3$/3HT in the range 1:10 to 1:1, which were conducted to determine the role of the molar ratio in determining the yield and molecular weight. Although, MALDI TOF MS is a powerful tool for the characterization of synthetic polymers, it is inappropriate for the detection of small molecules with molar mass under 500 Da because of the use of an organic matrix[35]. In contract, Surface-assisted Laser desorption/Ionization time of light mass spectrometry (SALDI TOF MS) using inorganic nanoparticle as an organic matrix-free can easily detect low-molecular-weight compounds[35,36]. Therefore, using SALDI TOF MS with titanium dioxide as the matrix, in the first time, the structure of oligomer (such as dimer, trimer, tetramer and pentamer) was confirmed, providing new insights into the mechanism of oxidative polymerization.

## 1.2 Experimental section

### *1.2.1 Materials*

3-Hexylthiophene and $FeCl_3$ were purchased from Tokyo Chemical Industry Ltd and used without any further purification. Anthralin (Nacalai Tesque Inc., Tokyo ) and Silver trifluoroacetate (Wako pure chemical industries Ltd) were applied as the matrix and cation agent in the MALDI-TOF MS, respectively. Hexane, chloroform (contains 0.3-1% ethanol as a stabilizer) and chloroform for HPLC (ethanol free, contains 150 ppm amylene as a stabilizer), nitrobenzene and acetonitrile for HPLC used in this study was from Wako Pure Chemical Industrials Ltd, dried by standing over 4A molecular sieves 24 hours, then purged with Argon gas for 25 minutes before using. Titanium oxide was used for SALDI TOF MS (Surface-Assisted Laser Desorption/Ionization Time-Of-Light Mass Spectrometry)

### *1.2.2 Equipment*

$^1$H NMR spectra (400MHz) and IR spectra were recorded on a Brucker Acsend 400 spectrometer and a Jasco FT/IR – 480 Plus, respectively. GPC was carried out in a system equipped with a Jasco PU-2080 Plus pump, and a Jasco RI-2031 plus intelligent RI detector. The molecular weight and molecular weight distribution of the polymers relative to polystyrene standard were analyzed using Chrom NAV software. Chloroform served as the polymer solvent and eluent in an equilibrated system at 40$^o$C. A Brucker autoflex speed-KE in reflector mode was used for the MALDI-TOF MS (Matrix-Assisted Laser Desorption/Ionization Time-Of-Light Mass Spectrometry) and SALDI-TOF MS (Surface-Assisted Laser Desorption/Ionization Time-Of-Light Mass Spectrometry) analysis. ESI (Electrospray Ionization) mass spectra were acquired with an AB Sciex Triple ESI TOF 4600 system in positive ion mode, for analysis, 20 µl of sample was injected (direct injection) into the mass spectrometer using chloroform/acetonitrile (10/90, v/v) as a solvent at a flow rate 10 µl/min (syringe pump).

### *1.2.3 Synthesis polymerization of 3HT*

All reactions in this study were conducted in an oven-dried Schlenk flask with a stop cock under an argon atmosphere. $FeCl_3$ (81 mg, 0.5 mmol) and anhydrous hexane (15 ml) were put into a Schlenk tube and the mixture was performed ultrasound treatment for 15 minutes. The hexane (5 mL) solution of 3HT (90 mg, 0.5 mmol) was dropped into a magnetically stirred suspension of $FeCl_3$. The obtained polymer was washed with methanol to remove any residual $FeCl_3$, and then it was extracted with acetone and chloroform using a Soxhlet extractor. The methanol soluble fraction was concentrated on a rotary evaporator then washed with deionized water and extracted with dichloromethane three times. Then the extract was dried over $Na_2SO_4$ and evaporated to give a yellow oil. Polymerization of 3HT was carried out with different ratios between 3HT and $FeCl_3$ in different solvents as above. However, when chloroform (containing 0.3-1% ethanol as a stabilizer) was used as a solvent, polymerization did not occur at a ratio of 1:1 between $FeCl_3$ and 3HT monomer. In this reaction the solution was concentrated on a rotary evaporator, then washed with deionized water and extracted three times with dichloromethane. Then the extract was dried over $Na_2SO_4$ and evaporated to give an orange oil.

## 1.3 Results and discussion

The synthesis of P3HT was conducted under the conditions described in the experimental section (Scheme 1.1). Table 1.1 summarizes all results of P3HT synthesized in hexane. As shown in Table 1.1 (entries 5-9), the P3HT were successfully synthesized even though the molar ratio of $FeCl_3$/3HT was lower than one. The regioregularity of P3HT was affected by the temperature, in detail; the lower regioregularity was obtained at the higher polymerization temperatures (entries 1-3 in Table 1.1). Lower temperatures support the self-assemble ability and durable aggregate of head-to-tail (HT) structure[27,37] that favor the production of the HT dimer more than the head-to-head (HH) dimer[34]. Therefore, lower temperatures improve the HT content of P3HT. The polymer yield was 30% after 2 h with the molar ratio between the monomer and oxidant was 1:1. Then the yield remained relatively constant around 30 % throughout the 72 h (entries 10-14, Table 1).

The same outcome was observed when the molar ratio of the monomer and oxidant was 1:4, under which conditions the polymerization reaction reached completion after 2 h [19]. In case of 3HT/$FeCl_3$ molar ratio of

1:1, the molecular weight of the polymer ($M_n$) was almost constant of 100 kDa, and was not affected by other polymerization condition such as temperatures and time. However, both polymer yield and $M_n$ value decreased by a 3HT/$FeCl_3$ molar ratio decreasing (entries 5-9, Table 1.1). In summary, the molar ratio between $FeCl_3$ and the monomer has both the polymer yield and the molecular weight of the polymer changed but does not affect the regioregularity of P3HT.

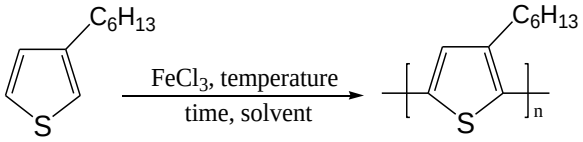


**Scheme 1.1 Synthetic scheme of poly(3-hexylthiophene)**

**Table 1.1: Oxidative polymerization of 3-hexylthiophene in hexane solvent**

| Entry | $FeCl_3$/3HT ratio | Temperature (°C) | Reaction time (h) | Yield (%) | | $M_n$[a], kDa | PDI[b] | % HT[c] |
|---|---|---|---|---|---|---|---|---|
| | | | | Acetone fraction [d] | Chloroform fraction [e] | | | |
| 1 | 1:1 | ***0*** | 2 | 1.3 | 26.5 | 105 | 2.2 | 77 |
| 2 | 1:1 | ***23*** | 2 | 3.1 | 26.7 | 109 | 2.2 | 71 |
| 3 | 1:1 | ***50*** | 2 | 1.8 | 19.0 | 102 | 2.3 | 69 |
| | | | | | | | | |
| 4 | 2:1 | 23 | 2 | 3.5 | 57.2 | 101 | 2.3 | 71 |
| 5 | ***1:1*** | 23 | 2 | 3.1 | 26.7 | 109 | 2.2 | 71 |
| 6 | ***1:2*** | 23 | 2 | 2.2 | 13.9 | 52 | 2.9 | 71 |
| 7 | ***1:4*** | 23 | 2 | 1.9 | 4.2 | 40 | 2.5 | 71 |
| 8 | ***1:8*** | 23 | 2 | 0.7 | 3.9 | 28 | 2.6 | 71 |
| 9 | ***1:10*** | 23 | 2 | 0.4 | 1.9 | 27 | 2.8 | 71 |
| | | | | | | | | |
| 10 | 1:1 | 23 | ***6*** | 3.1 | 29.1 | 120 | 2.6 | 71 |
| 11 | 1:1 | 23 | ***12*** | 1.2 | 28.8 | 112 | 2.5 | 71 |
| 12 | 1:1 | 23 | ***24*** | 2.1 | 27.3 | 125 | 2.2 | 71 |
| 13 | 1:1 | 23 | ***48*** | 1.2 | 28.4 | 115 | 2.4 | 71 |
| 14 | 1:1 | 23 | ***72*** | 2.3 | 27.2 | 106 | 2.4 | 71 |

[a] Determined by Gel-Permeation Chromatography (Polystyrene standard, solvent chloroform)
[b] Polydispersity Index. PDI = $M_w/M_n$
[c] HT: head to tail content, determined by $^1$H NMR
[d]: Acetone fraction: the polymer product was Soxhlet extracted with acetone
[e]: Chloroform fraction: the polymer product was Soxhlet extracted with chloroform

The results from the polymerization in HPLC-grade chloroform (ethanol-free, contains 150 ppm of amylene as a stabilizer) are summarized in Table 1.2. Previous literature on the oxidative polymerization of 3HT using $FeCl_3$ in chloroform[12,27,38] reported that at least a two-fold excess of $FeCl_3$ is required to produce P3HT, and that usually, a four-fold excess relative to the 3HT monomer was used. Oxidative polymerization did not occur when the molar ratio of $FeCl_3$ to 3HT was less than or equal to 1. In this study, we also confirmed that no polymer was formed in the oxidative polymerization of 3HT using $FeCl_3$ in chloroform containing 0.3 to 1% ethanol as a stabilizer (Table 1.2 Entry 7)[39]. Surprisingly, under the same polymerization conditions, P3HT was obtained in a 16.2% yield when ethanol-free chloroform (containing 150 ppm of amylene as stabilizer) was used. This result indicates that even a small amount of ethanol may work as an inhibitor of the oxidative polymerization reaction. In other words, it seems that a small amount of ethanol in chloroform will react with $FeCl_3$ to deactivate it [40] and prevent the coordination between the 3HT monomer and the $FeCl_3$ active sites. It is also possible that the presence of ethanol caused a decrease in the Lewis acidity of anhydrous $FeCl_3$[41]. As shown in Table 1.2, the oxidative polymerization of 3HT in chloroform (ethanol-free, containing 150 ppm of amylene as stabilizer) occurred not only when the molar ratio of $FeCl_3$/3HT was 1, but even at lower molar

ratios from 1:2 to 1:10 ($FeCl_3$/3HT). These results are noteworthy, similar to the polymerization reactions in hexane, where P3HT could be obtained even though the stoichiometric amount of $FeCl_3$ was lower than that of 3HT. The P3HT synthesized in chloroform has a larger molecular weight distribution (PDI) and smaller $M_n$ than the P3HT synthesized in hexane (Entries 5–9, Table 1.1 and Entries 2–6, Table 1.2). Moreover, the content of the HT dyad in P3HT was not affected by the molar ratio of $FeCl_3$:3HT. However, the yield of the polymer was less than that in hexane (as shown in Fig. 1).

**Table 1.2: Results from oxidative polymerization of 3-hexylthiophene in HPLC grade chloroform (ethanol-free, contains 150 ppm amylene as a stabilizer) at 23 °C for 2 h**

| Entry | $FeCl_3$/3HT ratio | Yield (%) | | $M_n$[a] x $10^{-3}$ | PDI[b] | % HT[c] |
|---|---|---|---|---|---|---|
| | | Acetone fraction [d] | Chloroform fraction [e] | | | |
| 1 | 2/1 | 1.3 | 43.8 | 40 | 3.5 | 72 |
| 2 | 1/1 | 1.6 | 14.6 | 38 | 3.6 | 72 |
| 3 | 1/2 | 1.4 | 4.1 | 32 | 3.2 | 72 |
| 4 | 1/4 | 0.8 | 1.3 | 30 | 3.3 | 72 |
| 5 | 1/8 | 0.5 | 1.2 | 29 | 3.2 | 72 |
| 6 | 1/10 | 0.3 | 1.0 | 30 | 3.1 | 72 |
| 7 | 1/1[f] | 0 | 0 | - | - | - |

[a] Determined by Gel-Permeation Chromatography (Polystyrene standard, solvent chloroform)
[b] Polydispersity Index. PDI = $M_w/M_n$
[c] Head to tail content, determined by $^1$H NMR
[d] Acetone fraction: the polymer product was Soxhlet extracted with acetone
[e] Chloroform fraction: the polymer product was Soxhlet extracted with chloroform
[f] Chloroform (contains 0.3–1% ethanol as a stabilizer)

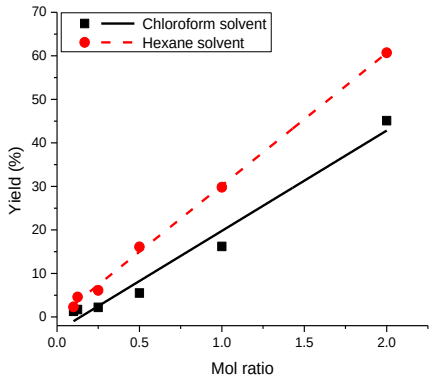


**Figure 1.1: Polymer yield as a function of different molar ratio of $FeCl_3$ and 3HT**

It is extremely impressive that the oxidative polymerization occurred even when the molar ratio between the $FeCl_3$ and monomer was as low as 1:10, although the yield varies depending on the molar ratio (Fig.1.1). This result is incompatible with any of the proposed polymerization mechanisms, such as the radical mechanism[40], carbocation mechanism[17], and radical cation mechanism[18], found in the literature.

Previous reports [27,40] have suggested that the solubility of $FeCl_3$ in a solvent affects the performance of the oxidative polymerization in terms of yield, regioregularity, and polydispersity. Due to the poor solubility of $FeCl_3$ in hexane and HPLC-grade chloroform, the oxidative polymerization in these solvents occurred in a heterogeneous system. It is said that the oxidative polymerization takes place on the active sites at the surface of the $FeCl_3$ crystals[40] . In order to further investigate this phenomenon, several 3HT oxidative polymerization reactions were carried out using two solvents—nitrobenzene and acetonitrile—which can both completely

dissolve $FeCl_3$. Due to the good solubility of $FeCl_3$ in nitrobenzene and acetonitrile, the oxidative polymerization in these solvents occurred in a homogeneous system. The results are summarized in Table 1.3.

**Table 1.3: Results from the oxidative polymerization of 3-hexylthiophene in nitrobenzene and acetonitrile at 23 °C for 2 h**

| Entry | Solvent | $FeCl_3$/3HT ratio | Yield (%) | | $M_n$[a] x $10^{-3}$ | PDI[b] | % HT[c] |
|---|---|---|---|---|---|---|---|
| | | | Acetone fraction [d] | Chloroform fraction [e] | | | |
| 1 | Nitrobenzene | 1:10 | 0.3 | 1.6 | 10 | 1.3 | 71 |
| 2 | Nitrobenzene | 1:1 | 6.3 | 12.1 | 14 | 1.7 | 71 |
| 3 | Acetonitrile | 1:10 | 0.2 | 0.6 | 13 | 1.5 | 70 |
| 4 | Acetonitrile | 1:1 | 3.9 | 9.3 | 9 | 1.2 | 70 |

[a] Determined by Gel-Permeation Chromatography (Polystyrene standard, solvent chloroform)
[b] Polydispersity Index. PDI = $M_w/M_n$
[c] Head to tail content, determined by $^1$H NMR
[d] Acetone fraction: the polymer product was Soxhlet extracted with acetone
[e] Chloroform fraction: the polymer product was Soxhlet extracted with chloroform

We were astonished to find that a polymerization similar to what was seen in the heterogeneous reactions in hexane and chloroform solvents could be obtained in both nitrobenzene and acetonitrile solvents, even when the stoichiometric ratio between $FeCl_3$ and 3HT was in the 1:1–1:10 range (Table 1.3). As shown in Table 1.3, the P3HT obtained in acetonitrile or nitrobenzene showed a smaller $M_n$ and a relatively narrow molecular weight distribution (PDI=1.2–1.7) compared with polymers obtained in hexane or chloroform (PDI=2.5–3.5) (Tables 1.1 and 1.2). Moreover, the polymer yield in the homogeneous reaction system was lower than in the heterogeneous system (Tables 1.1, 1.2, and 1.3). In the heterogeneous reaction system, the concentration of $FeCl_3$ did not affect the polymer yield, which agrees with previous reports[42]. However, in the homogeneous systems studied, it was found that the polymer yield clearly depended on the concentration of $FeCl_3$, as shown in Fig. 1.6. In these polymerization reactions, the molar ratio of $FeCl_3$/3HT was kept at 1:1, while the volume of the nitrobenzene / acetonitrile solvent was varied to change the concentration of $FeCl_3$.

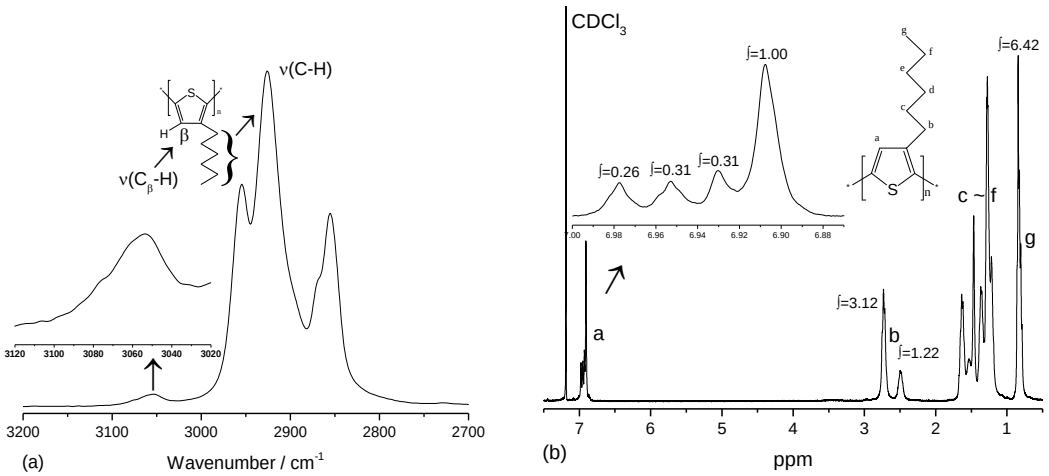


**Figure 1.2. FT-IR (a) and $^1$H NMR (b) of P3HT in hexane (Entry 9, Table 1.1)**

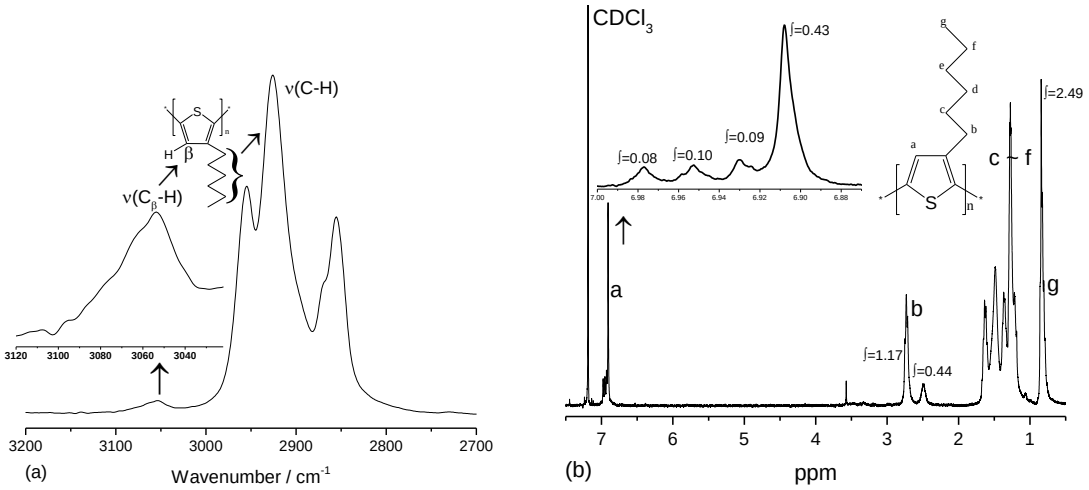


**Figure 1.3. FT-IR (a) and $^{1}$H NMR (b) of P3HT in HPLC-grade chloroform (Entry 6, Table 1.2)**

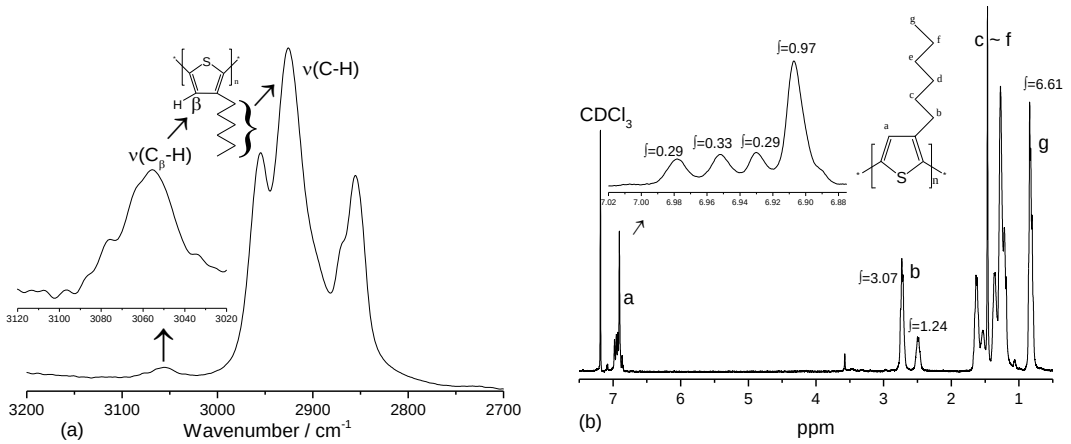


**Figure 1.4. FT-IR (a) and $^{1}$H NMR (b) of P3HT in nitrobenzene (Entry 1 Table 1.3)**

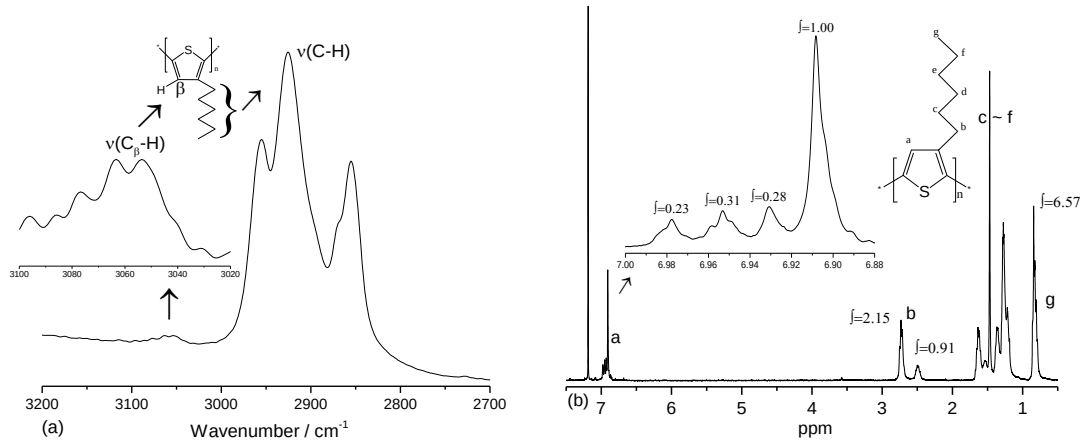


**Figure 1.5. FT-IR (a) and $^{1}$H NMR (b) of P3HT in acetonitrile (Entry 3 Table 1.3)**

The $^{1}$H NMR and FT-IR spectra of the P3HT synthesized in HPLC-grade chloroform, hexane, nitrobenzene, and acetonitrile (using a $FeCl_3$:3HT ratio of 1:10), are presented in Figs. 1.2, 1.3, 1.4, and 1.5, respectively. The absorptions in the 3000–2800 cm$^{-1}$ region of the FT-IR spectra are normally assigned to the C-H stretching

of the -$CH_3$ and >$CH_2$ groups in the hexyl chain [43,44] , while the bands at 3080–2980 $cm^{-1}$ are a feature of the backbone arising from the stretching vibration mode of thiophene at the 4-position ($C_\beta$-H)[43,44]. The intensities of the FT-IR spectra of P3HT synthesized from different solvents (in Figs. 1.2a, 1.3a, 1.4a and 1.5a) supports the conclusion that a side reaction takes place at the 4-position, the extent of which was estimated based on the anti-symmetric stretching vibration of the -$CH_3$ group at 2950 $cm^{-1}$. The signals in the $^1$H NMR at δ=0.87 are assigned to the methyl proton [45]. As summarized in Table 1.4, the peaks in the $^1$H NMR at δ=2.50 ppm and δ=2.80 ppm are due to the head-to-head (H-H) and head-to-tail (H-T) structure of P3HT, respectively[45]. The four moderate signals at δ=6.97 ppm, δ=7.00 ppm, δ=7.02 ppm and δ=7.05 ppm were assigned to four triad configurations as follows: HT-HT, TT-HT, HT-HH and TT-HH, respectively [45]. The ratio of the integral intensities of the peaks at δ=0.87 ppm and δ=7 ppm in the $^1$H NMR is consistent with the methyl group and 4-postion of 3HT, which is indicative of the occurrence of side reactions such as the chlorination at the 4-position or 2,4-coupling reaction [45]. The relative amounts of the two dyad and the four triad configurations of P3HT synthesized in different solvents is almost identical, indicating that the heterogeneous or homogeneous nature of the reaction does not affect the molecular characteristics of P3HT. Moreover, the ratios between the integral intensity of the methyl proton (δ=0.87) and four triad configurations (from δ=6.97 to δ=7.05) were 3.4 (hexane), 3.5 (HPLC-grade chloroform and nitrobenzene), and 3.6 (acetonitrile), respectively (Table 1.4). These results indicate that side reactions occurred to a slight extent in all samples, regardless of the solvent used.

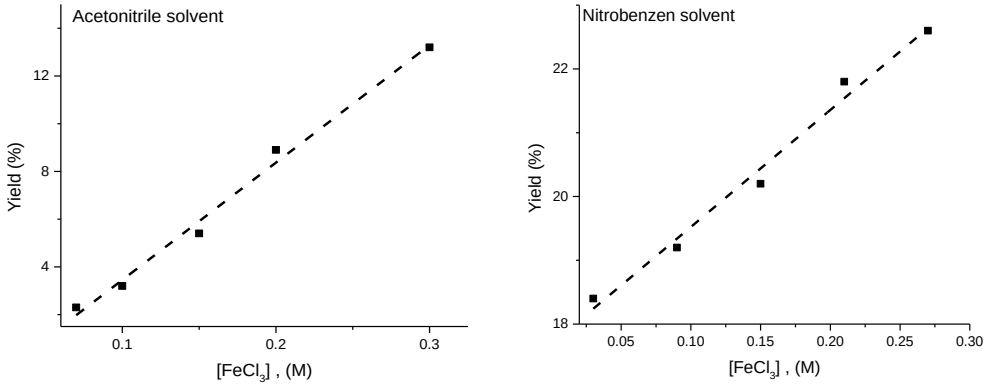


**Figure 1.6. Polymer yield as a function of the concentration of [$FeCl_3$] in acetonitrile (a) and nitrobenzene (b)**

**Table 1.4. Molecular characterization of P3HT samples synthesized with a molar ratio $FeCl_3$/3HT (1:10) in different solvents**

| Solvent | Dyads (%)* | | Triads (%)* | | | | Ratio of integral intensity of H from ($C_\beta$-H) and ($CH_3$)* |
|---|---|---|---|---|---|---|---|
| | HT | HH | HT-HT | HT-TT | HT-HH | TT-HH | |
| Hexane | 71 | 29 | 53 | 16 | 16 | 14 | 3.4 |
| HPLC chloroform | 72 | 28 | 61 | 13 | 14 | 12 | 3.5 |
| Nitrobenzene | 71 | 29 | 52 | 15 | 18 | 15 | 3.5 |
| Acetonitrile | 70 | 30 | 54 | 16 | 17 | 13 | 3.6 |

MALDI TOF MS, which is a powerful tool for the characterization of synthetic polymers, was run using anthralin as the matrix [46,47]. The MALDI TOF mass spectrum of the acetone extract of the P3HT synthesized in hexane using a $FeCl_3$:3HT stoichiometric ratio of 1:10, is shown in Fig 1.7. Similar spectra were also

obtained for the P3HT polymerized in other solvents. The adjacent peaks differ in mass by one monomer unit[48], and measuring the mass difference between the adjacent peaks in the same series gives the mass of the monomer unit [49, 50]. In the case of P3HT, the mass difference obtained was 166, consistent with the 3HT unit. The MALDI-TOF mass spectrum of P3HT shows three or more ion series such as [$166_m$ + 2H], [$166_m$+H+Cl], and [$166_m$+2Cl], which are similar to what has been reported previously[46]. This implies that the terminal proton at the 5-position of the thiophene ring in the oligomer was replaced with the chlorine generated from $FeCl_3$ [51,47]. The ion series [$166_m$+2H] and [$166_m$+H+Cl], having hydrogen termination, can take part in polymerization, but [$166_m$+2Cl] seems to suppress the polymerization rate[19]. From the repeat unit mass of the 3HT monomer (m/z = 166) and the calculated m/z of 1496.87, it was determined that the cluster peaks had a molecular weight where m=9 (m: repeat unit number). Similarly, P3HT ions corresponding to [$166_m$+H+Cl] and [$166_m$+2Cl] (with m=9) display mass-to charge ratios of 1531.98, and 1565.98, respectively, agreeing well with the calculated m/z values of 1531.93 and 1565.94.

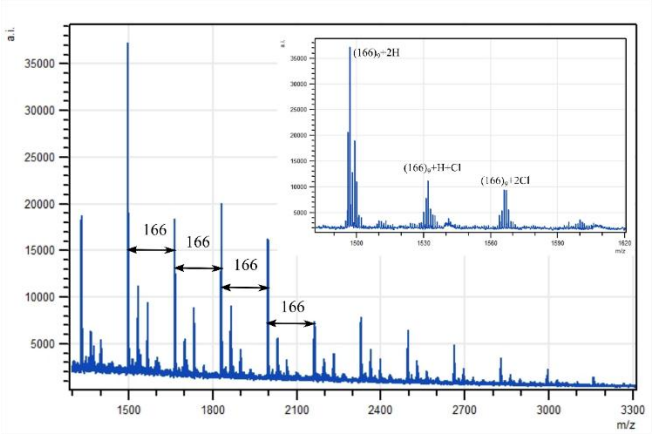


**Figure 1.7. MALDI TOF MS of P3HT (Entry 9, Table 1.1).**

The stabilizer in the chloroform solvent plays an important role in the oxidative polymerization of the 3HT monomer using $FeCl_3$. The ethanol contained in the chloroform could diminish the coordination between the monomer and Fe(III) active sites [40]. Moreover, the ethanol stabilizer in chloroform causes a decrease of the Lewis acidity of anhydrous $FeCl_3$[41]. When the stoichiometric ratio of $FeCl_3$/3HT is 4, the influence of ethanol can be ignored, which explains why previous literature reports state that P3HT with a high molecular weight can be obtained in a high yield[27,42]. However, when the stoichiometric ratio of $FeCl_3$/3HT is 1, due to the presence of ethanol, the amount of active $FeCl_3$ is insufficient to promote oxidative polymerization of the 3HT monomer in order to obtain P3HT. Under these polymerization conditions, when the reaction is stopped by methanol, there is no black precipitate, and the color of the solution remains yellow, indicating that polymerization did not occur. To investigate further, this solution was concentrated, washed with deionized water, and upon extraction with dichloromethane, was found to give a low-molecular-weight oligomer. Fig. 1.8 shows the $^1$H NMR spectrum of this oligomer. The two peaks at 2.5 ppm and 2.8 ppm are assigned to the α-CH2 protons, and the collection of peaks in the 6.6–7.0 ppm range are assigned to protons of four triad configuration of oligomer [45]. In addition, Fig. 1.9 show the SALDI TOF mass spectrum of this oligomer, analyzed using titanium oxide as a matrix. The SALDI TOF mass spectrum in Fig. 1.9 contains the ion series [166n + H + H] and [166n + H + Cl], with n = 4 and 5 (n is equal to the number of repeat units). These ions are displayed at m/z 666.353, 700.387, 832.408, and 866.317, in good agreement with the calculated m/z values of 666.342, 700.303, 832.423, and 866.384 (calculation by Isopattern), respectively. These results show that when the stoichiometric ratio of $FeCl_3$/3HT is 1, oxidative polymerization of 3HT with $FeCl_3$ in chloroform (with ethanol as a stabilizer) only produces an oligomer having a regiorandom structure and low molecular weight.

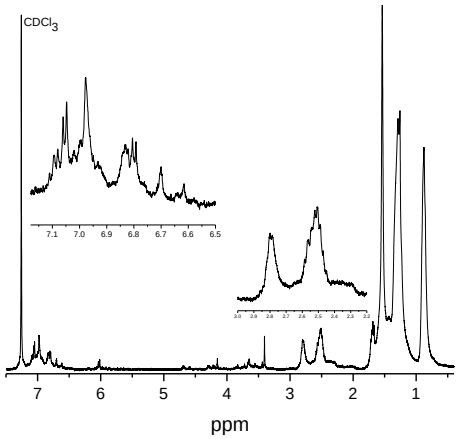


**Figure 1.8. $^{1}$H NMR spectrum of the oligomer extracted from the methanol–soluble fraction when 3HT was synthesized under the following conditions: 2 h, $FeCl_3$/3HT = 1:1, 23 °C, in chloroform solvent (contains 0.3–1% ethanol as stabilizer)**

As described above, P3HT was obtained in both heterogeneous and homogeneous systems, with $FeCl_3$/3HT molar ratios from 1:1 to 1:10. It has been reported that an oligomer ($M_n$ of 3300) with a regiorandom structure is present in the methanol soluble fraction[42] when oxidative polymerization of 3HT is conducted with a $FeCl_3$/3HT stoichiometric ratio of 4. Fig. 1.10 shows the $^{1}$H NMR spectra of the products extracted from the methanol soluble fraction when the $FeCl_3$/3HT ratio was 1:10. Furthermore, a representative ESI MS of the methanol soluble fraction, acquired in positive mode, shows peaks at m/z 169.1208 (Entry 9 Table 1.1), 169.1209 (Entry 6 Table 1.2), and 169.1679 (Entry 3 Table 1.3), as depicted in Fig. 1.11. These peaks correspond to $[M+H]^+$ of the 3HT monomer peak, and are consistent with the calculated 3HT monomer peak at a value of *m/z* 169.1045. This methanol soluble fraction (from Entry 9 in Table 1.1, Entry 6 in Table 1.2, and Entry 3 in Table 1.3) only contained the 3HT monomer, which indicates that a number of 3HT monomer molecules remain after the end of oxidative polymerization when using a $FeCl_3$/3HT molar ratio of 1:10.

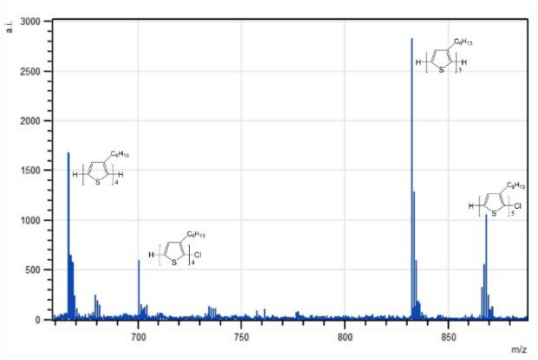


**Figure 1.9. SALDI TOF MS of oligomer extracted from methanol – soluble fraction when 3HT was synthesized followed conditions: 2 hour, $FeCl_3$/3HT is 1/1, 23ºC in chloroform solvent (contains 0.3-1% ethanol as stabilizer)**

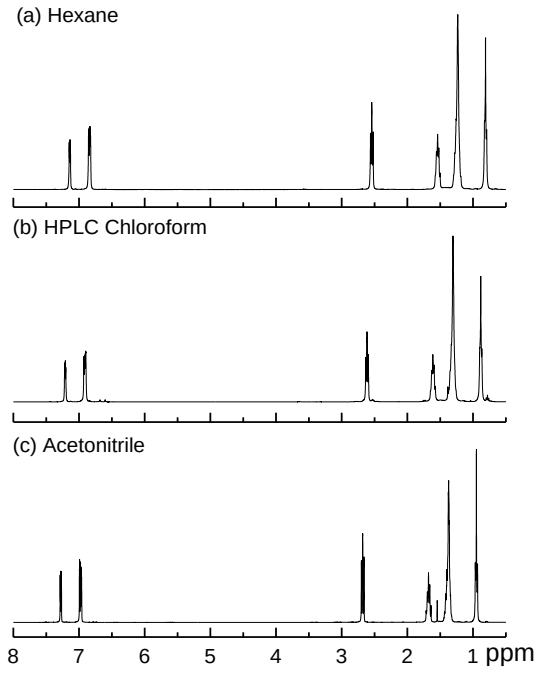


**Figure 1.10. $^{1}$H NMR spectra of the oligomer extracted from the methanol soluble fraction corresponding to Entry 9–Table 1.1 (a), Entry 6–Table 1.2 (b), and Entry 3–Table 1.3 (c)**

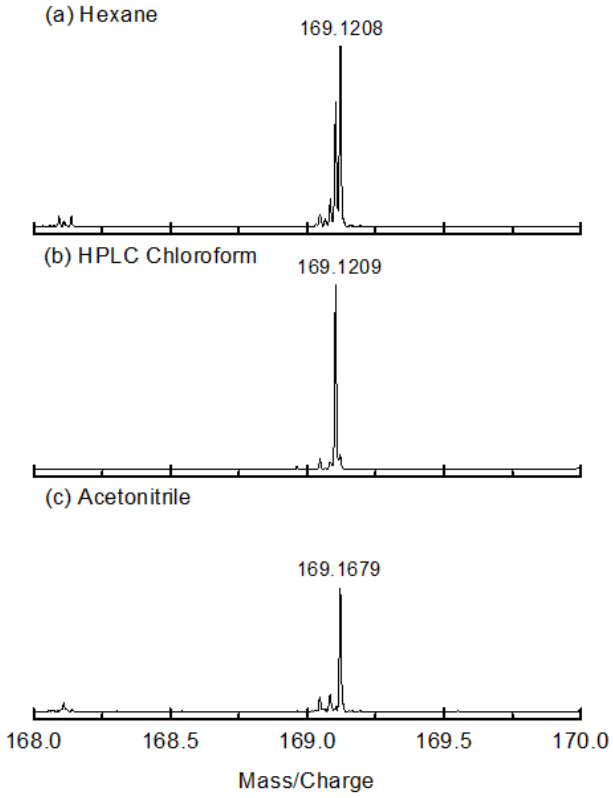


**Figure 1.11. ESI MS spectra, acquired in positive ion mode, of the oligomer extracted from the methanol–soluble fraction corresponding to Entry 9–Table 1.1 (a), Entry 6–Table 1.2 (b), and Entry 3–Table 1.3 (c)**

Fig. 1.12 shows the $^{1}$H NMR spectra of the products extracted from the methanol soluble fraction when the stoichiometric ratio of $FeCl_3$/3HT is 1:1. It is obvious that the spectrum of Fig. 1.12c is as same as the spectrum shown in Fig. 1.10, meaning that a number of 3HT monomers remain even after oxidative polymerization of 3HT using a $FeCl_3$/3HT ratio of 1:1 in acetonitrile solvent. In contrast to Fig. 1.12c, Figs. 1.12a and 1.12b show a series of peaks appearing from 0.5 to 7.5 ppm. The two peaks that appear at 2.6 ppm and 2.8 ppm are related to the HT and HH dyad contents, while the cluster of peaks in the 6.6–7.0 ppm range correspond to the four triad configurations that include HT-HT, TT-HT, HT-HH, and TT-HH segments[45]. In addition, Fig. 1.13 show the SALDI TOF mass spectrum of an oligomer (Entry 5 Table 1.1 and Entry 2 Table 1.2) for which are two types of peaks are observed: [166n + H + H] and [166n + H + Cl], with n = 4 and 5 (n is equal to the number of repeat units). These peaks are observed at m/z 666.360, 700.316, 832.402, and 866.301 (in Fig. 1.13), respectively, in accordance with the calculated m/z values of 666.342, 700.303, 832.423, and 866.384 (calculation by Isopattern). These results show that in a heterogeneous system (in hexane and chloroform), many low-molecular-weight oligomers with regiorandom structures (47–51% of HT content) are produced. However, in homogeneous systems (in acetonitrile) many 3HT monomers remain after oxidative polymerization when a $FeCl_3$/3HT ratio of 1:1 is used. This also explains why the polymer yield obtained in a heterogeneous system (in hexane or chloroform) is higher than that obtained in a homogeneous system (in nitrobenzene or acetonitrile) when a $FeCl_3$/3HT ratio in the 1:1–1:10 range is used (see Tables 1.1, 1.2 and 1.3).

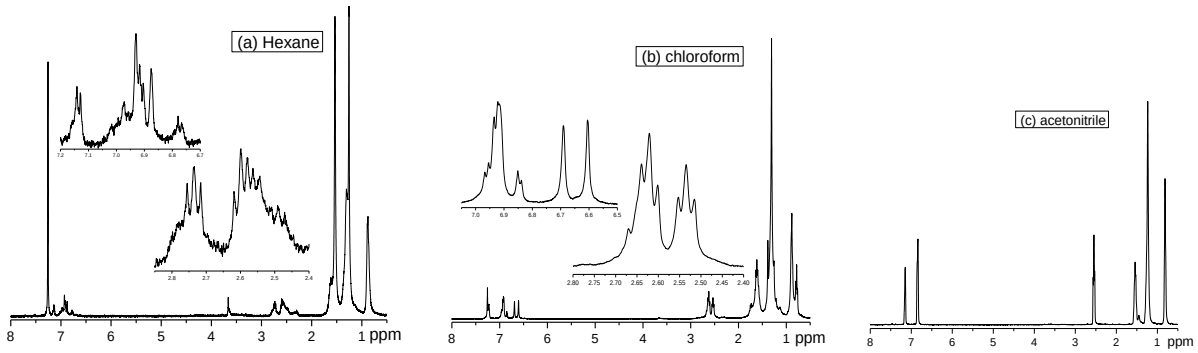


**Figure 1.12. $^{1}$H NMR spectrum of the oligomer extracted from the methanol–soluble fraction of Entry 5 in Table 1.1 (a), Entry 2 in Table 1.2 (b), and Entry 4 in Table 1.3 (c)**

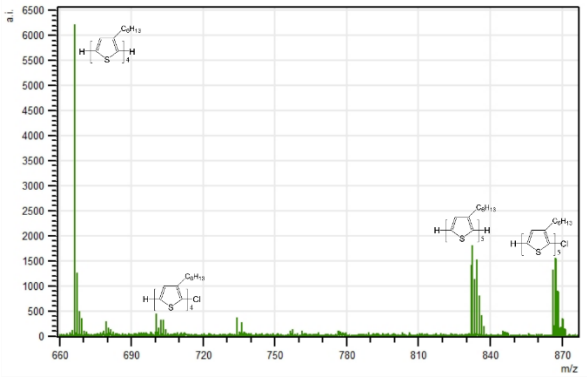


**Figure 1.13. SALDI TOF MS of the oligomer extracted from the methanol–soluble fraction of Entry 5 in Table 1.1 (a) and Entry 2 in Table 1.2 (b)**

The solubility of $FeCl_3$ in the solvent can play an important role in changing the yield of oxidative polymerization. In a heterogeneous system (in chloroform or hexane), the 3HT monomers are easily coordinated to Fe(III) at the active sites on the surface of the $FeCl_3$ crystals. The connections occur between the free electron pair of the sulfur atom and the free orbital of Fe(III)[40]. In a homogeneous system (in acetonitrile or nitrobenzene), the coordination between the 3HT monomer and Fe(III) is difficult due to the solubility of the $FeCl_3$ crystals in the solvent, resulting in a lower polymerization rate.

Many plausible mechanisms for the chemical oxidative polymerization of 3HT using $FeCl_3$ have been proposed for the case where the stoichiometric ratio of $FeCl_3$/3HT is 4 [18,27,40,42] For example, a dimer consisting of two 3HT monomers is formed initially, connected at the 2-position and 2'-position, and further oxidation reactions occur more easily in the oligomer than in the monomer [18,42]. In fact, in our research, the structure of 3HT dimer can be observed using SALDI TOF MS. Moreover, there are three possible routes in a plausible mechanism for oxidative polymerization: coupling between the oligomer and monomer, coupling between oligomers, and coupling between dimers[42]. In the case where the $FeCl_3$/3HT ratio is lower than 1, it is supposed that dimer assembly should be the primary process at the early stages of chemical oxidative polymerization. Based on the data described above, an enormous amount of oligomers and monomers remain in the mixture after the end of the polymerization process. These results are in good agreement with the hypothesis proposed in a previous paper[42], and indicate that coupling between oligomers was diminished, and the oxidation of the monomer was also kept at a minimum. Thus, a coupling between the oligomer and monomer (Scheme 1.2) should be favored for obtaining the regioregular-structured polymer[27,42].

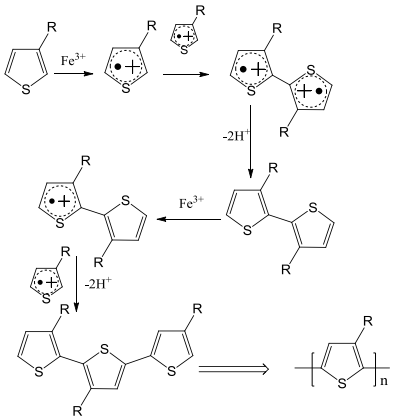

**Scheme 1.2. Proposed mechanism for the oxidative polymerization of P3HT**[27]

## 1.4 Conclusions

Solid $FeCl_3$ is a very effective catalyst for oxidative polymerization. Ethanol, used as a stabilizer in chloroform, significantly influences the performance of polymerization, especially when the $FeCl_3$/monomer ratio is equal to or lower than 1. The oxidative polymerization of the 3HT monomer can be conducted reliably both in hexane and ethanol-free chloroform using a $FeCl_3$/3HT ratio lower than 1 (from 1:1 to 1:10), and leads to a high-molecular-weight polymer. The polymer yield and $M_n$ obtained in heterogeneous systems are higher than those obtained in homogeneous systems. The yield of the oxidative polymerization is proportional to the molar fraction of the $Fe^{3+}$ used. A dimer could be formed at the initial stage of the oxidative polymerization. The coupling between oligomer and monomer should be favored in order to obtain P3HT with a regioregular structure. When the ratio of $FeCl_3$/3HT is in the 1:1–1:10 range, a large amount of low-molecular-weight oligomers and monomers remain in the mixture at the end of the oxidative polymerization.

## 1.5 References

(1) Li, J.; Liu, J.; Wei, C.-W.; Liu, B.; O'Donnell, M.; Gao, X. *Phys. Chem. Chem. Phys.* **2013**, *15*, 17006-17015
(2) Kim, D. Y.; Cho, H. N.; Kim, C. Y. *Prog. Polym. Sci.* **2000**, *25*, 1089-1139.
(3) Günes, S.; Neugebauer, H.; Sariciftci, N. S. *Chem. Rev.* **2007**, *107*, 1324−1338.
(4) Cheng, Y.-J.; Yang, S.-H.; Hsu, C.-S. *Chem. Rev.* **2009**, *109*, 5868–5923.
(5) McQuade, D. T.; Pullen, A. E.; Swager, T. M. *Chem. Rev.* **2000**, *100*, 2537-2574.
(6) Smela, E. *Adv. Mater.* **2003**, *15*, 481-494.
(7) Majumdar, H. S.; Bandyopadhyay, A. *J. Appl. Phys.* **2002**, *91*, 2433-2437.
(8) Facchetti, A. *Chem. Mater.* **2011**, *23*, 733–758.
(9) Sheina, E. E.; Liu, J.; Iovu, M. C.; Laird, D. W.; McCullough, R. D. *Macromolecules* **2004**, *37*, 3526-3528.
(10) Yokoyama, A.; Miyakoshi, R.; Yokozawa, T. *Macromolecules* **2004**, *37*, 1169-1171.
(11) Elsenbaumer, R. L.; Jen, K. Y.; Oboodi, R. *Synth. Met.* **1986**, *15*, 169-174.
(12) Sugimoto, R.; Takeda, S.; Gu, H. B.; Yoshino, K. *Chem. Express* **1986**, *1*, 635-638.
(13) Yoshino, K.; Hayashi, S.; Sugimoto, R. *Jpn. J. Appl. Phys.* **1984**, *23*.
(14) Roncali, J.; Garreau, R.; Yassar, A.; Marque, P.; Gamier, F.; Lemaire, M. *J. Phys. Chem.* **1987**, *91*, 6706-6714.
(15) Schopf, G.; Koßmehl, G. *Adv. Polym. Sci.* **1997**, *129*, 1-12.
(16) Niemi, V. M.; Knuuttila, P.; 0sterholm, J. E.; Korvola, J. *Polym. Rep.* **1992**, *33*, 1559-1562.
(17) Andersson, M. R.; Selse, D.; Berggren, M.; Jarvinen, H.; Hjertberg, T.; Inganas, O.; Wenerstrom, O.; Osterholm, J.-E. *Macromolecules* **1994**, *27*, 6503-6506.
(18) Barbarella, G.; Zambianchi, M.; Toro, R. D.; Martino Colonna, J.; Iarossi, D.; Goldoni, F.; Bongini, A. *J. Org. Chem.* **1996**, *61*, 8285-8292.
(19) Liu, Y.; Nishiwaki, N.; Saigo, K.; Sugimoto, R. *Bull. Chem. Soc. Jpn.* **2013**, *86*, 1076-1078.
(20) Dou, J.; Chen, Z.; Ma, C. *Synth. Met.* **2014**, *196*, 117-124.
(21) H.Bannock, J.; Xu, W.; Baïssas, T.; Heeney, M.; Mello, J. C. d. *Eur. Polym. J.* **2016**, *80*, 240-246.
(22) Yagci, Y.; Jockusch, S.; Turro, N. J. *Macromolecules* **2007**, *40*, 4481-4485.
(23) Aydogan, B.; Gunbas, G.; AsumanDurmus; Toppare, L.; Yagci, Y. *Macromolecules* **2010**, *43*, 101-106.
(24) Aoyama, Y.; Yamanari, T.; Murakami, T. N.; Nagamori, T.; Marumoto, K.; Tachikawa, H.; Mizukado, J.; Suda, H.; Yoshida, Y. *Polym. J.* **2015**, *47*, 26-30.
(25) Jung, Y. J.; Lee, S. J.; Choi, S. W.; Kim, J. H. *J. Polym. Sci. Part A: Polym. Chem.* **2008**, *46*, 5968-5975.
(26) Balasubramanian, A.; Ku, T.-C.; Shih, H.-P.; Suman, A.; Lin, H.-J.; Shih, T.-W.; Han, C.-C. *Polym. Chem* **2014**, *5*, 5928-5941.
(27) Fukumoto, H.; Omori, Y.; Yamamoto, T. *Polym. J.* **2013**, *45*, 462-465.
(28) Gadient, J.; Groch, R.; Lind, C. *Polymer* **2017**, *115*, 21-27.
(29) Hirai, T.; Nagae, Y.; White, K. L.; Kamitani, K.; Kido, M.; Uchiyama, T.; Nishibori, M.; Konishi, Y.; Yokomachi, K.; Sugimoto, R.; Saigo, K.; Ohishi, T.; Higaki, Y.; Kojio, K.; Takahara, A. *RSC Adv.* **2016**, *6*, 111993-111996
(30) Park, T.-J.; Kim, Y. S.; Kan, E.; Lee, S. H. *RSC Adv.* **2015**, *5*, 25590-25593
(31) Park, T.-J.; Lee, S. H. *Green Chem* **2017**, *19*, 910-913.
(32) Laakso, J.; Jarvinen, H. *Synth. Met.* **1993**, *55*, 1204–1208.
(33) Wang, Y.; Lucht, B. L.; Euler, W. B. *Polymer Preprints* **2002**, *43*, 1160.
(34) Amou, S.; Haba, O.; Shirato, K.; Hayakawa, T.; Ueda, M.; Takeuchi, K.; Asai, M. *J. Polym. Sci. Pol. Chem.* **1999**, *37*, 1943–1948.
(35) Yonezawa, T.; Asano, T.; Matsubara, M. *Bull. Chem. Soc. Jpn.* **2016**, *89*, 346-353.
(36) Guinan, T.; Kirkbride, P.; Pigou, P. E.; Ronci, M.; Kobus, H.; Voelcker, N. H. *Mass Spectrom. Rev.* **2015**, *34*, 627-641.
(37) Yamamoto, T.; Komarudin, D.; Arai, M.; Lee, B.-L.; Suganuma, H.; Asakawa, N.; Inoue, Y.; Kubota, K.; Sasaki, S.; Fukuda, T.; Matsuda, H. *J. Am. Chem. Soc.* **1998**, *120*, 2047-2058.
(38) Hirai, T.; Sato, M.; Kido, M.; Nagae, Y.; Kaetsu, K.; Kiyoshima, Y.; Fujii, S.; Ohishi, T.; White, K. L.; Higaki, Y.; Teraoka, Y.; Nishibori, M.; Kamitani, K.; Hanada, K.; Sugiyama, T.; Sugimoto, R.; Saigo, K.; Kojio, K.; Takahara, A. *J. Polym. Sci. Part A: Polym. Chem.* **2015**, *53*, 2075-2078.
(39) Hai, T. A. P.; Sugimoto, R. *J. Mol. Struct.* **2017**, *1146*, 660–668.
(40) Niemi, V. M.; Knuuttila, P.; 0sterholm, J.-E.; Korvola, J. *Polymer Reports* **1992**, *33*, 1559-1562.

(41) Toshima, N.; Hara, S. *Prog. Polym. Sci.* **1995**, *20*, 155-183.
(42) Amou, S.; Haba, O.; Shirato, K.; Hayakawa, T.; Ueda, M.; Takeuchi, K.; Asai, M. *J. Polym. Sci. Part A: Polym. Chem.* **1999**, *37*, 1943–1948.
(43) Brambilla, L.; Tommasini, M.; Botiz, I.; Rahimi, K.; Agumba, J. O.; Stingelin, N.; Zerbi, G. *Macromolecules* **2014**, *47*, 6730-6739.
(44) Yuan, Y.; Zhang, J. M.; Sun, J. Q.; Hu, J.; Zhang, T. P.; Duan, Y. X. *Macromolecules* **2011**, *44*, 9341-9350.
(45) Sato, M. A.; Morii, H. *Macromolecules* **1991**, *24*, 1196-1200.
(46) Liu, J.; Loewe, R. S.; McCullough, R. D. *Macromolecules* **1999**, *32*, 5777-5785.
(47) McCarley, T. D.; Noble, C. O.; IV; DuBois, C. J.; Jr.; McCarley, R. L. *Macromolecules* **2001**, *34*, 7999-8004.
(48) Montaudo, G.; Samperi, F.; Montaudo, M. S. *Prog. Polym. Sci.* **2006**, *31*, 277–357.
(49) Sato, H.; Nakamura, S.; Teramoto, K.; Sato, T. *J. Am. Soc. Mass Spectrom.* **2014**, 1-10.
(50) Dopke, N. C.; Lovett, T. N. *J. Chem. Educ.* **2007**, *84*, 1968-1980.
(51) Liu, Y.; Nishiwaki, N.; Saigo, K.; Sugimoto, R. *Polym. Bull.* **2015**, *72*, 1817–1826.

# Chapter 2:

# The catalytic oxidative polymerization of 3-hexylthiophene

## 2.1 Introduction

In previous chapter, we reported the effect of the oxidizer/3-hexylthiophene monomer molar ratio in the chemical oxidative polymerization and confirmed the proposed mechanism of 3HT with $FeCl_3$ as oxidant[1]. Recently, the reduction-oxidation process involving $FeCl_3$ was sufficiently described in detail and the reduction of Fe(III) to Fe(II) was confirmed by Fe K-edge X-ray absorption near-edge structure (XANES)[2]. Chemical syntheses of poly(3-alkylthiophene) (PAT) were conducted by metal-catalyzed cross-coupling polymerization using different transition metal acetylacetonate catalysts such as Pd(II), Ni(II) , Co(II), and Fe(III)[3] or oxidative polymerization using $FeCl_3$, [4] $MoCl_5$, or $RuCl_3$ [5], $AlCl_3/CuCl_2$ or $AlCl_3$ alone[6]. In addition, a new PAT was synthesized by the Curtis method, using Cu powder and a catalytic amount of $PdCl_2$ in pyridine.[7] Although cross-coupling in the presence of Ni and Pd catalyst can be applied to the potential synthesis of a selection of monomers, and producing perfectly regioregular structure, this method requires brominated monomer as well as water- and oxygen-free conditions for polymerization [8]. The oxidative polymerization of P3HT with $FeCl_3$ is simple and preferred for industrial production, however this method limits the extended conjugation length due to cross-linking at the 2,4 positions[8]. Recently, several interesting methods based on simple and inexpensive oxidative catalysis have been reported for the syntheses of 3HT and its derivatives with regioregularity and the desired properties[9-13]. Polythiophene nanoparticles with a narrow size distribution can be obtained by oxidative polymerization using $FeCl_3$ as a catalyst and hydrogen peroxide as an oxidant [13]. Furthermore, P3HT rich in head-to-head content can be obtained through palladium-catalyzed oxidative polymerization [9]. Instead of $FeCl_3$, the oxovanadium catalyst system was employed for the synthesis of regioregular head-to-tail poly(3-alkylphenylthiophene)[10]. The use of catalytic amounts of $CoCl_2$ with $FeCl_3$ was found to increase the molecular weight and regioregularity of P3HT [11]. The poly[3-(4-alkoxyphenyl)thiophene] with good regioregularity was obtained by oxidative coupling catalyzed by Cu(II) complexes [12].

In the case of the oxidative polymerization of 3HT with $FeCl_3$, in order to avoid the use of excess $FeCl_3$ [4,5,14-21], an oxidizer to assist the catalytic oxidative polymerization by oxidizing $Fe^{2+}$ to $Fe^{3+}$ was considered (Scheme 2.1). Some previous works demonstrated that $FeCl_2$ is oxidized to $FeCl_3$ when $CHCl_3$ is decomposed by exposure to UV light in the presence of oxygen.[2,22] In this study, we report the catalytic oxidative polymerization of 3-hexylthiophene with $FeCl_3$ in hexane using various oxidizing agents ($Cl_2$, BPO, $H_2O_2$, $ZrCl_4$, and $(NH_4)_2Ce(NO_3)_6$) capable of oxidizing $Fe^{2+}$ to $Fe^{3+}$.

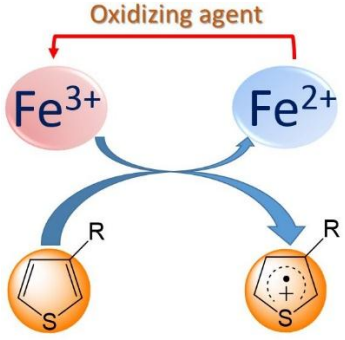


**Scheme 2.1. The catalytic oxidative polymerization**

## 2.2 Experimental section

### *2.2.1 Materials*

3-Hexylthiophene, $FeCl_3$, and $FeCl_2$ were purchased from Tokyo Chemical Industry Ltd. and used without any further purification. Anthralin (Nacalai Tesque Inc., Tokyo) and silver trifluoroacetate (Wako Pure Chemical Industries Ltd.) were applied as the matrix and cation agent in the MALDI-TOF MS, respectively. Hexane was received from Wako Pure Chemical Industries Ltd. and dried by 4Å molecular sieves for 24 h, then purged with Ar gas for 25 min before using. Benzoyl peroxide (BPO) (Nacalai Tesque Kyoto Chemical Industries Ltd.), $H_2O_2$ (Sann Toku Chemical Industries Ltd.), $ZrCl_4$ (Tokyo Chemical Industry Ltd.), and $(NH_4)_2Ce(NO_3)_6$ (Wako Pure Chemical Industries Ltd.) were used as oxidizers for the catalytic oxidative polymerization.

### *2.2.2 Equipment*

$^1H$ NMR (400 MHz) and IR spectra were recorded on a Bruker Ascend 400 spectrometer and a Jasco FT/IR–480 Plus, respectively. GPC was carried out in a system equipped with a Jasco PU-2080 Plus pump and a Jasco RI-2031 with an intelligent RI detector. The molecular weight and molecular weight distribution of the polymers relative to a polystyrene standard were analyzed using Chrom NAV software. Chloroform served as the polymer solvent and eluent in an equilibrated system at 40 °C. A Bruker Autoflex Speed-KE was used in reflector mode for the MALDI-TOF MS analysis. UV-Vis absorbance spectra and fluorescence emission spectra were measured at room temperature on a Jasco V-650 UV-Vis spectrometer and a Jasco spectrofluorometer FP-8300, respectively. ESI mass spectra were acquired with an AB Sciex Triple ESI TOF 4600 system; for the analysis, 20 μL of sample was injected (direct injection) into the mass spectrometer using chloroform/acetonitrile (10:90, v/v) as a solvent at a flow rate of 10 μL/min (syringe pump). Electrical conductivity of the iodine doped polymer film was measured with an Agilent 34401A $6^{1/2}$ Digit Multimeter resistometer by a four-probe method.

### *2.2.3 Synthesis and characterization of polymer products*

#### *2.2.3.1 Polymerization of 3HT using $FeCl_3$ with oxidizers*

All the reactions described in this study were conducted in an oven-dried Schlenk tube with stopcock under an atmosphere of argon. The polymerizations of 3HT were done according to the literature, except that the reagents and the ratios were changed.[4] In short, $FeCl_3$ (81 mg, 0.5 mmol) was added to anhydrous hexane (15 mL) in a Schlenk tube and stirred for 5 min. The mixture then underwent ultrasound treatment for 15 min. The hexane (5 mL) solution of 3HT (90 mg, 0.5 mmol) was dropped into the suspension of $FeCl_3$. After 24 h, various oxidative agents ($Cl_2$, BPO, $H_2O_2$, $ZrCl_4$, and $(NH_4)_2Ce(NO_3)_6$) were injected into the mixture, and the reactions continued for another 24 h. The resulting copolymer was washed with methanol to remove any residual $FeCl_3$, and then it was extracted with acetone and chloroform using a Soxhlet extractor.

#### *2.2.3.2 Polymerization of 3HT using $FeCl_2$ and $(NH_3)_2Ce(NO_3)_6$*

$FeCl_2$ (64 mg, 0.5 mmol), $(NH_3)_2Ce(NO_3)_6$ (275 mg, 0.5 mmol), and anhydrous hexane (15 mL) were placed in a Schlenk tube and stirred for 5 min. The mixture then underwent ultrasound treatment for 15 min. The hexane (5 mL) solution of 3HT (90 mg, 0.5 mmol) was dropped into the suspension of $FeCl_2$ and $(NH_3)_2Ce(NO_3)_6$, and the reaction mixture was stirred for 24 h. The resulting copolymer was washed with methanol to remove any residual $FeCl_2$ and $(NH_3)_2Ce(NO_3)_6$, and then it was extracted with acetone and chloroform using a Soxhlet extractor. The solvents were evaporated to collect the products.

## 2.3 Results and discussion

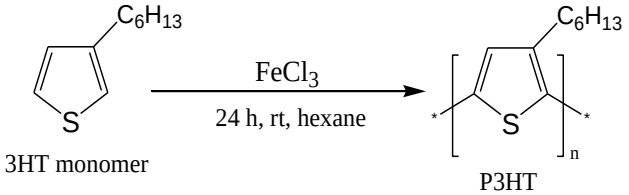


**Scheme 2.1 Synthesis of poly(3-hexylthiophene)**

The preparation of P3HT was carried out under the conditions shown in Scheme 2.1, and the ratio between $FeCl_3$ and 3-hexylthiophene monomer was varied from 1:1 to 4:1. The results of these experiments are summarized in Table 2.1.

**Table 2.1. Oxidative polymerization of 3-hexylthiophene in hexane at room temperature (23 °C)**

| Entry | $FeCl_3$/3HT ratio | Yield (%) | | $M_w$[a], kDa | PDI[b] | HT[c] |
|---|---|---|---|---|---|---|
| | | Oligomer[d] | Polymer[e] | | | |
| 1 | 1:1 | 3.1 | 26.7 | 114 | 2.2 | 67 |
| 2 | 2:1 | 2.2 | 55.5 | 112 | 2.5 | 67 |
| 3 | 3:1 | 4.6 | 70.6 | 115 | 2.2 | 67 |
| 4 | 4:1 | 3.5 | 85.4 | 106 | 2.4 | 67 |

[a] Determined by Gel-Permeation Chromatography (polystyrene standard, chloroform as solvent)
[b] Polydispersity Index, PDI = $M_w/M_n$
[c] HT: head to tail content, determined by $^1$H NMR
[d] Oligomer: the polymer product was Soxhlet extracted with acetone
[e] Polymer: the polymer product was Soxhlet extracted with chloroform

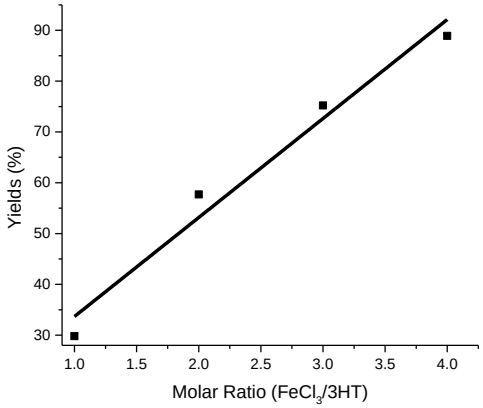


**Figure 2.1. Yield of P3HT as a function of the molar ratio of $FeCl_3$ to 3HT**

As shown in Table 2.1, the head-to-tail (HT) content of P3HT was nearly constant despite the changes in the molar ratio of $FeCl_3$/3HT, revealing that the formation of an HT unit is not affected by the amount of $FeCl_3$. The average molecular weight ($M_w$) and PDI are around 111000 Da and 2.2, respectively. However, the yields varied according to the change in the molar ratio of monomer and $FeCl_3$ (Fig. 2.1). The yield was drastically improved from 29.8% to 88.9% with the increase in the $FeCl_3$/3HT molar ratio from 1 to 4. It is remarkable that the oxidative polymerization occurs at all in this lowest molar ratio ($FeCl_3$/3HT = 1:1) which was explained in previous chapter [1]. In addition, the reduction of Fe(III) to Fe(II) has been confirmed definitely by Fe K-edge XANES[2]. In the oxidative polymerization of 3-hexylthiophene using $FeCl_3$ in hexane, $FeCl_3$ acts only as an oxidant. It has been suggested that the first step of oxidative polymerization is the formation of a radical cation and the reduction of Fe(III) to Fe(II).[23] During the reaction, $Fe^{3+}$ is consumed and $Fe^{2+}$ is formed, and the electrochemical potential of $Fe^{3+}/Fe^{2+}$ decreases over time[24]. Moreover, chloroform was oxidatively decomposed by exposure to UV light in the presence of oxygen, which facilitated the oxidation of Fe(II) to Fe(III).[2,22] It was considered that some oxidizing agent could oxidize $Fe^{2+}$ to $Fe^{3+}$ and that the polymerization could be catalyzed by the oxidation of $Fe^{2+}$ to $Fe^{3+}$ (Scheme 2.1). Various oxidative agents ($Cl_2$, BPO, $H_2O_2$, $ZrCl_4$, and $(NH_4)_2Ce(NO_3)_6$) were examined to determine which could effectively oxidize $Fe^{2+}$ to $Fe^{3+}$. After polymerization for 24 h at 23 °C, the oxidizing agents were added, and polymerization continued for another 24 h. The effects of the oxidizing agents in the polymerization of 3HT using $FeCl_3$ are summarized in Table 2.2.

**Table 2.2. The effect of the oxidizing agents in polymerization of 3HT using $FeCl_3$ in hexane**

| Entry | Oxidizing agent | Yield (%) | Insoluble (%) |
|---|---|---|---|
| 1 | none | 29–35 | - |
| 2 | $Cl_2$ | 28 | - |
| 3 | $H_2O_2$ | 27 | - |
| 4 | BPO | 5 | 54 |
| 5 | $ZrCl_4$ | 30 | - |
| 6 | $(NH)_4Ce(NO_3)_6$ | 53 | - |

$$Fe^{2+} + Cl_2 \rightarrow Fe^{3+} \qquad (1)$$

**Equation 2.1. Chlorine as an oxidizing agent**

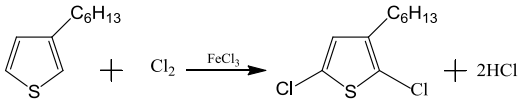


**Scheme 2.3. The halogenation of 3-hexylthiophene**

Although chlorine is known to easily oxidize $Fe^{2+}$ to $Fe^{3+}$ in basic inorganic chemistry, as shown in Eq. (2.1), it had no effect on the yield in this polymerization system. It is possible that a halogenation reaction of 3HT occurs under these reaction conditions (Scheme 2.3).[25] Since the chloro-substituted monomer is less reactive,[25] it is likely that species that causes the termination of the oxidative polymerization. Although chlorine can oxidize $Fe^{2+}$ to $Fe^{3+}$, it is not potent enough to improve the polymerization yield due to the presence of the halogenation reaction.

$H_2O_2$ has been well-known as a Fenton reagent for more than a century (Scheme 2.4), although its mechanism of action is still widely debated.[26] Equation (2.2) lists a series of transformations proposed by Barb et al.[27] to be involved in the free radial mechanism.

$$Fe^{2+} + H_2O_2 \rightarrow Fe^{3+} + OH^- + OH^{\cdot} \qquad (2.2a)$$
$$OH^{\cdot} + H_2O_2 \rightarrow HO_2^{\cdot} + H_2O \qquad (2.2b)$$
$$Fe^{3+} + HO_2^{\cdot} \rightarrow Fe^{2+} + H^+ + O_2 \qquad (2.2c)$$
$$Fe^{2+} + HO_2^{\cdot} \rightarrow Fe^{3+} + HO_2^- \qquad (2.2d)$$
$$Fe^{2+} + OH^{\cdot} \rightarrow Fe^{3+} + OH^- \qquad (2.2e)$$

**Equation 2.2. The Fenton reaction**

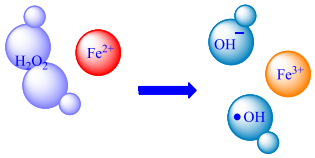


**Scheme 2.4. The reaction between $Fe^{2+}$ and $H_2O_2$**

Combination $FeCl_3/H_2O_2$ systems (catalyst/oxidant) have been utilized successfully for the oxidative polymerization of thiophene in the presence of a surfactant in aqueous medium.[13,28] However, hydrogen peroxide is usually received and used as an aqueous solution, and water is not miscible with hexane. Therefore, interactions between $H_2O_2$ molecules and $Fe^{2+}$ ions are hardly possible. In addition, as shown in Eq. (2.2c), hydroxyl radicals react with $Fe^{3+}$, and this reaction competes with the oxidation of $Fe^{2+}$.

Benzoyl peroxide (BPO) is also able to oxidize $Fe^{2+}$ to $Fe^{3+}$ (Scheme 2.5). P3HT was obtained in very high yields, as shown in Table 2.2, but the percentage of insoluble material obtained was quite high. This means that partial gelation of the resulting polymer occurs by a side reaction of 3HT at the 4-position.

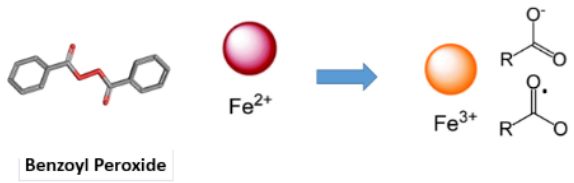


**Scheme 2.5: The reaction between $Fe^{2+}$ and BPO**

$4Fe^{2+} + Zr^{4+} \rightarrow 4Fe^{3+} + Zr$ ($E^0 = -4.63$ V with $E^0_{Fe^{2+}/Fe^{3+}} = -0.771$ V; $E^0_{Zr^{4+}/Zr} = -1.55$ V) (2.3a)

$Fe^{2+} + Ce^{4+} \rightarrow Fe^{3+} + Ce^{3+}$ ($E^0 = 0.99$ V with $E^0_{Fe^{2+}/Fe^{3+}} = -0.771$ V; $E^0_{Ce^{4+}/Ce^{3+}} = 1.76$ V) (2.3b)

(Standard reduction potentials obtained from the Handbook of Inorganic Chemistry)

**Equation 2.3. Oxidation $Fe^{2+}$ by $Zr^{4+}$ and $Ce^{4+}$**

$Ce^{4+}$ (diammonium cerium nitrate) was the most effective oxidant among those tried for the polymerization of 3HT. The yield of the polymer was typically in the range of about 29–35% without the addition of $(NH_4)_2Ce(NO_3)_6$, but the yield improved to 53% with its use. To predict what redox reaction would occur, the standard reduction potentials of Fe, Zr, and Ce are applied the diagonal rule (Equation 2.3). A positive value of $E^0$ shows that the forward reaction is favored, while a negative value of $E^0$ indicates that the reverse reaction is favored. This could explain why Ce increased the polymerization yield, while Zr had no effect.

P3HT obtained by adding $(NH_4)_2Ce(NO_3)_6$ was characterized by GPC and $^1H$ NMR, and its other properties were also analyzed. Table 2.3 (entries 1 and 2) shows the molecular weight of the oligomer and P3HT polymer synthesized with and without the addition of $Ce^{4+}$. The extracted oligomers of S1 and S2 had similar $M_w$'s (4500 and 5600 Da) with a PDI of 1.3–1.4, while S1 resulted in a P3HT polymer with higher $M_w$ than in S2 ($114 \times 10^3$ Da compared to $99 \times 10^3$ Da) with a PDI of 2.2–3.8. These results indicate that the molecular weight of the resulting polymer is nearly the same, with or without the addition of $Ce^{4+}$.

**Table 2.3. Effect of the $Ce^{4+}$ into polymerization of 3-hexylthiophene in hexane**

| Entry | Sample | Experiment | Oligomer[c] | | Polymer[d] | |
|---|---|---|---|---|---|---|
| | | | $M_w$[a] × $10^3$ Da | PDI[b] | $M_w$[a] × $10^3$ Da | PDI[b] |
| 1 | S1 | $Fe^{3+}$/3HT 1:1 | 4.5 | 1.4 | 114 | 2.2 |
| 2 | S2 | $Fe^{3+}$/3HT/$Ce^{4+}$ 1:1:1 | 5.6 | 1.3 | 99 | 3.8 |
| 3 | S3 | $Fe^{2+}$/$Ce^{4+}$/3HT 1:1:1 | 1.5 | 1.4 | 11 | 1.9 |

[a] Determined by Gel-Permeation Chromatography (Polystyrene standard, chloroform as solvent)
[b] Polydispersity Index, PDI = $M_w/M_n$
[c]: Oligomer: the reaction product was Soxhlet extracted with acetone
[d]: Polymer: the reaction product was Soxhlet extracted with chloroform

To confirm definitively the oxidizing ability of Ce(IV), a combination of $FeCl_2$ and $(NH_4)_2Ce(NO_3)_6$ was used to oxidatively polymerize 3HT (Table 2.3, entry 3). The obtained polymer (S3) had a molecular weight of 11000 Da (PDI = 1.9) and was obtained in 15% yield.

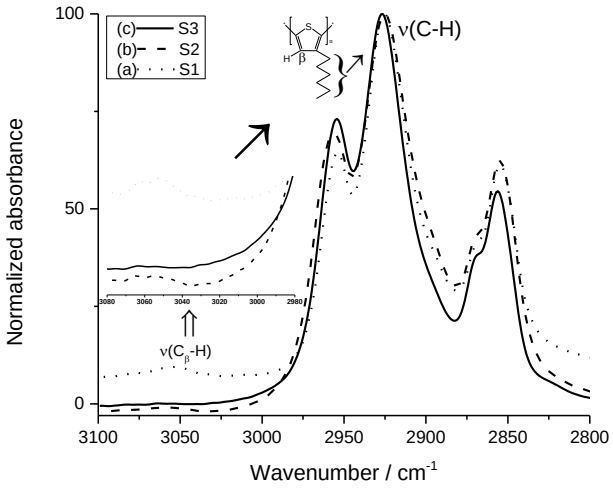


**Figure 2.2. FT-IR spectra of P3HT samples S1, S2, and S3**

Figure 2.2 shows the FT-IR spectra of the P3HT samples S1, S2, and S3. S1 and S2 were synthesized with a molar ratio of 3HT/$FeCl_3$ of 1 to 1. The absorptions in the 3000–2800 $cm^{-1}$ are usually assigned to the C-H stretching of the $CH_3$ and $CH_2$ groups of the hexyl chain, while the bands at 3080–2980 $cm^{-1}$ correspond to the stretching vibrations of the thiophene backbone at the 4-position ($C_\beta$-H).[29,30] The intensities of the FT-IR spectra were normalized based on the antisymmetric $CH_3$ stretching at 2930 $cm^{-1}$.There is no apparent difference between the peaks for the υ(C-H) band among the three P3HT samples. However, the vibration direction of the $C_\beta$-H out-of-plane deformation mode of S1, S2, and S3 were entirely different. These signals indicated that side reactions involving chlorination at the 4-position had occurred. As shown in Fig. 2.2, the intensities of the bands in the 3080–2980 $cm^{-1}$ region of S2 and S3 are very weak, which indicates that the side reaction occurred at the 4-position in these samples. However, the stretching of the υ($C_\beta$-H) in the 4-position of S1 is observed at 3061 $cm^{-1}$, which supports the notion that the side reaction was minimal to nonexistent in S1.

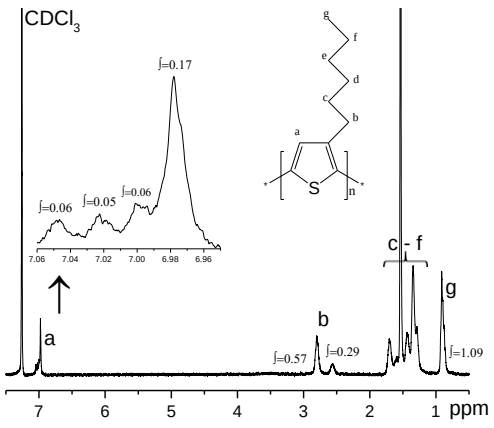


**Figure 2.3. $^1$H-NMR spectra of P3HT (S1)**

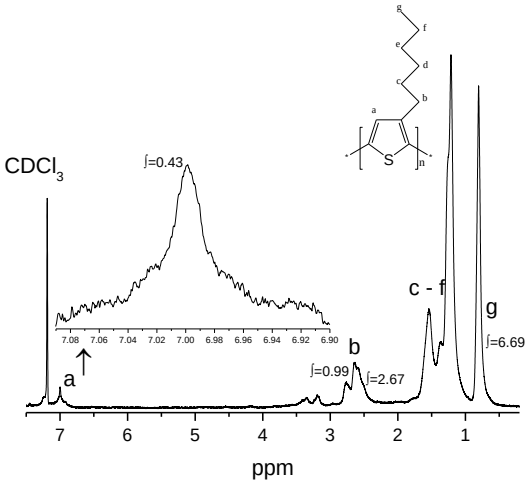


**Figure 2.4. $^1$H-NMR spectra of P3HT (S2)**

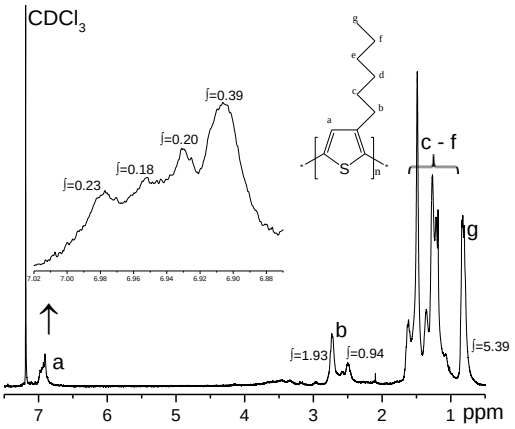


**Figure 2.5. $^{1}$H-NMR spectra of P3HT (S3)**

Figures 2.3, 2.4, and 2.5 present the $^{1}$H NMR spectra of samples S1, S2, and S3. The signals at δ = 0.87 are assigned to the methyl proton.[31] The peaks at δ = 2.50 and δ = 2.80 are related to head-to-head (HH) and head-to-tail (HT) signals, respectively.[31] The four moderate signals at δ = 6.97, δ = 7.00, δ = 7.02, and δ = 7.05 are assigned to the four triad configurations HT-HT, TT-HT, HT-HH, and TT-HH, respectively.[31] These results are summarized in Table 2.4. While S1 and S3 have similar HT and HH configurations, the two dyad configurations of S2 are entirely distinct. The four triad configurations of these samples are different; particularly in S2, only one intense peak at δ = 7.00 attributed to the HT-TT configuration appeared. These results led to the conclusion that the dyad and triad configurations are a result of the presence of $Ce^{4+}$. The intensity of the integral of the methyl proton (δ = 0.87) and the splitting of the peaks from the four triad configurations in the aromatic region (δ = 6.97–7.05) indicate a regulation of the side reaction of 3HT at the 4 position. As seen in Table 2.4, the ratio of the integral intensity at the methyl proton and the four triad configurations are 3.2 (S1), 5.3 (S3), and 15.5 (S2). These results indicate that the side reaction occurred in all samples (S1, S2, and S3), but this reaction takes place only slightly in S1. In agreement with the $^{1}$H NMR spectra, in the FT-IR spectra, the integral intensity of the υ($C_{\beta}$-H) stretching vibration is much more apparent in S1 than in S2 or S3, which suggests that many side reactions occurred at the 4-position in S2 and S3. Moreover, in Table 2.4, it is observed that the ratio of the integral intensity of H from ($C_{\beta}$-H) and ($CH_3$) in S2 is five times greater than that in S1 and three times greater than that of S3. These results confirmed that the reaction involving chlorination at the 4-position, or the 2,4-coupling reaction that occurred in S2, was greater than that in S3, and, in turn, the side reactions in S3 were greater than that in S1. In S1, side reactions at the 4-position still occur, but only slightly when $Ce^{4+}$ was injected to the reaction mixture. Addition of $Ce^{4+}$ increased the yield, but also increased the incidence of side reactions at the 4-position and changed the molecular characterization (only the TT-HT configuration was observed). Considering S3, in which a combination system including $Fe^{2+}$ and $Ce^{4+}$ was utilized for chemical oxidative polymerization of 3HT, it is clear that this system worked effectively, with only minor changes in molecular characterization and side reactions at the 4-position. Taking these results into account, it is indicated that $Ce^{4+}$ is able to oxidize $Fe^{2+}$ to $Fe^{3+}$.

**Table 2.4. Molecular characterization of P3HT samples S1, S2, and S3**

| Samples | Dyads (%)* | | Triads (%)* | | | | Ratio of integral intensity of H from ($C_\beta$-H) and ($CH_3$)* |
|---|---|---|---|---|---|---|---|
| | HT | HH | HT-HT | HT-TT | HT-HH | TT-HH | |
| S1 | 67 | 33 | 50 | 17 | 15 | 17 | 3.2 |
| S2 | 27 | 73 | 0 | 100 | 0 | 0 | 15.5 |
| S3 | 67 | 33 | 39 | 20 | 18 | 23 | 5.3 |

*Determined by $^1$H NMR

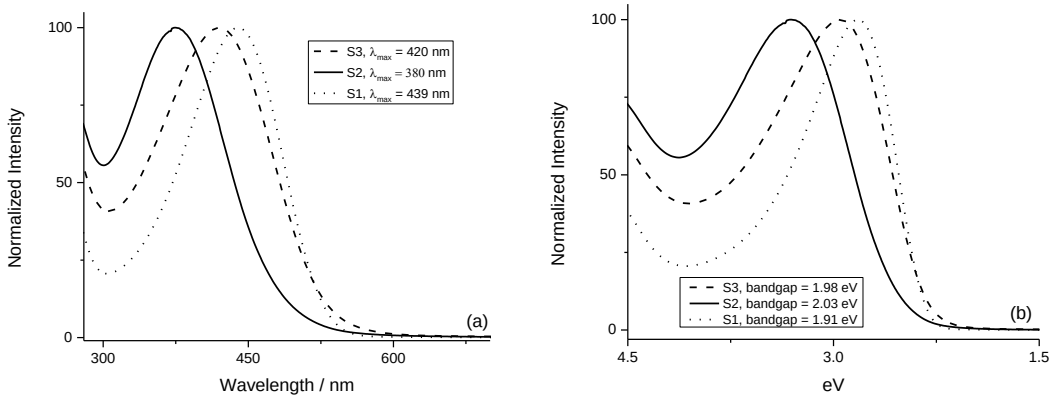


**Figure 2.6. UV-Vis spectra of P3HT (S1, S2, and S3) in chloroform**

UV-Vis spectra of each of the three samples (S1, S2, and S3) in chloroform (Fig. 2.6) show only one peak from P3HT molecules in the range of 380–439 nm. These peaks correspond to the $\pi$-$\pi^*$ transition that indicates the conjugation length of the conducting polymer.[32,33] The band gap energy is calculated from the onset wavelength of optical absorption (Fig. 2.6b). An energy band gap of S1 is 1.91 eV, while S2 and S3 show an energy band gap of 2.03 eV and 1.98 eV, respectively. The absorption spectra of the polymer samples exhibit shifts in wavelength, reflecting the change in molecular structure, self-organizing tendency, and optical gap.[34,35] The large shift of the UV-Vis peak between S1 and S2 (shift ($\Delta$) = 439-380 = 59 nm) is thought to arise from side chain branches at the 4-position and a large HH content (73%) of sample S2. The HT content of S3 remains the same (67%) as S1. However, the 420 nm peak of S3 shifts from 439 nm in S1 ($\Delta$ = 19 nm); this smaller shift shows that side reactions at the 4-position produced side chain branching, which affected the conjugation length of S3.

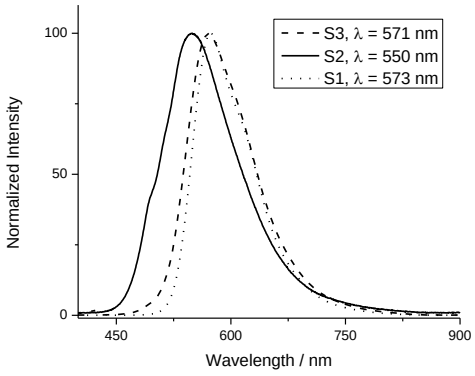


**Figure 2.7. Fluorescence spectra of P3HT samples (S1, S2 and S3) in chloroform**

Figure 2.7 shows the fluorescence spectra of the three samples S1, S2, and S3 in chloroform. The emission maximum of S1 and S3 was observed at 573 nm and 571 nm, respectively, while that of S2 appeared at 550

nm. With the appearance of side chain branches, the conjugation length of the polymer backbone varied, leading to a change in the absorption peak and, consequently, the emission spectrum as well.

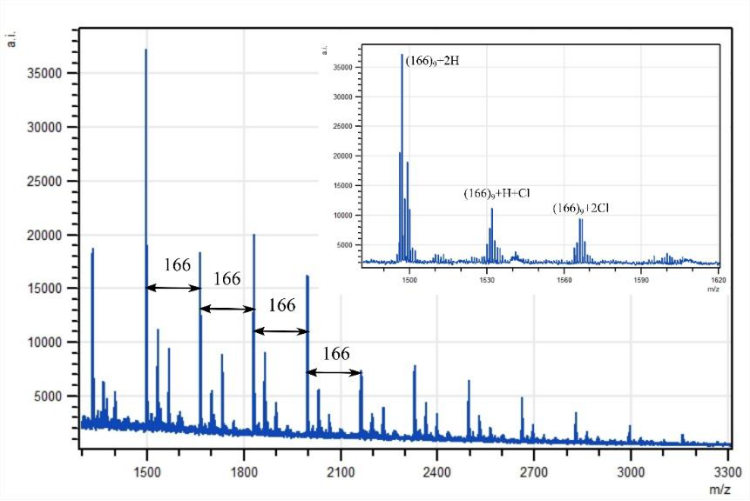


**Figure 2.8. MALDI TOF mass spectra of acetone-soluble fraction of P3HT (S1)**

Figure 2.8 shows the MALDI TOF mass spectra of the acetone-soluble fractions of the sample S1. The adjacent peaks differ in mass by one monomer unit,[36] and measuring the mass difference between the adjacent peaks in the same series gives the mass of the monomer unit.[37,38] The acetone-soluble fractions of S2 and S3 resulted in almost the same MALDI TOF mass spectra of S1. These MALDI TOF mass spectra of the P3HT samples S1, S2, and S3 show a mass difference of 166, which is consistent with the 3HT unit and shows common peaks such as [$166_m$ + 2H], [$166_m$ + H + Cl], and [$166_m$ + 2Cl]. These values are in agreement with those reported previously.[39] This implies that the terminal proton at the 5-position of the thiophene ring in the oligomer was replaced with the chlorine generated from $FeCl_3$.[40],[41] From the repeat unit mass of the 3HT monomer (m/z = 166) and the calculated m/z 1496.87, it was determined that the cluster peaks had a molecular weight of m = 9 (m: repeat unit number). Similarly, P3HT ions corresponding to [$166_m$ + H + Cl] and [$166_m$ + 2Cl] (with m = 9) result in mass-to-charge ratios of 1531.98 and 1565.98, respectively, agreeing well with the calculated m/z of 1531.93 and 1565.94.

**Table 2.5. Conductivity of P3HT (S1, S2, and S3) doped with Iodine**

| Samples | S1 | S2 | S3 |
|---|---|---|---|
| Conductivity (S/cm) | 0.9 | 0.09 | 0.6 |

As shown in Table 2.5, S1 and S3 show similar electrical conductivity (0.9 and 0.6 S/cm), but that of S2 (0.09 S/cm) is lower by about one order of magnitude. Previous works have demonstrated the effect of branched side chains on the physicochemical, photovoltaic, and conductivity properties of conjugated polymer [35,42-44]. The difference in conductivity between S1, S2, and S3 is influenced by the side reaction of 3HT at the 4-position (see the ratio of integral intensity of H from ($C_\beta$-H) and ($CH_3$) in Table 2.4), which could be related to the torsion angle between adjacent monomer units, resulting in steric hindrance on the π-π stacking of the conjugated polymer chain.

To ascertain whether $(NH_4)_2Ce(NO_3)_6$ can polymerize 3HT, a polymerization reaction with the $Ce^{4+}$/3HT ratio of 1:1 was conducted. However, no polymer product was obtained in this reaction. To identify the substance in the reaction mixture, it was concentrated and washed with deionized water and extracted with dichloromethane. Removal of the solvent gave a yellow oil. The yellow oil (called the extraction part) was analyzed by $^1$H NMR and direct infusion ESI-MS. The pure 3-hexylthiophene monomer was also analyzed by $^1$H NMR and direct infusion ESI-MS for comparison.

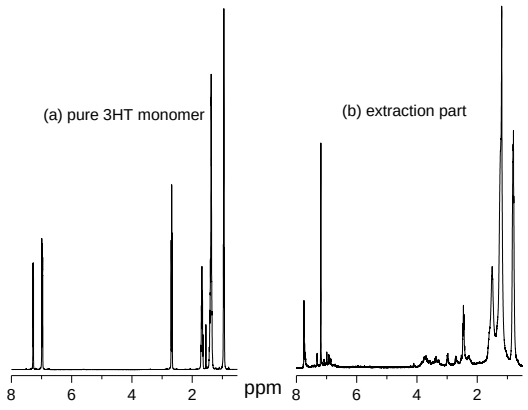


**Figure 2.9. $^{1}$H NMR of pure 3HT monomer (a) and extraction part (b).**

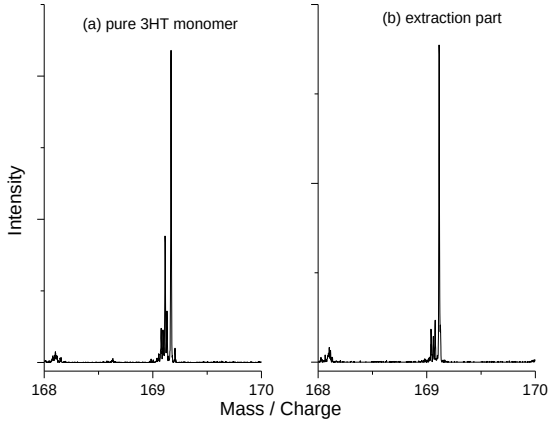


**Figure 2.10. ESI-MS spectra, acquired in positive ion mode, of pure 3HT monomer (a) and extraction part (b)**

As Fig. 2.9 shows, the extraction part includes only the 3HT monomer. Figure 2.10 shows the ESI-MS spectra, acquired in positive mode, of the extraction part (b), and (a) shows the pure 3HT monomer which revealed the same peaks at *m/z* 169.1142. These peaks correspond to $[M+H]^+$ of the 3HT monomer peak, consistent with the calculated 3HT monomer at the value of *m/z* 169.1045. These results imply that $(NH_4)_2Ce(NO_3)_6$ alone cannot polymerize 3HT, but it is adequate to oxidize $Fe^{2+}$ to $Fe^{3+}$.

## 2.4 Conclusions

In polymerizing 3HT using $FeCl_3$ as an oxidizing agent in hexane, it was proven that the yield of the polymer product was influenced when the ratio of $FeCl_3$ to 3HT was changed in the range of 1:1 to1:4. Various oxidative agents ($Cl_2$, BPO, $H_2O_2$, $ZrCl_4$, and $(NH_4)_2Ce(NO_3)_6$) were examined to find an effective oxidizing agent (for $Fe^{2+}$ to $Fe^{3+}$). $Ce^{4+}$ was the most effective oxidizer for the required reaction, though it is not strong enough to catalyze the chemical coupling oxidative polymerization of 3HT itself. As $Ce^{4+}$ induced a side reaction of 3HT at the 4-position, the structure and properties of P3HT were significantly affected. The side reaction of 3HT at the 4-position could result in steric effects due to the torsion angle of the adjacent monomer unit, which would influence the optical properties and the conductivity of P3HT.

## 2.5 References

(1) Hai, T. A. P.; Sugimoto, R. *J. Mol. Struct.* **2017**, *1146*, 660–668.

(2) Hirai, T.; Sato, M.; Kido, M.; Nagae, Y.; Kaetsu, K.; Kiyoshima, Y.; Fujii, S.; Ohishi, T.; White, K. L.; Higaki, Y.; Teraoka, Y.; Nishibori, M.; Kamitani, K.; Hanada, K.; Sugiyama, T.; Sugimoto, R.; Saigo, K.; Kojio, K.; Takahara, A. *J. Polym. Sci. Part A: Polym. Chem.* **2015**, *53*, 2075-2078.

(3) Lin, J. W.-P.; Dudek, L. P. *J. Polym. Sci. Pol. Chem.* **1980**, *18*, 2869–2873.

(4) Sugimoto, R.; Takeda, S.; Gu, H. B.; Yoshino, K. *Chem. Express* **1986**, *1*, 635-638.

(5) Yoshino, K.; Hayashi, S.; Sugimoto, R. *Jpn. J. Appl. Phys.* **1984**, *23*.

(6) Kovacic, P.; Jones, M. B. *Chem. Rev.* **1987**, *87*, 357-379.

(7) McClain, M. D.; Whittington, D. A.; Mitchell, D. J.; Curtis, M. D. *J. Am. Chem. Soc.* **1995**, *117*, 3887–3888.

(8) McCullough, R. D. *Adv. Mater.* **1998**, *10*, 93-116.

(9) Tsuchiya, K.; Ogino, K. *Polym. J.* **2013**, *45*, 281–286.

(10) Haba, O.; Hayakawa, T.; Ueda, M.; Kawaguchi, H.; Kawazoe, T. *React. Funct. Polym.* **1998**, *37*, 163-168.

(11) Pratt, C. M.; Foot, P. J. S.; Davis, R. *Polym. Polym. Compos.* **2016**, *24*, 185-190.

(12) Ricciotti, L.; Borbone, F.; Carella, A.; Centore, R.; Roviello, A.; Barra, M.; Roviello, G.; Ferone, C.; Minarini, C.; Morvillo, P. *J. Polym. Sci. Pol. Chem.* **2013**, *51*, 4351-4360.

(13) Jung, Y. J.; Lee, S. J.; Choi, S. W.; Kim, J. H. *J. Polym. Sci. Part A: Polym. Chem.* **2008**, *46*, 5968-5975.

(14) Laakso, J.; Jarvinen, H. *Synth. Met.* **1993**, *55*, 1204–1208.

(15) Wang, Y.; Lucht, B. L.; Euler, W. B. *Polymer Preprints* **2002**, *43*, 1160.
(16) Fukumoto, H.; Omori, Y.; Yamamoto, T. *Polym. J.* **2013**, *45*, 462-465.
(17) Amou, S.; Haba, O.; Shirato, K.; Hayakawa, T.; Ueda, M.; Takeuchi, K.; Asai, M. *J. Polym. Sci. Pol. Chem.* **1999**, *37*, 1943–1948.
(18) Niemi, V. M.; Knuuttila, P.; 0sterholm, J.-E.; Korvola, J. *Polym. Rep.* **1992**, *33*, 1559-1562.
(19) Sheina, E. E.; Liu, J.; Iovu, M. C.; Laird, D. W.; McCullough, R. D. *Macromolecules* **2004**, *37*, 3526-3528.
(20) Yokoyama, A.; Miyakoshi, R.; Yokozawa, T. *Macromolecules* **2004**, *37*, 1169-1171.
(21) Elsenbaumer, R. L.; Jen, K. Y.; Oboodi, R. *Synth. Met.* **1986**, *15*, 169-174.
(22) Hoggard, P. E.; Gruber, M.; Vogler, A. *Inorg. Chim. Acta* **2003**, *346*, 137-142.
(23) Barbarella, G.; Zambianchi, M.; Toro, R. D.; Martino Colonna, J.; Iarossi, D.; Goldoni, F.; Bongini, A. *J. Org. Chem.* **1996**, *61*, 8285-8292.
(24) Andersson, M. R.; Selse, D.; Berggren, M.; Jarvinen, H.; Hjertberg, T.; Inganas, O.; Wenerstrom, O.; Osterholm, J.-E. *Macromolecules* **1994**, *27*, 6503-6506.
(25) Liu, Y.; Nishiwaki, N.; Saigo, K.; Sugimoto, R. *Bull. Chem. Soc. Jpn.* **2013**, *86*, 1076-1078.
(26) Barbusiński, K. *Ecological Chemistry and Engineering s* **2009**, *16*, 347-358.
(27) Bar, W. G.; Baxenda, J. H.; E, P. G.; Hargra, K. R. *Trans. Faraday Soc.* **1951**, *47*, 462-500.
(28) Lee, J. M.; Lee, S. J.; Jung, Y. J.; Kim, J. H. *Curr. Appl. Phys.* **2008**, *8*, 659–663.
(29) Yuan, Y.; Zhang, J. M.; Sun, J. Q.; Hu, J.; Zhang, T. P.; Duan, Y. X. *Macromolecules* **2011**, *44*, 9341-9350.
(30) Brambilla, L.; Tommasini, M.; Botiz, I.; Rahimi, K.; Agumba, J. O.; Stingelin, N.; Zerbi, G. *Macromolecules* **2014**, *47*, 6730-6739.
(31) Sato, M. A.; Morii, H. *Macromolecules* **1991**, *24*, 1196-1200.
(32) Zhang, D.; Qina, J.; Xue, G. *Synth. Met.* **1999**, *100*, 285-289.
(33) Ong, C.; Bayley, P. M.; Winther-Jensen, O.; Winther-Jensen, B. *Polym. J.* **2013**, *45*, 391–395.
(34) Vezie, M. S.; Few, S.; Meager, I.; Pieridou, G.; Dörling, B.; Ashraf, R. S.; Goñi, A. R.; Bronstein, H.; McCulloch, I.; Hayes, S. C.; Campoy-Quiles, M.; Nelson, J. *Nat. Mater.* **2016**, 1-9.
(35) Cui, C.; Sun, Y.; Zhang, Z.; Zhang, M.; Zhang, J.; Li, Y. *Macromol. Chem. Phys.* **2012**, *213*, 2267−2274.
(36) Montaudo, G.; Samperi, F.; Montaudo, M. S. *Prog. Polym. Sci.* **2006**, *31*, 277–357.
(37) Sato, H.; Nakamura, S.; Teramoto, K.; Sato, T. *J. Am. Soc. Mass Spectrom.* **2014**, 1-10.
(38) Dopke, N. C.; Lovett, T. N. *J. Chem. Educ.* **2007**, *84*, 1968-1980.
(39) Liu, J.; Loewe, R. S.; McCullough, R. D. *Macromolecules* **1999**, *32*, 5777-5785.
(40) Liu, Y.; Nishiwaki, N.; Saigo, K.; Sugimoto, R. *Polym. Bull.* **2015**, *72*, 1817–1826.
(41) McCarley, T. D.; Noble, C. O.; IV; DuBois, C. J.; Jr.; McCarley, R. L. *Macromolecules* **2001**, *34*, 7999-8004.
(42) Chang, Y.; Mohanty, A. D.; Smedley, S. B.; Abu-Hakmeh, K.; Lee, Y. H.; Morgan, J. E.; Hickner, M. A.; Jang, S. S.; Ryu, C. Y.; Bae, C. *Macromolecules* **2015**, *48*, 7117-7126.
(43) Holliday, S.; Ashraf, R. S.; Wadsworth, A.; Baran, D.; Yousaf, S. A.; Nielsen, C. B.; Tan, C. H.; Dimitrov, S. D.; Shang, Z.; Gasparini, N.; Alamoudi, M.; Laquai, F.; Brabec, C. J.; Salleo, A.; Durrant, J. R.; McCulloch, I. *Nat. Commun.* **2016**, 1-11.
(44) Roncali, J.; Garreau, R.; Yassar, A.; Marque, P.; Gamier, F.; Lemaire, M. *J. Phys. Chem.* **1987**, *91*, 6706-6714.

# Chapter 3:

## Syntheses, characterizations and applications of conjugated polymers

### 3.1 Introduction:

In this chapter, we focus on the use of $FeCl_3$ oxidative polymerization to synthesize random copolymers based on 3-hexylthiophene and explore their applications. Because of their unique conjugated properties, polythiophene derivatives have attracted much attention the chemical and physical fields over the last quarter of a century. These polymers have been used in many attractive academic and industrial applications such as solar cells, molecular electronics, sensors and other applied electric devices [1-3]. Several studies on polythiophene have been carried, with focus on the molecular assembly properties of polythiophene [4], synthesis and characterization of poly(3-hexylthiophene) block polystyrene for photovoltaic applications [5], molecular structure of regio-regular oligo and poly(3-hexylthiophene) single crystals[6], crystallinity of poly(3-hexylthiophene) blocks with other polymers[7], and improvement of well-controlled poly(3-hexylthiophene) nanofibrils by ultrasound – assisted crystal segregation[8]. A diblock copolymer composed of poly(3-hexylthiophene) and poly(N,N-dimethylamino-2-ethylmethacrylate-random-2-hydroxyethyl methacrylate), synthesized via quasi-living Grignard metathesis (GRIM) polymerization were easily converted into ammphiphilic diblock copolymers[9]. A diblock copolymer of poly(3-hexylthiophene)-block-poly(dimethylsiloxane) was synthesized for use as a donor material for organic photovoltaic devices[10]. A facile synthetic route to well-defined poly(3-hexylthiophene)-block-poly(methylmethacrylate) copolymer was designed based on the anionic coupling reaction[11].

Polymers with a carbazole group were widely investigated owing to their special electronic properties such as high photoluminescence. A series of conjugated copolymers containing the carbazole group were applied to organic solar cells[12], enhancement of bright pure blue-violet light with a high quantum yield[13], recording media[14] and other interesting applications. This carbazole containing polymer was applied as a chemical sensor, as the nitrogen atom of the carbazole molecule has a lone pair of electrons [15-23]. Because of their remarkable characteristics, carbazole and its derivatives have attracted much attention for application in the construction of fluorescent sensors [17,18,20,22,24]. Moreover, polymers with a high carbazole content show high thermal stability [25-28]. The conjugated copolymer of thiophene and carbazole derivatives can be expected to have better properties for various applications. However, to date, there is no report on thiophene derivatives and carbazole molecule(s) built into a linear polymer main chain, and the structure of this copolymer is still unknown.

Polyfluorenes (PFs) are a vital class of conjugated polymers with unique properties such as emission in a wide variety of colors with high efficiency and low operating voltage [29], enhancement of OLED performance [30], high photoluminescence quantum efficiency and good thermal stability[31] [32]. Recently, much research has been conducted to modify the structure of PF by blending, grafting, or copolymerization in order to improve the performance of this polymer. Examples of such work include manipulation of aggregate/excimer formation in PF with different end groups through nickel-mediated polymerization [33], and control of the side chain structures during the solution-crystallization of PF derivatives [34]. The solubility of PF, which has a planar structure with a tendency of aggregate, could be improved by copolymerization with 3-hexylthiophene. Copolymers comprising thiophene and fluorene derivatives could allow for simple and effective tuning of the optical properties [35], which is important for their application in organic photovoltaics (OPVs) [36], and thus aid the formation of high-quality, freestanding films with tunable fluorescence properties [37]. In addition, a copolymer based on fluorene derivative and thiophene derivative has been developed to control and enhance the surface interactions in the active layer of OPVs, giving the favorable donor and acceptor properties of fluorene and thiophene, respectively [38].

Methods for synthesizing copolymers based on conjugated polymers were segregated into three distinct categories: cross-coupling polycondensation [36,39,40], oxidative polymerization [35,41,42] and electrical

methods [37,43,44]. Among these methods, oxidative polymerization, which was proposed three decades ago, is still being widely used on an industrial scale because it can be performed under mild reaction conditions[45].

In this chapter, we report the design of novel copolymer of 9-ethylcarbazole (9EC) and 3-hexylthiophene (3HT) (Scheme 3.1) (in the first part), and a copolymer of fluorene (F) and 3HT ( in the second part) (Scheme 3.5) through $FeCl_3$ oxidative copolymerization. The relationship between the structure and properties of these copolymers was also studied.

## 3.2 Experimental section

### *3.2.1 Materials and equipment*

#### *3.2.1.1 Materials*

3-Hexylthiophene, anhydrous $FeCl_3$, fluorene and 9-ethylcarbazole were purchased from Tokyo Chemical Industry Ltd and used without any further purification. Anthralin (Nacalai Tesque Inc Tokyo ) and Silvertrifluoro acetate (Wako pure chemical industries Ltd) were applied as the matrix and cation agent in the MALDI-TOF MS, respectively. Tri-n-butylborane (TBB) and tetra-n-butylammonium fluoride (TBAF) were from Nippon Aluminum Alkyls Ltd and Wako pure chemical industries Ltd, respectively. Rhodamine B (Wako Pure Chemical Industries Ltd) was used as the reference material for the relative quantum yield method.

#### *3.2.1.2 Equipment*

$FeCl_3$ was weighed in the UNICO UN 650 F mode box under an atmosphere of argon. $^1$H-NMR spectra (400MHz) was recorded in the Bruker Acsend 400 spectrometer. SEC was carried in a system equipped with a Jasco PU-2080 Plus pump, and Jasco RI-2031 plus intelligent RI detector. The molecular weight and molecular weight distribution of the polymers relative to polystyrene standard was analyzed by the Chrom NAV software. Chloroform served as the polymer solvent and eluent in an equilibrated system at 40$^o$C. Bruker autoflex speed-KE in a reflector mode was used to analyze MALDI-TOF MS. UV-vis absorbance spectra and Fluorescence emission spectra were measured at room temperature on a Jasco V-650 UV-vis spectrometer and Jasco spectrofluorometer FP-8300, respectively. Thermogravimetric (TG) analysis was carried out in air condition with flow rate of 100ml/min by using a Hitachi Thermal Analysis System STA 7200 RV.

### *3.2.2 Synthesis of copolymer of 3HT and 9EC*

#### *3.2.2.1 The effect of reaction conditions*

All polymerization reactions in this study were conducted in an oven-dried schlenk flask with stop cock under an atmosphere of argon. Polymerization was carried out at room temperature (25 $^o$C) according to the literature except for changing the reagent and the ratio[46]. $FeCl_3$ and chloroform were put into a schlenk flask and the mixture was performed ultrasonic treatment for 15 minutes. 9-ethylcarbazole (9EC) and 3-hexylthiophene (3HT) were dropped into a magnetically stirred suspension of $FeCl_3$ and the reaction mixture was stirred for 2 hours under an atmosphere of argon. The obtained copolymer was washed with methanol to remove the remaining $FeCl_3$ and then extracted in the order of acetone and chloroform by the soxhlet extractor. Copolymerization of 9EC and 3HT using hexane or nitrobenzene instead of chloroform was carried out in order to investigate the solvent effect of this polymerization. In order to further investigate the effect of the polymerization temperature and polymerization time, polymerization was conducted at 0$^o$C, 25$^o$C and 50$^o$C and reaction time was 2 hours, 12 hours and 24 hours respectively.

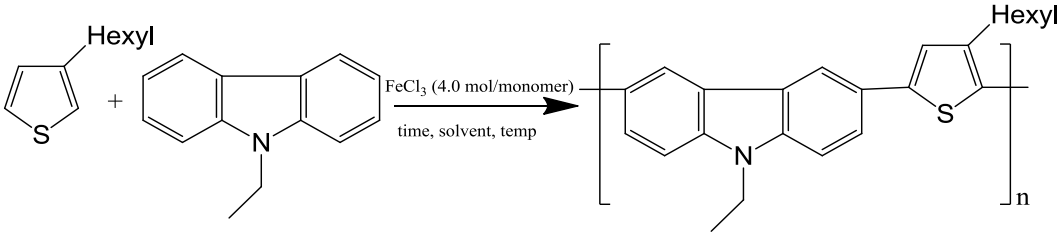


**Scheme 3.1: Synthetic scheme of 9-ethylcarbazole and 3-hexylthiophene copolymers**

### *3.2.2.2 Synthesis of complex of 3HT/9EC copolymer and tri-n-butylborane (TBB)*

THF solution of the 3HT/9EC copolymers (0.02 mmol as carbazole unit) and 0.1M THF solution of TBB (0.02 mmol) was mixed into a flask under atmosphere of argon and was stirred for 12 hours. Gummy complexes of 3HT/9EC copolymer and TBB were obtained after removal of solvent.

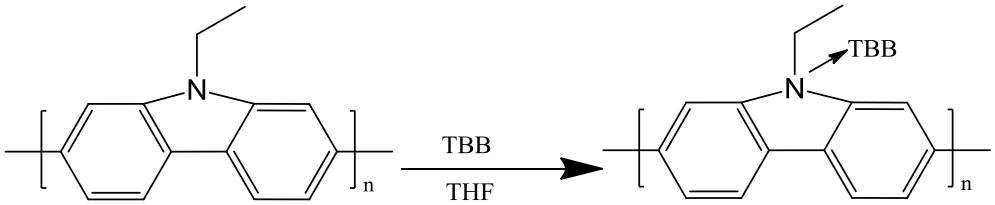


**Scheme 3.2: Synthetic scheme of complex of poly(9-ethylcarbazole) and TBB (Complex 1)**

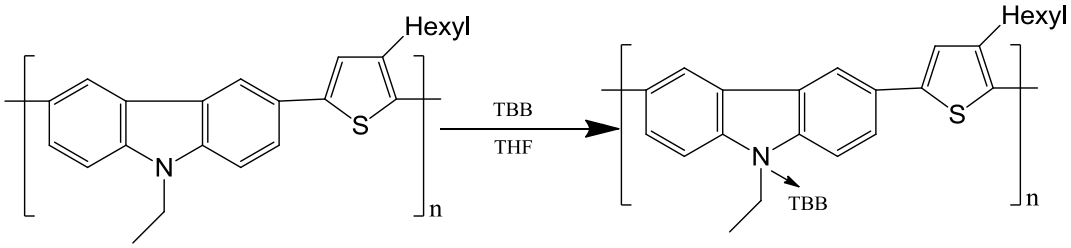


**Scheme 3.3: Synthetic scheme of complex of 3HT/9EC copolymer and TBB (Complex 2)**

There are two types of TBB complexes: Complex 1 is the complex of poly(9-ethylcarbazole) (P9EC) and TBB, and complex 2 is the complex of 3HT/9EC copolymer and TBB.

### *3.2.2.3 Fluorescence titration with Fluorine anion of TBB complexes*

THF solution (0.5mM) of complex 1 and complex 2 was prepared, then 3ml of these solution and 1 ml of various concentration of tetra-n-butylammonium fluoride (TBAF) solution (from 62.5 to 312.5 µM) were introduced in a quartz cells. The fluorescence spectra were recorded at room temperature.

### *3.2.3 Synthesis of copolymer of 3HT and F*

All reactions in this study were conducted in an oven-dried Schlenk flask with a stopcock, under argon atmosphere. $FeCl_3$ and $CHCl_3$ were placed in a Schlenk flask that was cooled to 0°C in an ice bath. 3-Hexyl thiophene and fluorene were dropped into a magnetically stirred suspension of $FeCl_3$, and the reaction mixture was stirred for 2 h under argon atmosphere. The obtained copolymer was washed with methanol to remove residual $FeCl_3$, and then extracted with acetone and chloroform by the Soxhlet extractor. The integrated fluorescence intensity was calculated by the Spectra Analysis software.

## 3.3 Results and discussion

### *3.3.1 Copolymer of 3HT and 9EC*

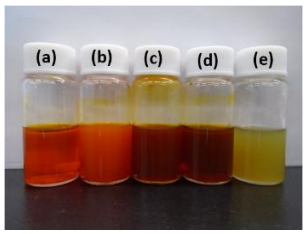


**Figure 3.1. Images of polymer samples with different mol ratio dissolved in THF: (a) P3HT, (b) 3HT/9EC (50/50), (c) 3HT/9EC (40/60), (d) 3HT/9EC (33/67) and (e) P9EC (Table 3.4, entries 1-5)**

*3.3.1.1 The effect of solvent on the 3HT/9EC copolymerization*

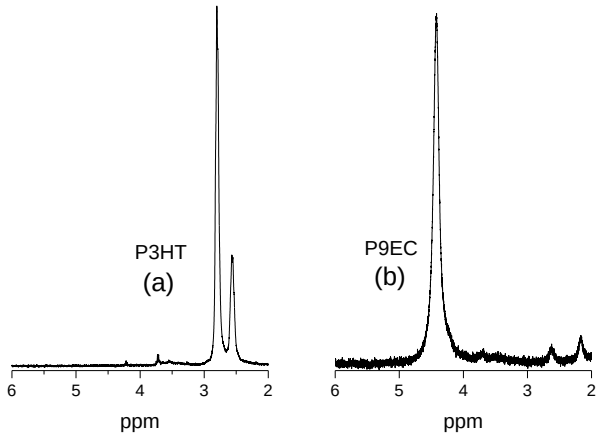


**Figure 3.2. $^1$H NMR spectra of P3HT (a) and P9EC (b)**

Copolymerization of 9EC and 3HT with the monomer ratio 50:50 was carried out in the presence of 4 mol equivalent of ferric chloride as oxidant under nitrogen atmosphere for 2 hours at 25$^o$C according to Scheme 3.1, and results of copolymerization in different solvents (hexane, chloroform, and nitro benzene) were summarized in the Table 3.1 and Figure 3.3. As shown in Table 3.1, the copolymerization in hexane solvent give the highest yield with 38% while the yield in chloroform and nitrobenzene are 26% and 17%, respectively. Figure 3.3 shows $^1$H-NMR spectra of resulting polymers of copolymerization in various solvents (hexane, chloroform, and nitro benzene). Two signal groups at $\delta$ = 4.0 – 5.0 ppm region and $\delta$ = 2.0 – 3.0 ppm region are clearly observed in the polymer produced in hexane. These peaks at $\delta$ = 2.0 – 3.0 ppm region (Figure 3.2a and Figure 3.3a) corresponded to the α-methylene protons in the poly(3-hexylthiophene) (P3HT) and the signal at $\delta$ = 4.0 – 5.0 ppm (Figure 3.2b and Figure 3.3a) was assigned to the ethylene group of poly(9-ethylcarbazole) (P9EC) respectively. The carbazole content in copolymer can be calculated because the ratio between integration of two peak areas indicated the mol ratio of 3HT and 9EC. As summarized in Table 3.1, the copolymer obtained in hexane solution, was included about 30% of the carbazole. In contrast, the copolymer obtained in other solvent, carbazole content in copolymer was very low (0% in chloroform and 5% in nitrobenzene). The result indicates that solvent has remarkably influenced the copolymerization. It can be explained that the $FeCl_3$ must be solid state to be active as an oxidant in copolymerization [47], and in this case $FeCl_3$ does not dissolve in hexane, while it can partly dissolve in chloroform and completely dissolve in nitrobenzene.

**Table 3.1: The effect of solvents on the 3HT/9EC (50/50) copolymerization (Reaction time 2 hours, 25$^o$C)**

| Entry | Solvent | Yield of copolymer (wt./wt.%) | Carbazole content in copolymer(%) (**) | Molecular weight of copolymer(*) $M_n$ | $M_w$ | PDI |
|---|---|---|---|---|---|---|
| 1 | $C_6H_{14}$ | 38 | 30 | 10100 | 29800 | 2.9 |
| 2 | $CHCl_3$ | 26 | 0 | 35000 | 126000 | 3.6 |
| 3 | $C_6H_5NO_2$ | 17 | 5 | 10800 | 17500 | 1.6 |

(*) determined by GPC, (**) determined by $^1$H-NMR

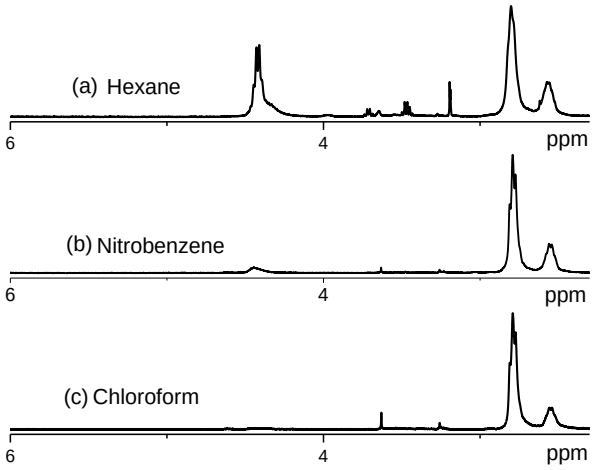


**Figure 3.3: $^{1}$H NMR spectra of 3HT/9EC (50/50) copolymer in different solvents: (a) Hexane, (b) Nitrobenzene and (c) Chloroform**

*3.3.1.2 The effect of temperature and reaction time on the 3HT/9EC copolymerization*

Copolymerization of 9EC and 3HT with the monomer ratio 50:50 was carried out in hexane with the presence of 4 mol equivalent of ferric chloride as an oxidant under nitrogen atmosphere for 2 hours by three different temperatures (0ºC, 25ºC and 50ºC) according to Scheme 3.1 and results of copolymerization were summarized in Table 3.2 and Figure 3.4. As shown in the Table 3.2, yields of copolymer were 36% at 25ºC and 30% at 50ºC, respectively. In addition, the carbazole content reached a high percent (30%) at room temperature (25ºC) and a lower percentage with 19% at 50ºC. In contrast, at the lowest temperature (0ºC) no polymerization product was obtained. These results revealed that incorporation of carbazole unit in copolymer is favored by a room temperature, it maybe form a stable aggregates by through self-assembly [48] to form aggregates between carbazole and thiophene during the copolymerization at room temperature.

**Table 3.2: The effect of temperature on the 3HT/9EC (50/50) copolymerization (Hexane solvent, reaction time: 2 hours)**

| Entry | TempºC | Yield of copolymer (wt./wt.%) | Carbazole content in copolymer(%) (**) | Molecular weight of copolymer(*) $M_n$ | $M_w$ | PDI |
|---|---|---|---|---|---|---|
| 1 | 0 | 0 | 0 | - | - | - |
| 2 | 25 | 36 | 30 | 10100 | 29800 | 2.9 |
| 3 | 50 | 30 | 19 | 66100 | 110000 | 1.6 |

(*) determined by GPC, (**) determined by $^{1}$H-NMR

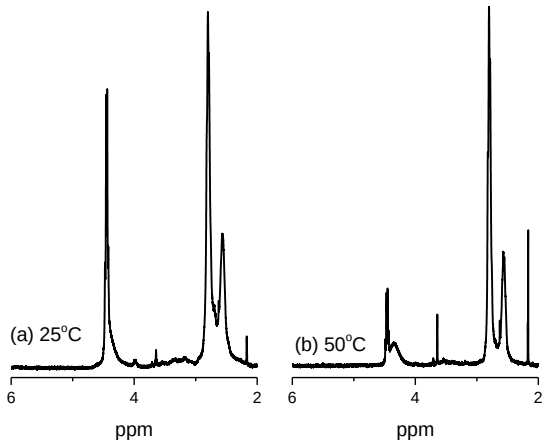


**Figure 3.4: $^1$H NMR spectra of 3HT/9EC (50/50) copolymer at different temperature: (a) 25°C and (b) 50°C**

The provided Table 3.3 compares the difference of yield as changing reaction time. The more reaction time is, the more yield of the product is. In this case, the highest yield (50%) was obtained by 24 hours, although the carbazole content in copolymer remained unchanged.

**Table 3.3: The effect of reaction time on the 3HT/9EC (50/50) copolymerization (Hexane solvent, 25°C)**

| Entry | Time (h) | Yield of copolymer (wt./wt.%) | Carbazole content in copolymer(%) (**) | Molecular weight of copolymer(*) $M_n$ | $M_w$ | PDI |
|---|---|---|---|---|---|---|
| 1 | 2 | 36 | 30 | 11500 | 30500 | 2.6 |
| 2 | 12 | 41 | 30 | 10100 | 29800 | 2.9 |
| 3 | 24 | 50 | 30 | 12300 | 32300 | 2.6 |

(*) determined by GPC, (**) determined by $^1$H-NMR

*3.3.1.3 The effect of the ratio of 3HT and 9EC on copolymerization*

Copolymerization of 3HT and 9EC with the different monomer ratio (by changing the 3HT/9EC molar ratio from 100/0 to 0/100) was carried out in the presence of 4 mol equivalent of ferric chloride as an oxidant under nitrogen atmosphere in hexane solvent at 25°C for 24 hours according to Scheme 3.1, and results were summarized in the Table 3.4 and Figure 3.5. 3-Hexylthiophene homopolymer (P3HT) has the highest molecular weight while each molecular weight of these copolymers decreased as the increase of 9EC in copolymer. The Figure 3.1 indicated the color of the solution of different 3HT/9EC copolymers depend on the 9EC content in copolymer. The ratio between integration of two peak areas was indicated to be mol ratio of 3-hexylthiophene and 9-ethylcarbazole and 9EC content of copolymer was calculated. As a result, the ratio contents of the copolymers with different monomer proportion (3HT/9EC from 100/0 to 0/100 in Table 3.4) were estimated from the region scale of peaks in two ranges. As the Figure 3.5 and Table 3.4 shown, content of 9EC in copolymer was obviously dependent on the ratio of 9EC and reached the highest value (47%) when 9EC molar ratio in feed was 60.

**Table 3.4: Polymerization results of 3HT and 9EC with different molar ratio (Hexane solvent, reaction time 24 hours, 25ºC)**

| Entry | 3HT/9EC molar ratio in feed | Yield of copolymer (wt./wt.%) | Carbazole content in copolymer(%) (**) | Molecular weight of copolymer(*) $M_n$ | $M_w$ | PDI |
|---|---|---|---|---|---|---|
| 1 | 100/0 | 61 | 0 | 50000 | 160000 | 3.2 |
| 2 | 50/50 | 50 | 30 | 12300 | 32300 | 2.6 |
| 3 | 40/60 | 42 | 47 | 3500 | 3900 | 1.1 |
| 4 | 33/67 | 46 | 38 | 3300 | 3500 | 1.1 |
| 5 | 0/100 | 70 | 100 | 2200 | 2400 | 1.1 |

(*) determined by GPC, (**) determined by $^1$H-NMR

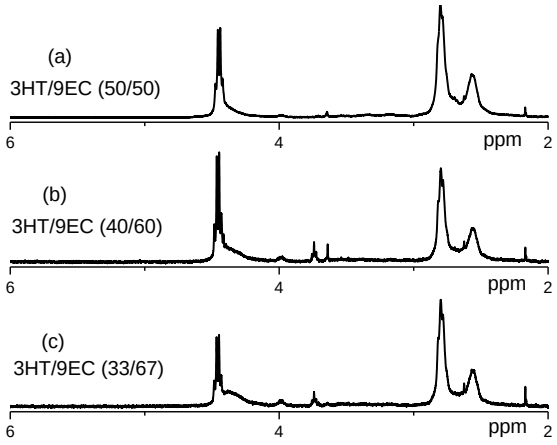


**Figure 3.5: $^1$H NMR spectra of 3HT/9EC copolymer at different molar ratio in feed.**

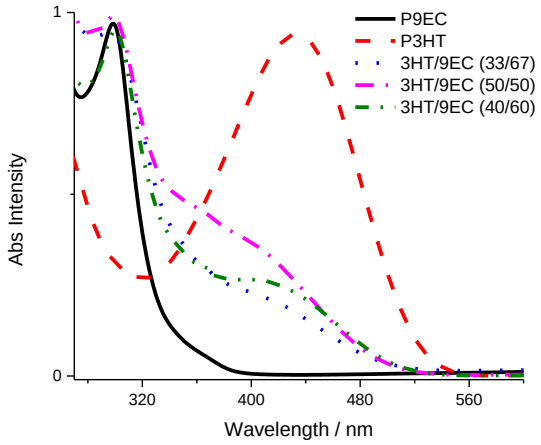


**Figure 3.6. UV-vis spectra of homopolymers and copolymers in THF at room temperature.**

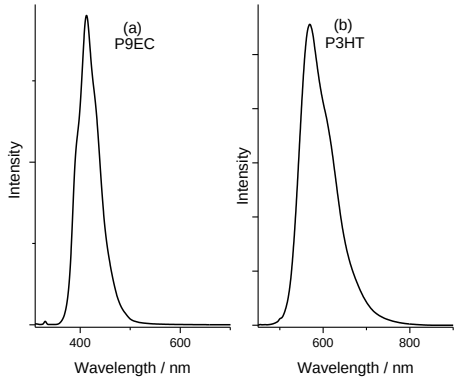


**Figure 3.7. Fluorescence spectroscopy of (a) P9EC and (b) P3HT (Table 3.4, entry 1 and 5)**

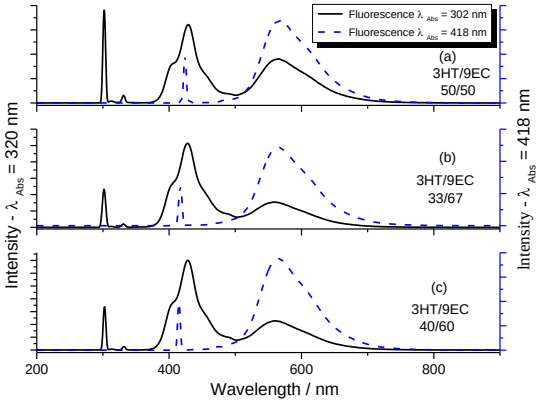


**Figure 3.8. Fluorescence spectroscopy of (a) 3HT/9EC (50/50) and (b) 3HT/9EC (33/67) and (c) 3HT/9EC (40/60) (Table 3.4, entries 2-4)**

Figure 3.6 shows UV-vis spectra of P3HT, P9EC and 3HT/9EC copolymers in THF at room temperature. P3HT (Table 3.4, entry 1) and P9EC (Table 3.4, entry 5) shows the simple UV-vis peak at 440 nm and 302 nm respectively, while other copolymers (Table 3.4, entry 2 to entry 4) shows multiple obvious peaks in a range of 302 nm and 418 nm. In 3HT/9EC copolymers, the UV-vis peak at 302 nm was not changed, but the peak at 440nm shifted slightly to the shorter wavelength side (from 440nm to 418 nm). The emission fluorescence spectra of homopolymers and copolymers in THF solution at room temperature are shown in Figure 3.7 and 3.8 for comparison. P3HT (Table 3.4, entry 1) and P9EC (Table 3.4, entry 5) shows only one emission peak at 424 nm and 580 nm respectively (Figure 3.7), while other copolymers show two different emission regions by two different wavelengths. For instance, in case of 3HT/9EC (50/50) (Table 3.4, entry 2) there are two emission peaks in a range of 400-600 nm at $\lambda_{excitation}$ = 302 nm and one emission peak in a range of 500-700 nm at $\lambda_{exitation}$ = 418 nm (Figure 3.8a).

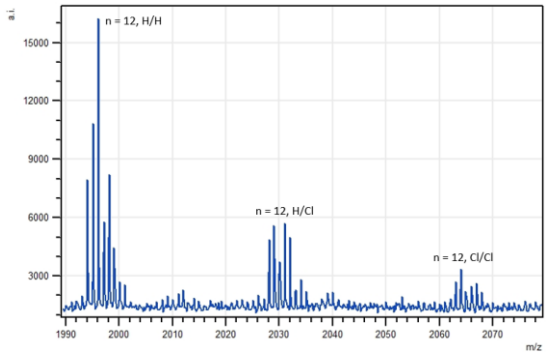


**Figure 3.9. MALDI TOF MS of P3HT (Table 4, entry 1)**

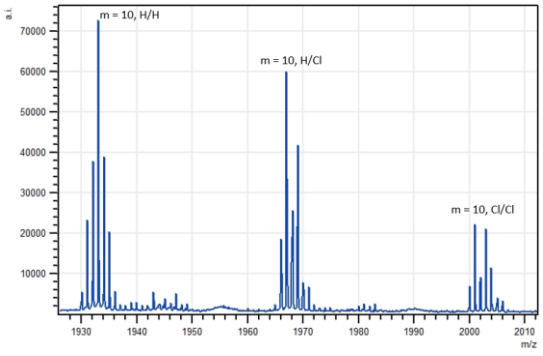


**Figure 3.10. MALDI TOF MS of P9EC (Table 4, entry 5)**

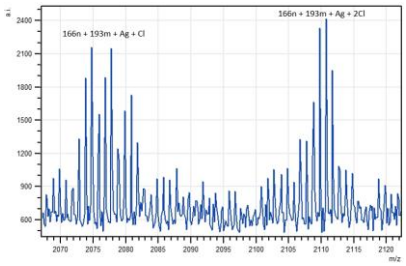


**Figure 3.11. MALDI TOF MS of 3HT/9EC (50/50) copolymer (Table 3.4, entry 2)**

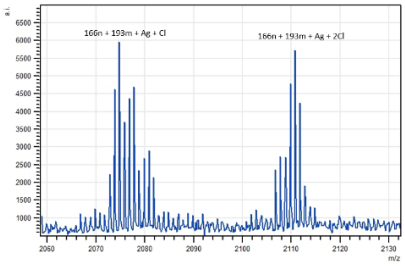


**Figure 3.12. MALDI TOF MS of 3HT/9EC (40/60) copolymer (Table 3.4, entry 3)**

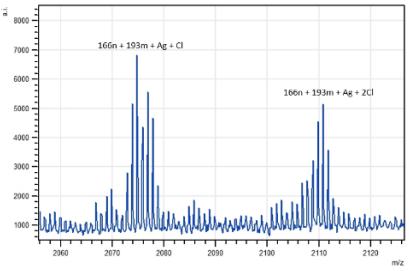


**Figure 3.13. MALDI TOF MS of 3HT/9EC (33/67) copolymer (Table 3.4, entry 4)**

To confirm that both 3-hexylthiophene and 9-ethylcarbazole monomer units were incorporated into the resultant polymer main chain, acetone-soluble copolymers and homopolymers were analyzed by MALDI-TOF MS (matrix-assisted laser desorption/ionization mass).

In general, the MALDI-TOF MS of P3HT shows common peaks such as [$166_n$ + H], [$166_n$ + Cl] and [$166_n$ + 2Cl] (Figure 3.9). And that of poly 9-ethylcarbazole shows similar peaks such as [$193_m$ + H], [$193_m$ + Cl] and [$193_m$ + 2Cl] (Figure 3.10). In contrast, since both 3-hexylthiophene unit and 9-ethylcarbazole unit were included in the copolymers, a variety of different peaks appeared in the MALDI-TOF MS (Figures 3.11, 3.12 and 3.13). In Figures 3.11, 3.12 and 3.13, n of (m+n) is thiophene units and m of (m+n) is carbazole units, respectively. By matching one of the peak patterns of Figure 3.11, 3.12 and 3.13 to the calculated isotopic distributions of these ions, each peak was identified obviously. For instance, the peak pattern of (m+n=11) in Figure 3.11 (3HT/9EC (50/50) Table 3.4, entry 2) was identified as the peak [$166_n$ + $193_m$ + Ag + Cl]. This indicates that 3HT/9EC copolymer included both 3-hexylthiophene and 9-ethylcarbazole monomer units. Similarly, each MALDI-TOF mass spectra of other samples (3HT/9EC (40/60) - Table 3.4, entry 3 and 3HT/9EC (33/67) - Table 3.4, entry 4) shows well-defined peaks clusters (Figure 3.12 and 3.13) proven that copolymers of 3-hexylthiophene and 9-ethyl carbazole in other ratio ( 3HT/9EC (40/60) and 3HT/9EC (33/67) ) were also prepared smoothly. However, each mixing ratio of 3-hexylthiophene and 9-ethylcarbazole unit in those copolymers was varied according to carbazole amount in copolymer. In the case of 3HT/9EC (50/50) sample copolymer (in the Figure 3.11, entry 2), its peak cluster showed m+n=11 at 2079.80 m/z. Considering the fact that the copolymer contains 30% carbazole, it is concluded that n=7, m=4.

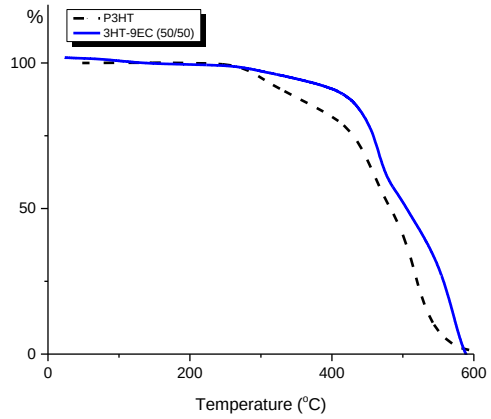


**Figure 3.14. The comparison of TG of P3HT and 3HT/9EC (50/50) copolymer**

To study the effect of carbazole on the thermal property of copolymer, thermogravimetric (TG) analysis was performed. As the Figure 3.14 shown, the weight loss of the poly 3-hexyl thiophene undergoes thermal degradation beginning at 350ºC, but the 3HT/9EC (50/50) copolymer undergoes thermal degradation beginning at 437ºC. These results revealed that the presence of 9-ethylcarbazole in polymer main chain significantly improved the thermal stability of copolymer.

### *3.3.1.4 Synthesis of complex of 3HT/9EC copolymers and tri-n-butylborane (TBB)*

Complex 1 and complex 2 were synthesized according to Schemes 3.2 and 3.3. $^{11}$B NMR spectrum of TBB was shown in Figure 3.15a with one peak at δ = 80.0 – 90.0 ppm region, and $^{11}$B NMR spectra of complex 1 and 2 were shown in Figure 3.15b, and the main peak shift to upper field region at δ = 0.0 – 40.0 ppm. However, in case of the mixture of P3HT and TBB, the peak of $^{11}$B NMR spectra of the mixture did not shift, that mean P3HT and TBB does not form a complex. The absorbance and emission wavelength of UV-vis and Fluorescence spectrum of complexes 1 and 2 shows same absorbance and emission wavelength of 3HT/9EC copolymers in the absence of TBB.

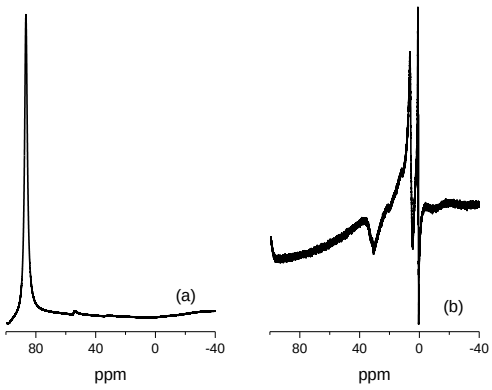


**Figure 3.15. $^{11}$B NMR spectra of TBB (a) and the complexes (complex 1 and 2) (b)**

### *3.3.1.5 Detecting of fluorine anions*

Fluorine anions (from tetra-n-butyl ammonium fluoride (TBAF)) in various concentrations (from 62.5 µM to 312.5 µM) were injected to the THF solution of complexes of 3HT/9EC copolymer and TBB, then fluorescence response of these samples were measured fluorometer. The results are shown in Figure 3.16. According to this Figure, in three cases (b), (c) and (d) (polymers including 9EC unit), the fluorescence intensity decreases gradually with increasing concentrations of fluorine anion. But in case of (a) (P3HT and TBB), any spectra change was not observed. And it means the complex of P3HT/TBB is not formed. This

phenomenon is known as the formation of new complex caused by the reaction between TBB and TBAF[15] (Scheme 3.4). In addition, different 9EC amounts also effect on the slope of the plot of $F_0/F$ as a function of the $F^-$ anion concentrations (Figure 3.17). That is, complex of 3HT/9EC copolymer is usable as the fluorine anion detectable material.

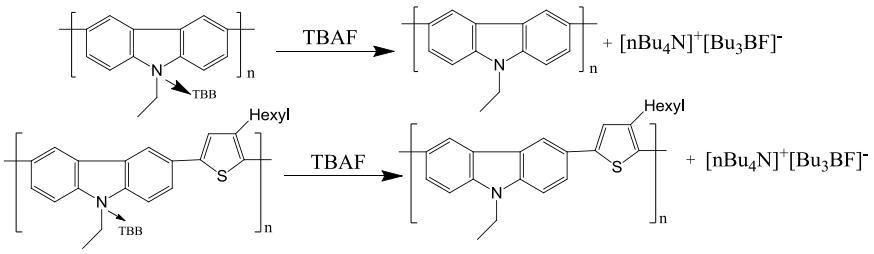


**Scheme 3.4. Reaction between TBAF and complex 1 or complex 2**

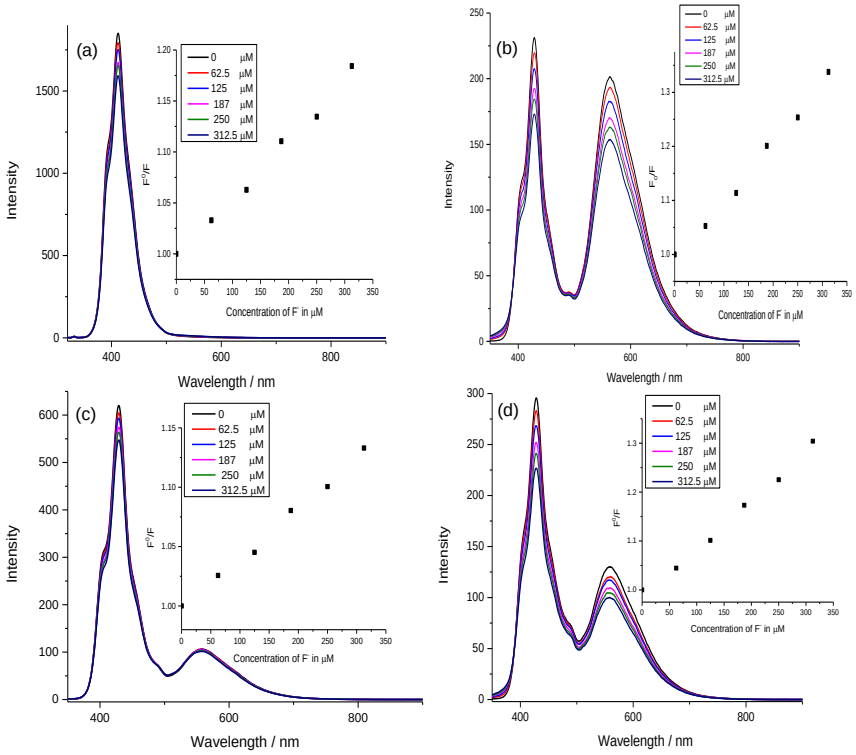


**Figure 3.16. Fluorescence response of complex of TBB and (a) P3HT homopolymer, (b)3HT/9EC (50/50) copolymer, (c) 3HT/9EC (40/60) copolymer, (d) 3HT/9EC (33/67) copolymer at varied concentration of $F^-$ anion in solution from 0 – 350 µM (excitation wavelength of 302 nm) and a plot of $F_0/F$ as a function of the $F^-$ anion concentrations**

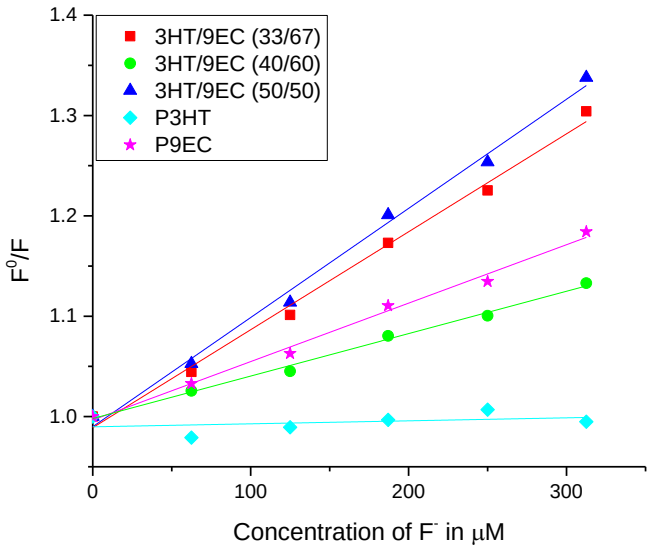


**Figure 3.17. Comparison plot of $F_0/F$ as a function of the $F^-$ anion concentrations with different complexes**

### *3.3.2 Copolymer of 3HT and F*

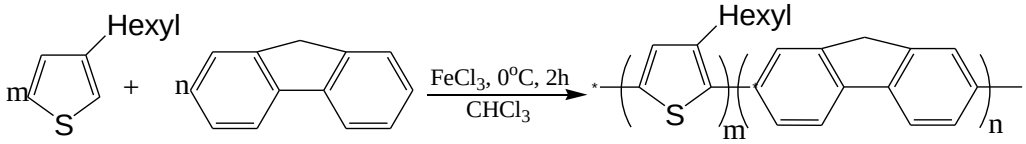


**Scheme 3.5: Synthesis of 3-hexylthiophene and fluorene copolymers.**

The polymerization of 3-hexylthiophene (3HT) and fluorene (F) was carried out at 0°C in the presence of 4 mol equivalent of $FeCl_3$ as the oxidant under nitrogen atmosphere in chloroform, and the results are summarized in Table 3.5. All the obtained 3-hexylthiophene and fluorene homopolymers and copolymers were soluble in chloroform. While poly(3-hexylthiophene) (P3HT) had the highest molecular weight, polyfluorene (PF) had the lowest molecular weight. From the results, it may be seen that with an increase in the fluorene monomer content, the molecular weight of the copolymer decreased. In addition, it can be seen that oxidation of fluorene is more difficult than that of 3-hexylthiophene. In detail, the oxidation potential of 3-hexylthiophene is around 1.32 V while that of fluorene is about 1.61 V[37]. These values indicated that oxidative polymerization of F is more difficult than that of 3HT. In fact, as the shown in the Table 3.5, the $M_w$ of P3HT (162 kDa) is higher than that of PF (1300). Additionally, the small difference between the oxidation potentials of thiophene and fluorene implied that the two monomers could be easily oxidized by the oxidative polymerization method. When the feed ratio of 3HT/F was varied, for example, in the case of 3HT/F (35/65), the oxidation potential of the copolymer could be lower than that of PF; thus, the copolymer 3HT/F (35/65) was easily oxidized, and the obtained copolymer had a higher molecule weight than PF. As shown in the Table 3.5, with the increase in 3HT concentration, the oxidation potential decreased, proving that both the 3HT and F monomers were simultaneously oxidized in the copolymer chain.

**Table 3.5: Polymerization results for 3HT and fluorene**

| Entry | 3HT/F molar ratio in feed | Yield of copolymer (wt/wt%) | Fluorene content in copolymer(%) (**) | Molecular weight of copolymer(*) $M_n$ | $M_w$ | PDI |
|---|---|---|---|---|---|---|
| 1 | 100/0 | 51 | 0 | 40200 | 162000 | 4.0 |
| 2 | 75/25 | 43 | 22 | 7600 | 29200 | 3.8 |
| 3 | 65/35 | 65 | 31 | 6400 | 22700 | 3.5 |
| 4 | 50/50 | 54 | 50 | 3800 | 12700 | 3.3 |
| 5 | 35/65 | 55 | 63 | 2600 | 5600 | 2.1 |
| 6 | 25/75 | 59 | 71 | 1600 | 2800 | 1.7 |
| 7 | 0/100 | 42 | 100 | 980 | 1300 | 1.3 |

Abbreviations: 3HT: 3-hexylthiophene; F: fluorene; PDI: polydispersity index

(*) Determined by GPC

(**) Determined by 1H NMR

A representative IR spectrum of the copolymer 3HT/F (50/50) is shown in Fig. 3.18. The weak peak in the range 3000 to 3050 $cm^{-1}$ is due to aromatic C-H stretching vibrations. The two peaks at 3000-2800 $cm^{-1}$ are characteristic of the hexyl group of 3HT. The relative intensity at 1500, 1450 $cm^{-1}$ originates from the stretching modes of C=C and C-C and should be attributed to the aromatic ring of fluorene and thiophene. The sharp peak at 980 $cm^{-1}$ belongs to the C-S-C stretching modes. These results indicate that both fluorene and 3-hexylthiophene units are present in the copolymer. Additionally, the absorbance of the peaks at 1500-1450 $cm^{-1}$ gradually becomes stronger with an increase in the fluorene content from 25 to 100 (Figure 3.19).

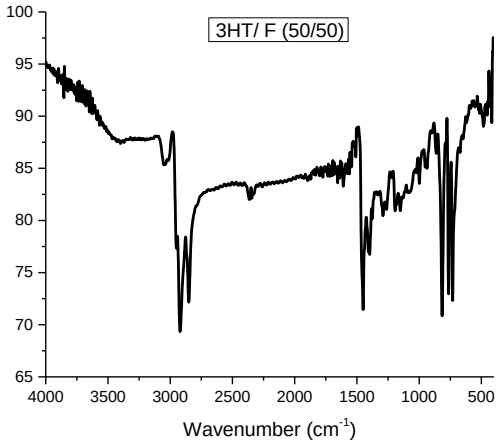


**Figure 3.18. IR spectrum of copolymer 3HT/F (50/50)**

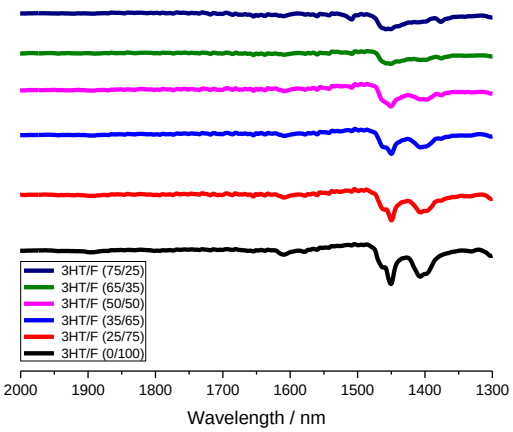


**Figure 3.19: IR spectra of polyfluorene and copolymers of fluorene.**

Although fluorene and PF have many advantageous properties such as high fluorescence quantum yield and high hole mobility, fluorene can be easily oxidized into fluorenone, and this may have a negative impact on the original properties of fluorene. Additionally, the carbonyl group is a characteristic of fluorenone. Thus, to identify the presence of fluorenone in PF and copolymers, IR spectra of those samples were measured to ensure that the fluorene (co)polymer was not oxidized. Normally, peaks at around 1700 $cm^{-1}$ are attributed to C=O groups. As shown in Fig. 3.19, no carbonyl group was observed in any of the (co)polymer samples, which confirmed that only PF and fluorene (co)polymers were formed.

Fig. 3.20 shows the $^{1}$H NMR spectra of the obtained P3HT (Table 3.5, entry 1), PF (Table 3.5, entry 7) homopolymer, and copolymer 3HT/F (50/50) (Table 3.5, entry 4). The $^{1}$H NMR spectrum of the copolymer of 3-hexylthiophene and fluorene is characterized by two signals corresponding to the α-methylene protons and the methylene group. The peaks in the δ 2.3–3.0 ppm region (Fig. 3.20 (b)) correspond to the α-methylene protons in P3HT, and the signal at δ 3.8–4.2 ppm (Fig. 3.20 (a)) is assigned to the methylene group of polyfluorene. In addition, the $^{1}$H NMR spectrum of copolymer 3HT/F (50/50) reveals two signal groups at δ 2.3–3.0 ppm and δ 3.8–4.2 ppm (Fig. 3.20 (c)). These signals should be assigned to the α-methylene of the 3-hexyl thiophene units and the methylene group of the fluorene units, which means that 3-hexylthiophene and fluorene are copolymerized. Based on a comparison of the peak area of the α-methylene protons (δ = 2.3–3.0 ppm) on P3HT and F units with the methylene proton peak (δ = 3.8–4.2 ppm), the ratio of PF to P3HT units on the copolymers can be calculated; the results are shown in Table 3.5. As a result, the actual fluorene content in the copolymers with different fluorene monomer proportions (from 0 to 100) can be estimated from the region scale of the peaks in two ranges (at (δ = 2.3–3.0 ppm) and (δ = 3.8–4.2 ppm), respectively). In detail, the number of the actual fluorene content was calculated by dividing the peak area at (δ = 3.8–4.2 ppm) by the sum of two peaks areas at (δ = 2.3–3.0 ppm) and (δ = 3.8–4.2 ppm). Although the actual fluorene content is slightly lower than the feed fluorene content for all copolymers, it is still proportional to feed fluorene content. For instance, as shown in the Table 3.5, fluorene content is 22 when the fluorene feed content is 25, and this number reaches 71 at the fluorene feed content of 75.

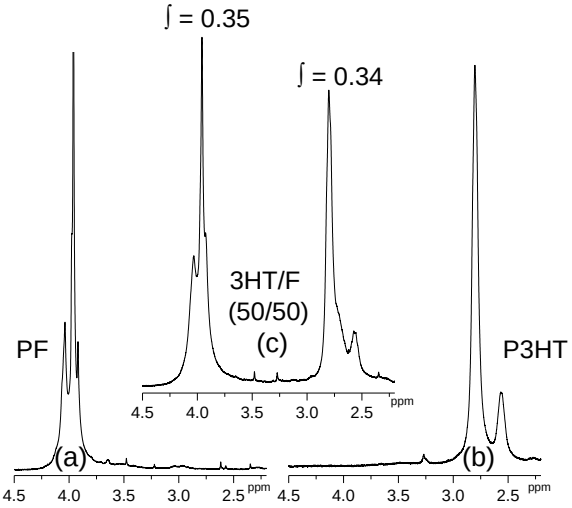


**Figure 3.20. $^{1}$H NMR spectra of PF (a), P3HT (b), and copolymer 3HT/F (50/50) (c) in $CDCl_3$ at room temperature.**

The $^{1}$H-NMR spectra of remain copolymers are similar to that of 3HT/F (50/50) copolymer, except the fluorene content depend on fluorene feeding (illustrated in supporting information).
To confirm that both 3-hexylthiophene and fluorene monomer units were included in the copolymers, acetone-soluble oligomers in copolymers and homopolymers were analyzed by MALDI-TOF MS (matrix-assisted laser desorption/ionization mass).

P3HT shows a typical MALDI-TOF MS spectrum, as illustrated in Fig.2 (a), in Supporting Information (SI). Adjacent peaks differ in mass by one unit monomer, [49] and measuring the mass difference between adjacent peaks of the same series gives the mass of the monomer unit [50]. In this case of P3HT, the obtained mass difference is 166, which is consistent with the 3-hexylthiophene unit. In general, the MALDI-TOF spectrum of P3HT shows common peaks such as [$166_m$ + H], [$166_m$ + H + Cl], and [$166_m$ + 2H]. This implies that the terminal proton at the 4-position of the thiophene ring in the oligomer was replaced with the chlorine generated from $FeCl_3$ [51]. In Fig. 2 (a) in SI, the cluster peaks of 3HT are clearly identified, for instance, from the repeat unit mass of 3HT monomer (m/z = 166), and the calculated m/z 1670.55, it was found that this cluster peak

has a molecular weight of m = 10 (m: repeat unit number). Similarly, repeat unit numbers for other cluster peaks were calculated. In the case of PF, the observed mass difference was 164, which was consistent with the fluorene unit (Fig. 2 (b), Supporting Information). Based on the mass of the monomer unit, the value of the repeat units for each cluster peak was calculated. Thus, a variety of peaks such as [$164_n$ + 2H] and [$164_n$ + Ag] (with n = 10 and 11) are seen in a typical MALDI-TOF mass spectrum of PF. Fig. 3.21 reveals the mass spectrum of 3HT/F (50/50) with multiple cluster peaks. These peaks dispense primarily in the mass range 1100 to 1700 m/z. Because of the equivalent in the mass values of the 3HT and F monomer units (166 and 164, respectively), the MALDI-TOF mass spectrum of the 3HT/F (50/50) copolymer is similar to the spectra of P3HT and PF. Thus, to identify the distribution of the copolymer compositions, the peak pattern (1491.734 m/z) at m + n = 9 was zoomed in and matched to the calculated compass isotope pattern (Fig. 4). The isotope pattern peak of [$166_7$ + $164_2$] at *m/z* 1491.704 is close to the peak of [$166_m$ + $164_n$] at *m/z* 1491.734 that assumed m=7 and n=2 (m and n denote the thiophene and fluorene units, respectively). This indicates that the copolymer of 3-hexylthiophene and fluorene included both the 3-hexylthiophene and fluorene monomer units.

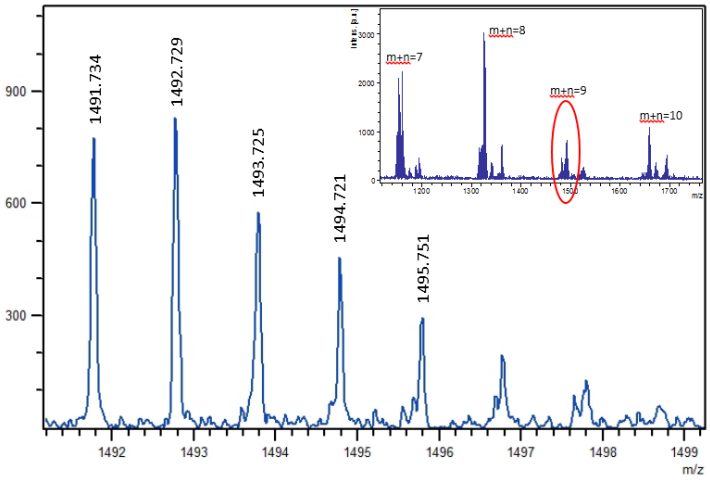


**Figure 3.21: MALDI-TOF MS spectra of 3HT/F (50/50) oligomer.**

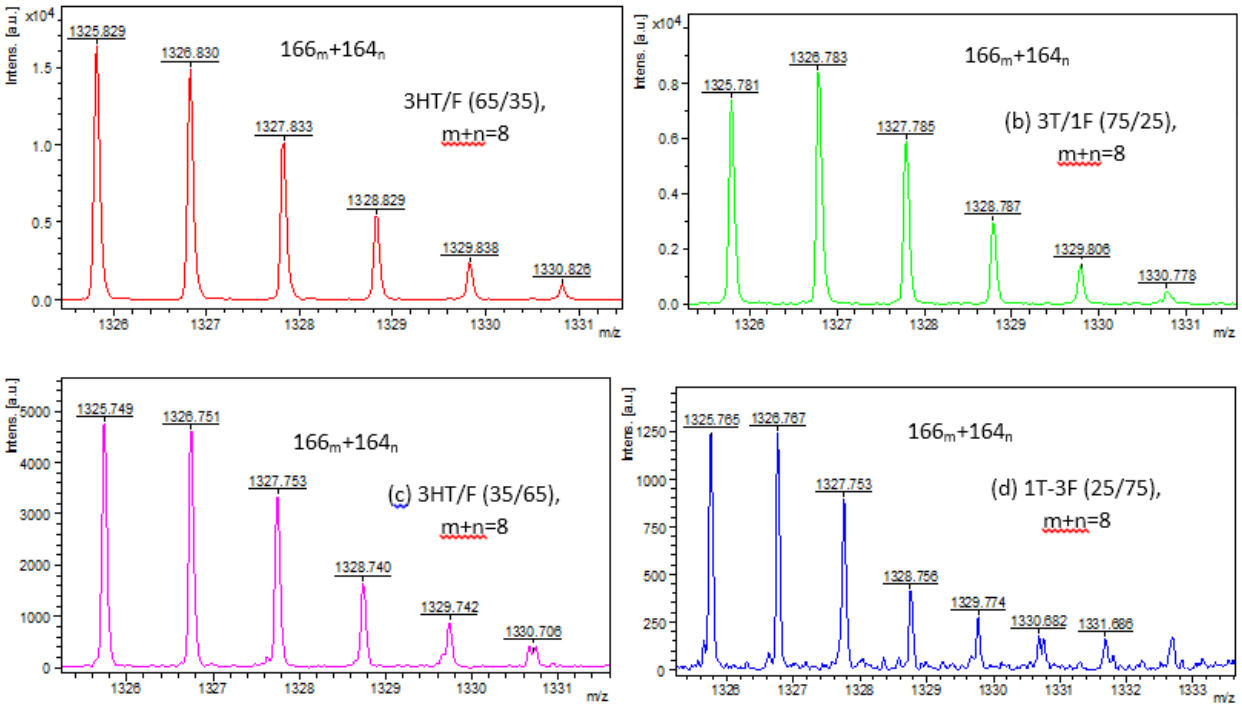


**Figure 3.22: MALDI-TOF MS spectra of (a) 3HT/F (65/35) oligomer, (b) 3HT/F (75/25) oligomer, (c) 3HT/F (35/65) oligomer and (d) 3HT/F (25/75) oligomer at peak m+n=8**

Similarly, the MALDI-TOF mass spectra of other samples (3HT/F molar ratios of 65/35, 75/25, 35/65, and 25/75) showed well-defined peak clusters (see the wide range full MALDI-TOF mass spectra in Supporting Information). Figs. 3.22 (a), (b), (c), and (d) show images of the peaks that were zoomed at the value m+n=8. By matching the calculated compass isotope pattern program with these peaks, the formation of copolymers of 3-hexylthiophene and fluorene in various molar ratios (3HT/F molar ratios of 65/35, 75/25, 35/65, and 25/75) could be demonstrated.

Fig. 3.23 shows the UV-vis spectra of P3HT (Table 3.5, entry 1), PF (Table 3.5, entry 7) homopolymers, and copolymers (Table 3.5, entry 2 to entry 6) with the corresponding absorbance maximum ($\lambda_{max}$). The absorbance maxima ($\lambda_{max}$) of P3HT and PF were observed at 440 and 329 nm, respectively, indicating that the corresponding optical band gaps were 2.82 and 3.77 eV. A broad band with a shoulder that shifted to lower wavelength region was observed in the spectrum of the copolymers with an increase in the feed fluorene amount from 25 to 75. In other words, when the fluorene content increased in the copolymer, the absorbance maximum shifted to short wavelength. The presence of fluorene in the copolymer may cause a continuous variation in the wavelength, thus confirming that a copolymer comprising two monomers was formed by oxidative polymerization. Additionally, the fluorene unit, in conjunction with the 3-hexylthiophene unit in the copolymers, extended the conjugation length of the copolymer backbone, leading to a change in the band gap [35] and thus, a change in the absorption peaks of the copolymers.

To differentiate the copolymer from a simple mixture of P3HT and PF homopolymers, the absorbance and emission intensity of a mixture of P3HT and PF (ratio 3:1) were measured. Obviously, in case of the mixture of homopolymers, two separated peaks were observed, whereas only one broadened peak was observed in the case of the copolymer (Figs. 5 and 6 in Supporting Information). In addition, the mixture of homopolymers showed two different emission regions with two different wavelengths ($\lambda_{max}$ = 330 nm and 440 nm, Fig. 6 in Supporting Information), while the copolymer showed only one emission region at $\lambda_{max}$ = 337 nm, with two peaks (Fig. 5 in Supporting Information). Therefore, from the absorbance and emission spectroscopy analyses, it was confirmed that a copolymer of fluorene and 3-hexyl thiophene was successfully prepared.

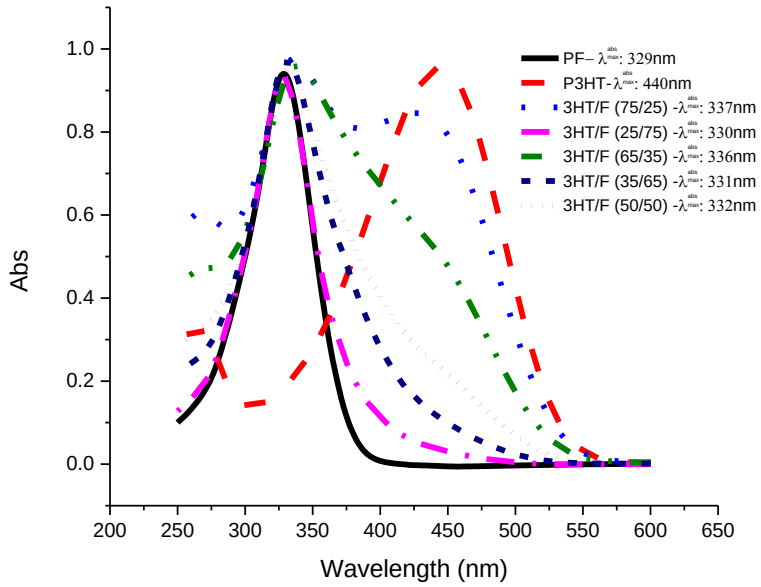


**Figure 3.23: UV-vis spectra of homopolymer and copolymers in $CHCl_3$ at room temperature.**

Furthermore, to calculate the quantum yield (φ) of the samples, the relative determination method was applied[52,53]. First, several solutions with different concentrations of the samples were prepared, and their absorbance and emission intensity were recorded. Second, a graph of the integrated fluorescence intensity versus the absorbance maximum was plotted to calculate the gradient of the straight line.

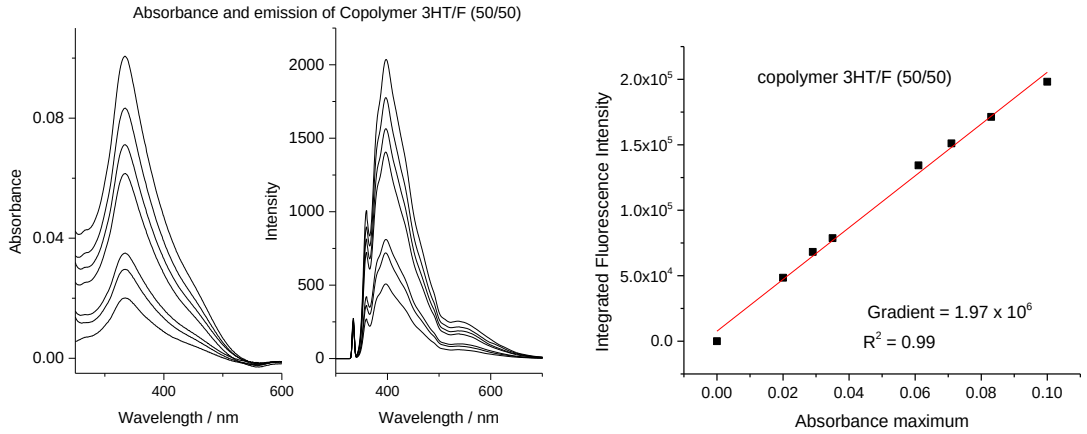


**Figure 3.24: Absorbance and emission spectra of 3HT/F (50/50) (left), and linear plot of integrated fluorescence vs. absorbance maximum (right).**

The fluorescence spectrum of a solution of 3HT/F (50/50) in chloroform is illustrated in Fig. 3.24. The emission maximum of 3HT/F (50/50) was observed at 408 nm. Furthermore, to understand the effect of the fluorene content on the optical properties of the copolymers, the relative quantum yields were determined. Fig. 3.24 shows the absorbance maximum and emission intensity of the 3HT/F (50/50) (Table 3.5, entry 4) copolymer and a linear plot of the integrated fluorescence vs. the absorbance maximum. The results for the other copolymers are described in Figure 5 - Supporting Information. The quantum yield based on the relative method was calculated according to the following equation[54,55]:

$$\Phi_x = \phi_{st} \frac{Grad\ x}{Grad\ st} \frac{\eta_x^2}{\eta_{st}^2}$$

($\varphi_x$ and $\varphi_{st}$ : quantum yield of the sample and the standard, respectively;
$\eta_x$ and $\eta_{st}$ : refractive index of the sample and the standard, respectively;
$Grad_x$ and $Grad_{st}$: Gradient from the plot of integrated intensity and absorbance maximum)

In this study, Rhodamine B (RB) was used as the standard sample. The gradient for RB calculated according to the abovementioned relative determination method is $1.59\times10^6$, and the quantum yield of RB in the literature is 0.31 [56]. Since the gradient value of the samples was calculated (Fig. 3.24, right side), the quantum yields of the other samples were obtained, and are summarized in the Table 1 of Supporting Information and Fig. 3.25.

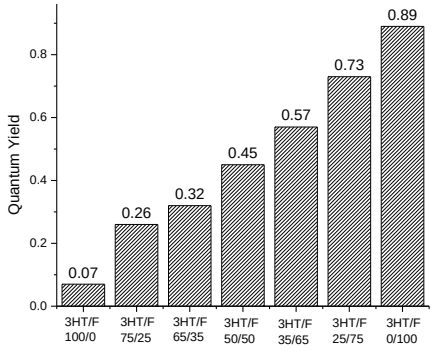


**Figure 3.25: Quantum yields of the samples.**

As shown in Fig. 3.25, the quantum yield of the copolymers was obviously influenced by the fluorene content. The quantum yield of 3-alkylthiophene was the lowest, while that of PF was the highest. In the case of the copolymers, the quantum yield value increased with the increase in fluorene content. It can be elucidated that the band gap of the copolymers changes with the presence of fluorene. In other words, this band gap decreases

with increasing fluorene content in the resulting copolymer, which helps in tuning the emission and thus leads to a high quantum yield.

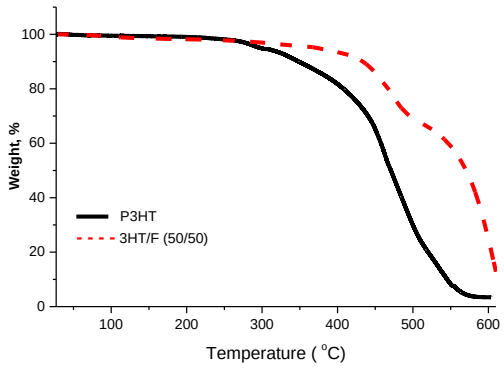


**Figure 3.26. Comparison of TG results for P3HT and 3HT/F (50/50)**

Thermal stability is one of the most important properties that determine the potential applications of a material. In order to investigate the degradation effect of fluorene on the copolymer, thermal analysis of P3HT and 3HT/F (50/50) was performed. Figure 3.26 shows the TG curves of P3HT and the copolymer 3HT/F (50/50) under air flow. The weight loss for P3HT commenced at 325°C and up to 40% decomposition was observed when the temperature reached 450°C. This weight loss could be attributed to the degradation of the polymer backbone chains of P3HT in air. With increasing fluorene content, the decomposition temperature of the copolymers clearly increased. For instance, weight loss for 3HT/F (50/50) commenced at around 420°C. Comparison of these data for P3HT and copolymer 3HT/F (50/50) indicated that the fluorene content plays a significant role in improving the thermal stability of the copolymers because fluorene has high thermal stability [1,2,37,57].

## 3.4 Conclusions

In this study novel copolymers based on 9-ethylcarbazole and 3-hexylthiophene have been synthesized successfully by oxidation polymerization with $FeCl_3$ in hexane solvent at room temperature, and they have been identified by Nuclear Magnetic Resonance ($^1$H-NMR), MALDI-TOF MS, UV–visible absorption, fluorescence spectroscopy, Size Exclusion Chromatography (SEC) and Thermal Gravity Analysis (TGA). It is firstly confirmed that the 9-ethylcarbazole and 3-hexylthiophene molecule(s) were built into the polymer main chain. The solubility of oxidant ($FeCl_3$) in different solvents (hexane, chloroform and nitrobenzene) influences the copolymerization of 3HT and 9EC. The presence of 9EC in the polymer main chain obviously improved the thermal stability of 3HT/9EC copolymer. A complex consisting of 3HT/9EC copolymer and tributylborane (TBB) (1:1) was also prepared smoothly and characterized by $^{11}$B NMR. By adding fluorine anion to the complex of 3HT/9EC and TBB in THF solution, the fluorescence intensity was decreased because of increasing concentrations of fluorine anion. In other words, it was confirmed that this complex of 3HT/9EC copolymer and TBB may have possibility of being used as detecting material for fluorine anion. Copolymers of 3-hexylthiophene and fluorene were also synthesized utilizing $FeCl_3$ as an oxidizing agent in $CHCl_3$. Incorporation of 3-hexylthiophene and fluorene units into the resultant polymer main chain was evident from the results of MALDI-TOF MS, $^1$H-NMR, UV-vis, and fluorometry analysis. The copolymer structure and the effects of the different amounts of the monomers present in the copolymer chain are clearly indicated in the MALDI-TOF mass spectra and $^1$H NMR spectra. GPC analysis indicated a decrease in the molecular weight of the copolymer when the fluorene content was increased. Although there was a small difference between the feed molar ratio and the actual molar ratio, the actual molar ratio of fluorene in the copolymers was proportional to the feed molar ratio. Oxidation of fluorene at the 9-position was not observed in the copolymers. Incorporation of fluorene in 3-hexylthiophene resulted in an increase in the emission intensity of the copolymer because the emission intensity of PF is higher than that of P3HT. In addition, the quantum yield

of the copolymer increased with an increase in the amount of fluorene. In addition, fluorene was demonstrated to play an important role in enhancing the thermal stability of the copolymers.

## 3.5 Supporting information

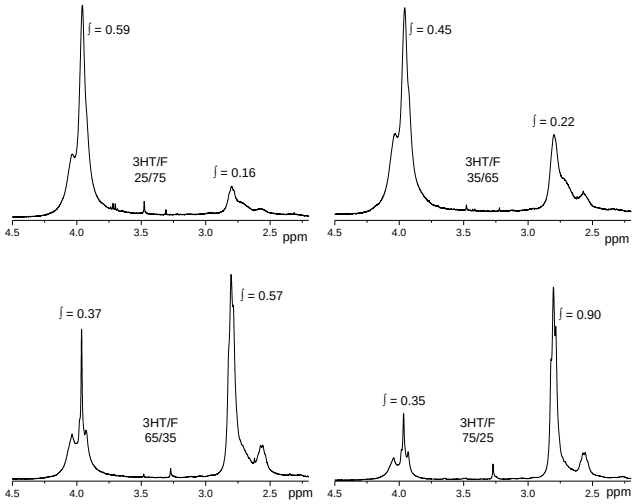


*Figure 1: $^1$H NMR spectra of copolymers 3HT/F (25/75), 3HT/F (35/65), 3HT/F (65/35), 3HT/F (75/25) in $CDCl_3$ at room temperature*

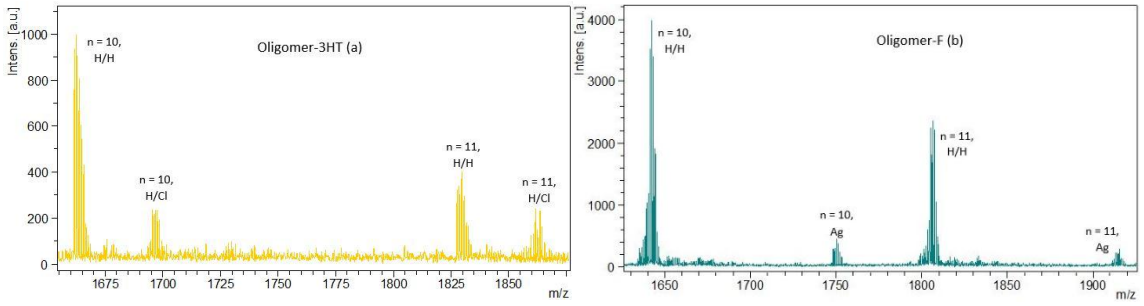


*Figure 2: MALDI-TOF MS spectra of Oligomer 3HT (a) and Oligomer F (b)*

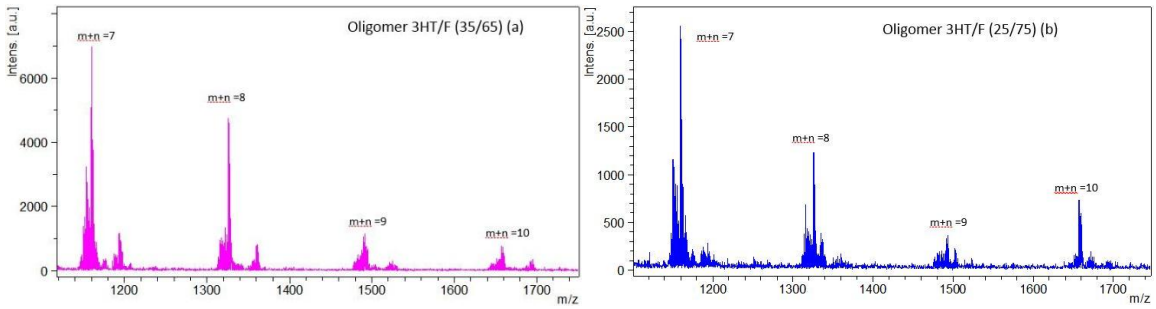


*Figure 3: MALDI-TOF mass spectra of oligomer 3HT/F (35/65) (a) and oligomer 3HT/F (25/75) (b)*

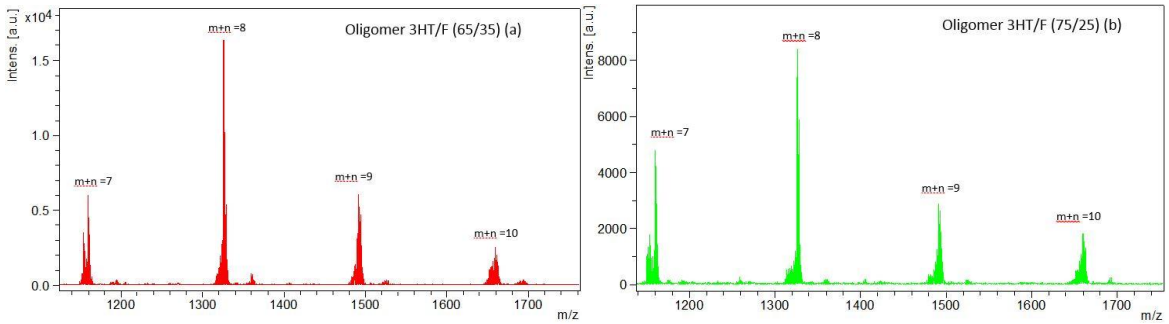


*Figure 4: MALDI-TOF MS spectra of oligomer 3HT/F (65/35) (a) and oligomer 3HT/F (75/25) (b)*

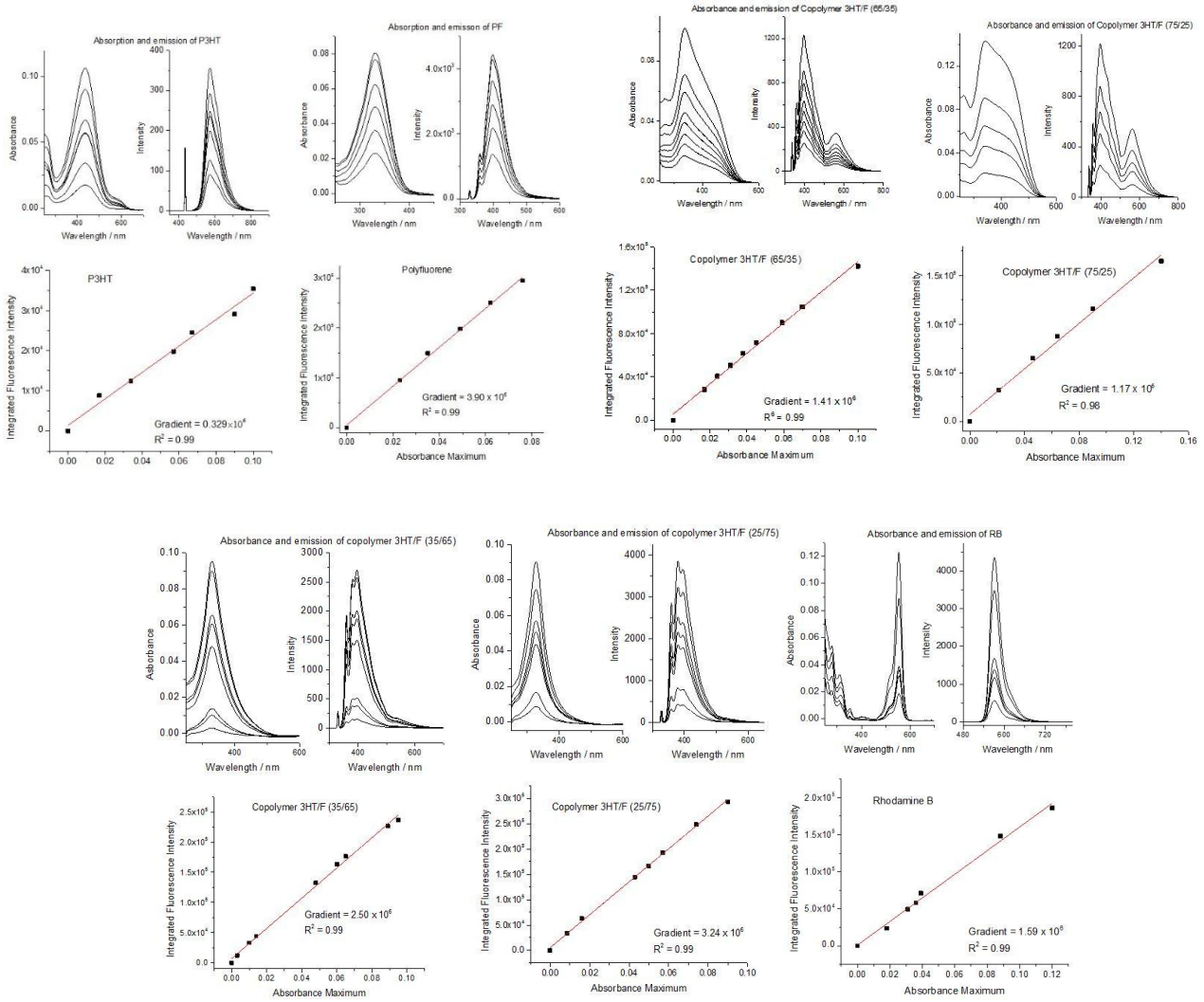


*Figure 5: Absorbance, emission and linear plot of integrated fluorescence vs absorbance maximum (bottom) of 3HT/F copolymer samples*

*Table 1: Gradient values of samples*

| Samples | Gradient value×$10^{-6}$ | Quantum Yield |
|---|---|---|
| P3HT | 0.329 | 0.07 |
| 3HT/F (75/25) | 1.17 | 0.26 |
| 3HT/F (65/35) | 1.41 | 0.32 |
| 3HT/F (50/50) | 1.97 | 0.45 |
| 3HT/F (35/65) | 2.50 | 0.57 |
| 3HT/F (25/75) | 3.24 | 0.73 |
| PF | 3.90 | 0.89 |

*The refractive index of water and chloroform are 1.33 and 1.44 respectively (Reference: S. Kedenburg, M. Vieweg, T. Gissibl, and H. Giessen, Optical Materials Express, (2012), Vol. 2, No. 11, 1588-1611)*

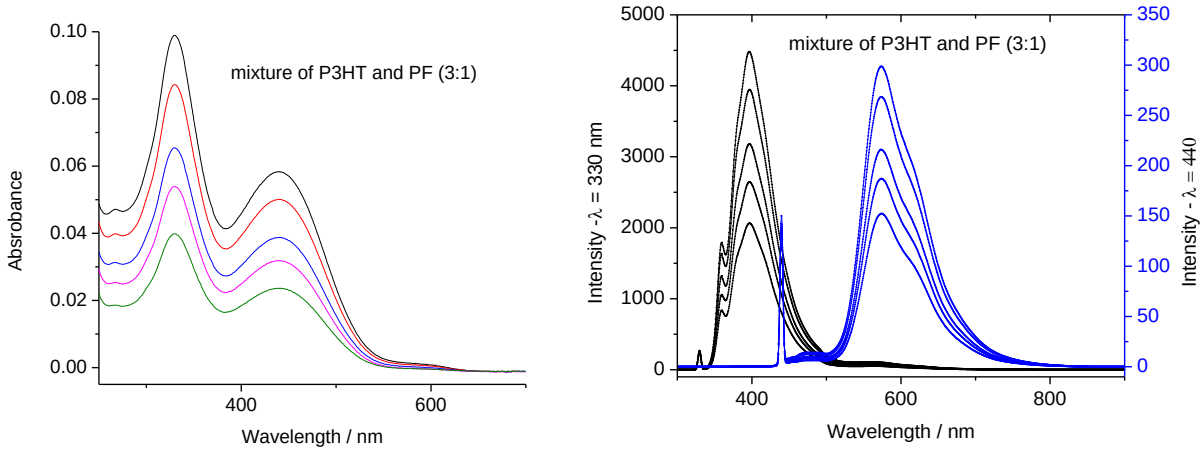


*Figure 6: Absorbance (top) and emission (bottom) of mixture of P3HT and PF (3:1).*

## 3.6 References


(1) Roncali, J. *Chem. Rev.* **1992**, *92*, 711-738.
(2) McCullough, R. D. *Adv. Mater.* **1998**, *10*, 93-116.
(3) MacDiarmid, A. G. *Angew. Chem. Int. Ed.* **2001**, *40*, 2581-2590.
(4) Yamamoto, T. *NPG ASIA MATERIALS* **2010**, *2*, 54-60.
(5) Gu, Z.; Tan, Y.; Tsuchiya, K.; Shimomura, T.; Ogino, K. *Polymers* **2011**, *3*, 558-570.
(6) Brambilla, L.; Tommasini, M.; Botiz, I.; Rahimi, K.; Agumba, J. O.; Stingelin, N.; Zerbi, G. *Macromolecules* **2014**, *47*, 6730-6739.
(7) Zhang, X.-F.; Xi, Q.; Zhao, J. *J. Mater. Chem.* **2010**, *20*, 6726-6733.
(8) Lee, S.; Jeon, H.; Jang, M.; Baek, K.-Y.; Yang, H. *ACS Appl. Mater. Interfaces* **2015**, *7*, 1290-1297.
(9) Nguyen, T. A.; Nguyen, T. T.; T.Nguyen, L.-T.; Le, T. V.; TranNguyen, H. *Synth. Met* **2016**, *217*, 172-184.
(10) KousukeTsuchiya; Ando, K.; Shimomura, T.; Ogino, K. *Polymer* **2016**, *92*, 125-132.
(11) Moon, H. C.; Anthonysamy, A.; Kim, J. K.; Hirao, A. *Macromolecules* **2011**, *44*, 1894–1899.
(12) Patra, D.; Sahu, D.; Padhy, H.; Kekuda, D.; Chu, C.-W.; Lin, H.-C. *J. Polym. Sci. Pol. Chem* **2010**, *48*, 5479-5489.
(13) Siove, A.; Ade`s, D. *Polymer* **2004**, *45*, 4045-4049.
(14) Andries, A.; Abaskin, V.; Achimova, E.; Meshalkin, A.; Prisacar, A.; Sergheev, S.; Robu, S.; Vlad, L. *Phys. Status Solidi A* **2011**, *208*, 1837-1840.
(15) Okamoto, Y.; Takahata, K.; Saeki, K. *Chem. Letters* **1998**, 1247-1247.
(16) Cai, T.; Zhou, Y.; Wang, E.; Hellstrom, S.; Zhang, F.; Xu, S.; Inganas, O.; Andersson, M. R. *Solar Energy Materials & Solar Cells* **2010**, *94*, 1275-1281.
(17) Chen, L.-X.; Niu, C.-G.; Zeng, G.-M.; Huang, G.-H.; Shen, G.-L.; Yu, R.-Q. *Analytical Science* **2003**, *19*, 295-299.
(18) Curiel, D.; Cowley, A.; Beer, P. D. *Chem. Commun.* **2005**, 236-238.
(19) Jiao, C.-X.; Shen, Q.; Huan, S.-Y.; Shen, G.-L.; Yu, R.-Q. *Analytica Chimica Acta* **2005**, *528*, 229-234.
(20) Mahapatra, A. K.; Hazra, G.; Sahoo, P. *Beilstein Journal of Organic Chemistry* **2010**, *2010*, 1-8.
(21) Wade, C. R.; Broomsgrove, A. E. J.; Aldridge, S.; Gabbaı, F. o. P. *Chem. Rev.* **2010**, *110*, 3958-3984.
(22) Zhang, J.; Zhang, L.; Wei, Y.; Chao, J.; Wang, S.; Shuang, S.; Dong, Z. C. a. C. *Anal. Methods* **2013**, *5*, 5549-5554.
(23) Kaur, M.; Yoon, B.; Rajesh Kumar; Cho, M. J.; Kim, H. J.; Kim, J. S.; Choi, D. H. *Bull. Korean Chem. Soc.* **2014**, *35*, 3437-3443.
(24) Yang, R. H.; Chan, W. H.; Lee, W. M.; Xia, P. F.; Zhang, H. K.; Li, K. A. *J. Am. Chem. Soc.* **2003**, *125*, 2884-2885.
(25) Morin, J. F.; Leclerc, M. *Macromolecules* **2002**, *35*, 8413-8417.
(26) Grazulevicius, J. V.; Strohriegl, P.; Pielichowski, J.; Pielichowski, K. *Prog. Polym. Sci.* **2003**, *28*, 1297-1353.
(27) Catargiu, A. M.; Ivan, T.; Vacareanu, L.; Grigoras, M. *Rev. Roum. Chim.* **2013**, *58*, 113-119.
(28) Jiang, H. J.; Zhang, J. l. *Polymer. Adv. Tech.* **2014**, *25*, 644-650.
(29) Leclerc, M. *J. Polym. Sci. Pol. Chem.* **2001**, *39*, 2867–2873.
(30) Schelkle, K. M.; Bender, M.; Jeltsch, K.; Buckup, T.; Mullen, K.; Hamburger, M.; Bunz, U. H. F. *Angew. Chem. Int. Ed.* **2015**, *54*, 1-5.

(31) Chou, C.-H.; Hsu, S.-L.; Dinakaran, K.; Chiu, M.-Y.; Wei, K.-H. *Macromolecules* **2005**, *38*, 745-751.
(32) Kreyenschmidt, M.; Klaerner, G.; Fuhrer, T.; Ashenhurst, J.; Karg, S.; Chen, W. D.; Lee, V. Y.; Scott, J. C.; Miller, R. D. *Macromolecules* **1998**, *31*, 1099-1103.
(33) Lee, J.-I.; Lee, V. Y.; Miller, R. D. *ETRI Journal* **2002**, *24*, 409-414.
(34) Perevedentsev, A.; Stavrinou, P. N.; Smith, P.; Bradley, D. D. C. *J. Polym. Sci. Pt. B-Polym. Phys* **2015**, *53*, 1492–1506.
(35) Ouyang, M.; Xiang, W. Q.; Xu, Y.; Zhang, Y. J.; Lou, Q. P.; Zhang, C. *Polym. Polym. Compos.* **2012**, *20*, 21-26.
(36) Lin, Y.-H.; Smith, K. A.; Kempf, C. N.; Verduzco, R. *Polym. Chem.* **2013**, *4*, 229-232.
(37) Wang, X.; Chen, B.; Xu, J.; Zhou, W.; Pu, S. *Journal of Applied Polymer Science* **2008**, *108*, 1924–1933.
(38) Kuang, H.; Janik, M. J.; Gomez, E. D. *J. Polym. Sci. Pt. B-Polym. Phys* **2015**, 1-7.
(39) Sui, A.; Shi, X.; Tian, H.; Geng, Y.; FosongWang. *Polym. Chem* **2014**, *5*, 7072–7080.
(40) Hardeman, T.; Koeckelberghs, G. *Macromolecules* **2015**, *48*, 6987-6993.
(41) Raj, V.; Madheswari, D.; Ali, M. M. *Journal of Applied Polymer Science* **2012**, *124*, 1649-1658.
(42) Li, X. G.; Huang, M. R.; Jin, Y.; Yang, Y. L. *Polymer* **2001**, *42*, 3427-3435.
(43) Wang, X.; Chen, B.; Xu, J.; Zhou, W.; Pu, S. *J. Appl. Polym. Sci.* **2008**, *108*, 1924–1933.
(44) Kumagai, A.; Fukumoto, H.; Yamamoto, T. *J. Phys. Chem. B* **2007**, *111*, 8020-8026.
(45) Cai, T.; Zhou, Y.; Wang, E.; Hellström, S.; Zhang, F.; Xu, S.; Inganäs, O.; Andersson, M. R. *Sol. Energy Mater. Sol. Cells* **2010**, *94*, 1275–1281.
(46) Sugimoto, R.; Takeda, S.; Gu, H. B.; Yoshino, K. *Chemistry Express* **1986**, *1*.
(47) Niemi, V. M.; Knuuttila, P.; 0sterholm, J. E.; Korvola, J. *Polym. Rep.* **1992**, *33*, 1559-1562.
(48) Szyma´nski, J. K.; Temprano-Coleto, F.; Pe´rez-Mercader, J. *Phys. Chem. Chem. Phys* **2015**, *17*, 6713-6717.
(49) Montaudo, G.; Samperi, F.; Montaudo, M. S. *Prog. Polym. Sci.* **2006**, *31*, 277–357.
(50) Sato, H.; Nakamura, S.; Teramoto, K.; Sato, T. *J. Am. Soc. Mass Spectrom.* **2014**, 1-10.
(51) Liu, Y.; Nishiwaki, N.; Saigo, K.; Sugimoto, R. *Polym. Bull.* **2015**, *72*, 1817–1826.
(52) William, A. T. R.; Winfield, S. A.; Miller, J. N. *Analyst* **1983**, *108*, 1067.
(53) Wurth, C.; Grabolle, M.; Pauli, J.; Spieles, M.; Resch-Genger, U. *Nature protocols* **2013**, *8*, 1535-50.
(54) Williams, A. T. R.; Winfield, S. A. *Analyst* **1983**, *108*, 1067-1071.
(55) William, A. T. R.; Winfield, S. A.; Miller, J. N. *Analyst* **2013**, *108*, 1067.
(56) Magde, D.; Rojas, G. E.; Seybold, P. *Photochem. Photobiol* **1999**, *70*, 737.
(57) Groenendaal, L. B.; Zotti, G.; Aubert, P. H.; Waybright, S. M.; Reynolds, J. R. *Adv. Mater.* **2003**, *15*, 855-880.

# Chapter 4:

# Modification of polyolefin surface through grafting poly(3-hexylthiophene)

## 4.1 Introduction

A growing interest in polymer surface modification for the development of macromolecules to improve their properties and performance has been perceived in recent years. Reported methods to modify polymers can be classified into three categories: blending, grafting, and curing[1]. Polypropylene (PP), one of the most commodity polymers, is used in a wide variety of applications such as packaging, textile, automotive materials and so forth [2-4]. However, the highly non-polar nature and low surface energy of PP needs to be modified for improving the surface properties such as wettability, adhesion, and dye-ability. Several methods have been reported for the PP surface modification; including impulse corona discharges[5], surfactant immobilization[6], direct melt grafting using twin-screw extrusion[7], plasma treatment[8,9], ultraviolet photo-grafting process[10], air dielectric barrier discharge (DBD)[11], and diazonium chemistry[12]. Several applications based on graft polyolefin have also been reported [13-16].

Conjugated polymers are of interest to physicists and chemists because of their novel properties that allow them to be utilized in semiconductors, transistors, sensors, solar cells, and other electrical devices[17,18]. Poly(3-hexylthiophene) (P3HT) and its derivatives are special conjugated materials that have been used in organic solar cells [19-21], transistors [17,22], polymer light-emitting diodes[23], chemical sensors[24], non-linear optics, and energy storage devices[25].

Recently, in-situ vapor-phase polymerization has been used to coat conducting polymers on fibrous PP films for the fabrication of capacitor electrodes[26]. In addition, a thin PP film coated with polypyrrole (PPy) was produced by a dipping method, and this was subsequently applied for water desalination[27]. Furthermore, a novel colleting electrode for the removal of fine particles, was fabricated by coating conductive polyaniline (PANI) on a PP plate [28]. A novel conductive composite fibers made of PP and poly(3,4-ethylenedioxythiophene) (PEDOT) was prepared for gas sensing [29]. In addition, electrically conductive polymer composites containing PANI, PPy, and polyolefins (PP and polyethylene (PE)) have been applied as the semiconducting layer of a polymer cable [30-32]. The main purpose of these studies was the synthesis of the composite materials, whereas, the goal of our research was to graft conjugated polymers such as P3HT onto the surface of PP. Because of the outstanding properties of PP, such as high abrasion resistance, chemical inertness, stretchability, and low density, the PP textile industry has developed these polymers since the 1950s [33,34]. During the production and utilization of PP fibers, the surface can easily become charged, which can result in serious problems such as damage to sensitive electronic equipment. Grafting of conjugated polymers on the PP surface may improve the antistatic properties of PP because the conjugated structure can transfer the static charges.

In general, a method comprising of three steps - bromination, substitution and oxidative polymerization - was utilized for the grafting of polythiophene (PT) onto polyethylene (PE) [35]. In addition, vinyl monomers were reportedly grafted onto the polyolefin surface by using triorganoboranes and oxygen in air [36-39].

In this chapter, a new methodology for grafting P3HT onto PP surfaces (film and powder) is reported. This process involves two simple reaction steps (Scheme 4.1). In the first step, 3-(4-ethenylphenyl)thiophene (EPT) is grafted onto the PP surface (PEPT-g-PP) using the radicals formed by mixing tri-*n*-butylborane (TBB) and oxygen molecules in air. In the second step, P3HT is grafted onto the PP surface via the chemical oxidative polymerization of PEPT-g-PP and 3HT monomers using $FeCl_3$ as the oxidant.

## 4.2 Experimental section

### *4.2.1 Chemicals*

Isotactic polypropylene (iPP) film and powder were purchased from Toyobo (Pylen Film-CT) and Mitsui Chemicals, respectively. 3-Hexylthiophene (3HT), 3-bromothiophene, and anhydrous $FeCl_3$ were obtained from Tokyo Chemical Industry Ltd. and used without further purification. Tri-n-butylborane and styrene monomers were supplied by Nippon Aluminum Alkyls Ltd. and Wako Pure Chemical Industry Ltd.,

respectively. 4-Vinylphenylboronic acid was obtained from Sigma-Aldrich and used as received. Tetrakis(triphenylphosphine) palladium, sodium carbonate, and disodium sulfate were purchased from Wako Pure Chemical Industry Ltd. Analytical grade solvents such as ethanol, benzene, chloroform, methanol, and hexane were purchased from Wako Pure Chemical Industry Ltd. and used as received. Hexane was used as the reaction solvent because of its low polarity, higher affinity for PP, [37] and the insolubility of $FeCl_3$ in hexane.[40] The hexane was dried by standing over 4-Å molecular sieves for 8 h and purged with argon gas for 20 min before use.

### *4.2.2 Measurement*

UV-Vis spectra were obtained by measuring the diffuse reflectance of the samples at room temperature on a Jasco V-650 UV-Vis spectrometer set in absorbance photometric mode with a bandwidth of 0.2 nm, a data interval of 1.0 nm, and scan speed of 400 nm $min^{-1}$. Thermogravimetric analysis was carried out in air from 20 to 900 °C at a flow rate of 25 mL $min^{-1}$ and a heating rate of 10 °C $min^{-1}$ using a Hitachi thermal analysis system (STA 7200 RV). X-ray diffraction patterns were obtained using grazing incidence X-ray diffraction (GIXD) with a Rigaku Smartlab diffractometer with graphite-monochromatized Cu-Kα radiation (λ = 1.5418 Å) in steps of 0.02° over a 2θ range of 2−90°. TEM images were obtained using a JEOL JEM-2100F microscope. Energy dispersive X-ray mappings and line scan spectra were acquired on an Oxford INCA Energy TEM250 instrument. $^1$H NMR spectra (400 MHz) were recorded on a Bruker Ascend 400 spectrometer, and Raman spectra were measured on an HR800 Horiba Raman spectrometer. High-resolution mass spectra were measured on an AB Sciex Triple electrospray ionization–time of flight (ESI-TOF) 4600 system; typically, 20 μL of the sample solution was injected directly into the spectrometer using chloroform/acetonitrile (10:90, v/v) as the solvent at a flow rate of 10 μL $min^{-1}$ (syringe pump). Gel permeation chromatography (GPC) was carried out in a system equipped with a Jasco PU-2080 Plus pump and a Jasco RI-2031 Plus intelligent refractive index (RI) detector. The molecular weights and molecular weight distributions of the polymers relative to a polystyrene standard were analyzed using Chrom NAV software. Chloroform was used as the polymer solvent and eluent in an equilibrated system at 40°C. The electric conductivity was measured with an Agilent 34401A $6^{1/2}$ Digit Multimeter resistometer using a four-probe method.

### *4.2.3 Synthesis of 3-(4-ethenylphenyl)thiophene*

3-(4-Ethenylphenyl)thiophene was synthesized via Suzuki-Miyaura cross-coupling reaction (Scheme 2). [41-43] 3-Bromothiophene (10 mmol) and 10 mL of an aqueous solution of $Na_2CO_3$ (2 M) were added to 0.3 mmol of tetrakis(triphenylphosphine)palladium dissolved in 20 mL of benzene. An ethanol solution (5 mL) of 4-vinylphenylboronic acid (11 mmol) was added to this solution and the reaction mixture was stirred at 80 °C under an argon atmosphere for 6 h. Subsequently, 5 mL of a 30% $H_2O_2$ solution was added to the reaction mixture at 23 °C to oxidize the residual 4-vinylphenylboronic acid. The product was extracted using diethyl ether, and the organic extracts were washed with a saturated NaCl solution and dried over $Na_2SO_4$. The product was obtained in 70% yield after the removal of diethyl ether using a rotary evaporator.

### *4.2.4 Grafting of PEPT onto the PP surface*

The grafting method used in this work is similar to the previously reported procedure for the grafting of vinyl monomers onto PP surfaces with TBB and diffuse molecular oxygen in air[37-39]. The PP film (25 mg, 1 × 1 $cm^2$, 0.3 mm thickness), 3-(4-ethenylphenyl)thiophene monomer (10 mmol), and TBB (0.3 mL) were stirred gently for 1 h under argon. The molar ratio of TBB and 3-(4-ethenylphenyl)thiophene was 1:20. After stirring for 1 h, TBB was reacted with oxygen by exposing the reaction mixture to air for 1 h. Subsequently, the reaction was stopped, and the mixture was stirred gently for 24 h. The reaction mixture was then transferred to a Soxhlet extractor for 24 h to extract the PEPT homopolymer using chloroform. The desired poly(3-(4-ethenylphenyl)thiophene) grafted PP (PEPT-g-PP) film was dried under vacuum for 12 h. The grafting of PEPT onto PP powder was carried out using a procedure similar to that described above.

### *4.2.5 Grafting of P3HT onto the PP surface*

Chemical oxidative polymerization was conducted in an oven-dried Schlenk flask fitted with a stopcock under an inert argon atmosphere.[40,44] $FeCl_3$ (0.37 g), PEPT-g-PP (25 mg), and hexane (7 mL) were placed in the Schlenk flask and the mixture was ultrasonicated for 20 min. A solution of 3-hexylthiophene (95 mg) in hexane (3mL) was dropped to a stirred suspension of the mixture, and the reaction was stirred for 24 h under an atmosphere of argon at room temperature (23 °C). Subsequently, the product was taken out and washed with methanol to remove the residual $FeCl_3$, followed by extraction with chloroform to eliminate any free P3HT homopolymer. The desired product, poly(3-hexylthiophene) grafted onto PP (or P3HT-g-PP), was dried under reduced pressure for 12 h. The grafting of 3HT onto the PP powder was carried out following a procedure similar to that described above.

## 4.3 Results and Discussion

### *4.3.1 Grafting P3HT on PP through $FeCl_3$ oxidative polymerization PEPT-g-PP and 3HT monomers*

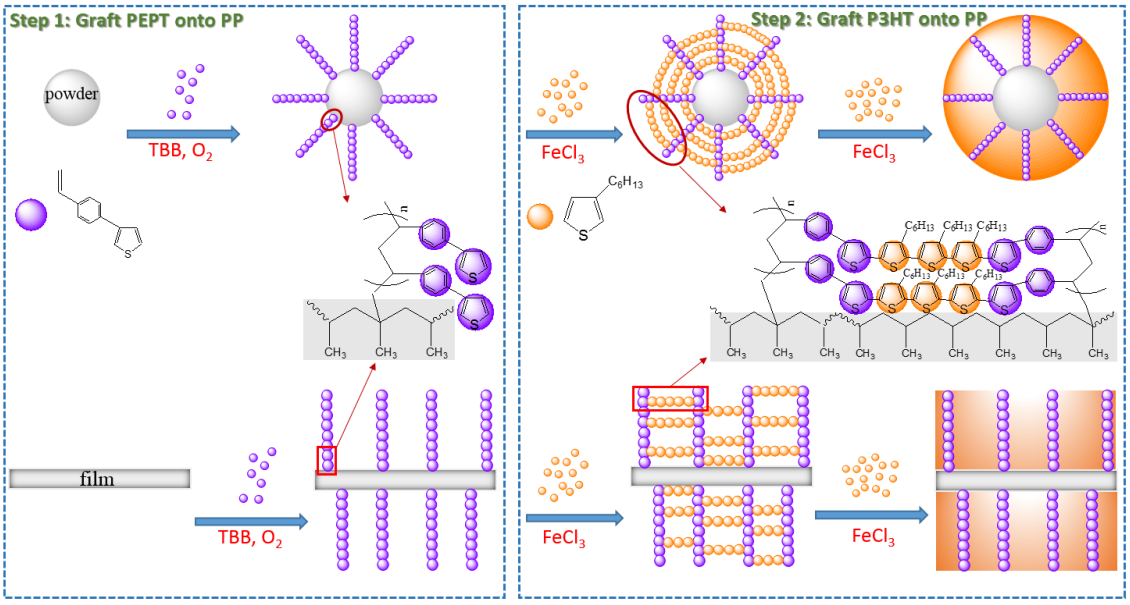


**Scheme 4.1. Grafting of PEPT and P3HT onto PP film and powder**

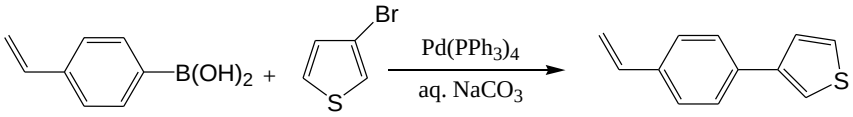


**Scheme 4.2. Palladium-catalyzed cross coupling reaction for the synthesis of 3-(4-ethenylphenyl)thiophene**

The monomer 3-(4-ethenylphenyl)thiophene was synthesized via the Suzuki-Miyaura cross-coupling reaction between phenylboronic acid and haloarenes in the presence of a base (Scheme 4.2). [41-43] The structure of the monomer was confirmed by $^{1}H$-, $^{13}C$-, and DEPT $^{13}C$ -NMR (as shown in Figures 4.1, 4.2, and 4.3). The high-resolution mass spectra of this compound indicated a mass of 187.0570, which is in good agreement with the calculated value of 187.0576.

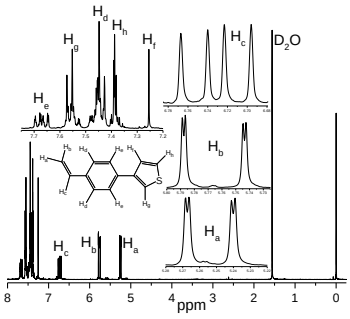


**Figure 4.1. $^{1}$H-NMR spectrum of 3-(4-ethenylphenyl)thiophene**

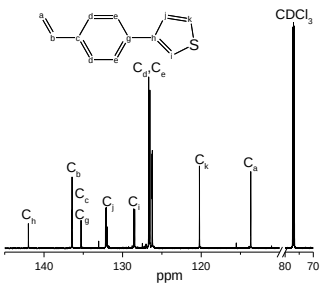


**Figure 4.2. $^{13}$C-NMR spectrum of 3-(4-ethenylphenyl)thiophene**

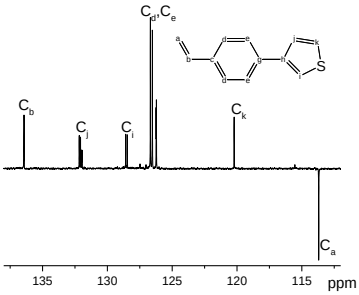


**Figure 4.3. DEPT $^{13}$C-NMR spectrum of 3-(4-ethenylphenyl)thiophene**

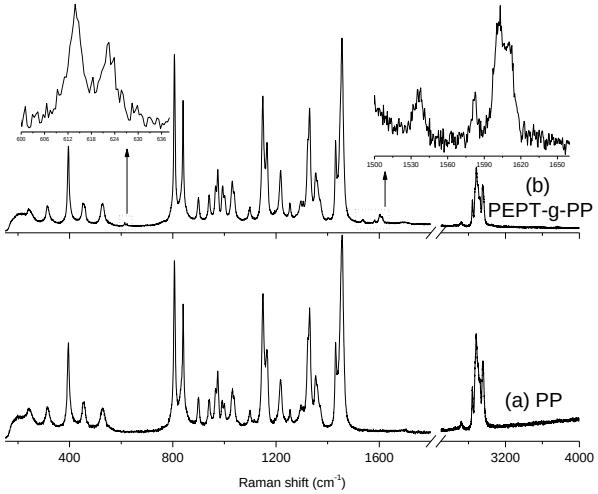


**Figure 4.4. Raman spectra of (a) PP and (b) PEPT-g-PP**

The Raman spectra of neat PP and PP modified by grafting with PEPT are shown in Figure 4.4. Several studies have been published that discuss the Raman spectrum of PP.[45-48] The characteristic strong absorption peak at 805 $cm^{-1}$ is attributed to $CH_2$ rocking, C–C backbone stretching, and C–$CH_3$ stretching vibrations. Several identical vibrations are responsible for the intense, characteristic skeletal bands observed at 2876, 1455, 1330, and 1147 $cm^{-1}$. Furthermore, several sharp peaks of medium intensity are observed in the range of 890–1100 $cm^{-1}$, corresponding to $CH_3$ rocking, CH bending and twisting, $CH_2$ wagging, and C–C backbone stretching vibrations. A few new peaks appear in the Raman spectrum of PEPT-g-PP (as shown in Figure 4.4b), indicating that PEPT was successfully grafted onto the PP surface. A low-intensity peak observed in the range of 1500–1650 $cm^{-1}$ arises from the C=C aromatic ring chain vibrations of 3-(4-ethenylphenyl) thiophene. The peaks observed in the range 600–636 $cm^{-1}$ belong to the CH out-of-plane vibrations of the aromatic moieties.[45]

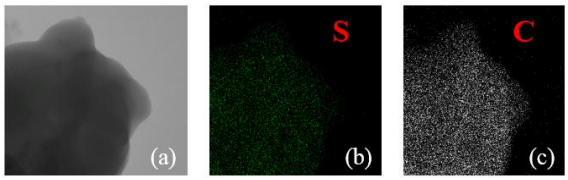


**Figure 4.5. EDX mapping images of PEPT-g-PP**

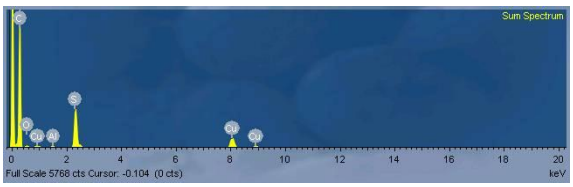


**Figure 4.6. EDX spectrum of PEPT-g-PP**

A TEM image of PEPT-g-PP powder is shown in Figure 4.5a, and the EDX mappings that show the distribution of the elements corresponding to the TEM image are shown in Figures 4.5b and 4.5c. As shown

in Figure 4.6, carbon and sulfur are found in the PEPT-g-PP sample. These observations suggest that the sulfur originated from the grafting of EPT onto the PP sample.

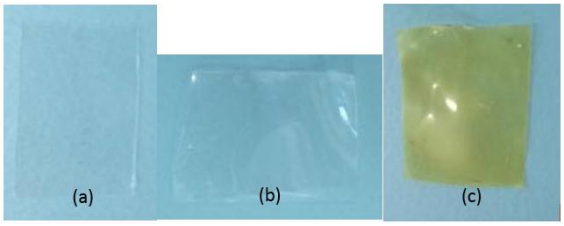


**Figure 4.7. Images of (a) PP, (b) PEPT-g-PP, and (c) P3HT-g-PP films**

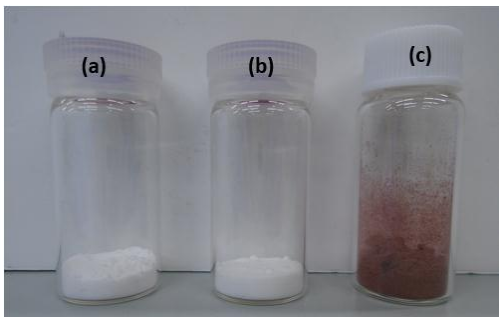


**Figure 4.8. Images of (a) PP, (b) PEPT-g-PP, and (c) P3HT-g-PP powders**

The graft ratios ($G_r$) of PEPT and P3HT onto PP were calculated according to Equation (1) [37,39]:

$$G_r = \frac{m_g - m_o}{m_o} \times 100\% \qquad (1)$$

where $G_r$ refers to the graft ratio of PEPT on PP, $m_o$ and $m_g$ are the weights of PP before and after grafting, respectively. In the case of P3HT, $m_o$ and $m_g$ are the weights of PEPT-g-PP before and after grafting of PP with P3HT, respectively.

The reaction of TBB with diffused oxygen produces the free radicals required for graft polymerization.[38,39] In this work, hexane was used as a solvent because it is non-polar and miscible with PP. Moreover, weak Van der Waals forces between TBB and hexane result in absorption of TBB onto the PP surface.[37] In addition, the insolubility of $FeCl_3$ in hexane increases its activity as an oxidant in the polymerization reaction. [40] The graft ratio of PEPT onto the PP film is only 0.6% and has a value of 2.2% in the case of grafting of PEPT onto the powdered form of PP. This may be explained by the higher surface area of the powder compared to the film. The oxidative polymerization of PEPT-g-PP and 3HT monomers for the grafting of P3HT onto the PP surface was carried out in hexane with $FeCl_3$ at 23 °C for 24 h. The incorporation of the thiophene derivative and 3HT monomer has been discussed in a previous report.[49] The graft ratio of 3HT on PEPT-g-PP was also affected by the surface area in a significant manner. In fact, the grafting of P3HT onto the PEPT-g-PP powder had a high grafting ratio of 5.6 %, while this value was just 1.8% in the case of grafting P3HT onto the PEPT-g-PP film. During the grafting process, P3HT-g-PP underwent a color change that was easily discernible with the naked eye (as shown in Figures 4.7 and 4.8). The PP film (Figure 4.7b) and powder (Figure 4.8b) grafted with PEPT were transparent and white, respectively, similar to the PP film (Figure 4.7a) and powder (Figure 4.8a) before the grafting reaction. However, the P3HT-g-PP polymer showed very different colors: a yellow film (Figure 4.7c) and red powder (Figure 4.8c). In addition, both the film (Figure 4.7c) and powder (Figure 4.8c) became orange upon immersion in chloroform.

During the grafting of P3HT onto PP, the self-polymerizations of 3HT occurred concurrently with the graft polymerization of 3HT onto PP. The ungrafted 3HT polymers were extracted from the grafted products with chloroform. The chacracterization of the extracted P3HT is shown in Figure 4.9.

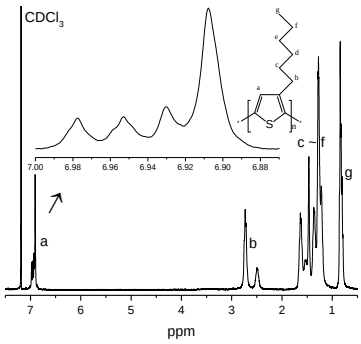


**Figure 4.9. $^{1}$H-NMR spectrum of extracted P3HT**

The $^{1}$H-NMR spectrum of extracted P3HT is shown in Figure 4.9. The signals at 2.5 and 2.7 ppm are assigned to head-to-head (H-H) and head to tail (H-T) configurations, respectively, while the cluster of peaks around 6.8-7.0 ppm correspond to four triad configurations as follows HT-HT, TT-HT, HT-HH and TT-HH, respectively. [50] Furthermore, GPC measurements of the extracted P3HT indicate that the number-average molecular weight ($M_n$) is 90000 Da and the polydispersity index (PDI) is 2.3.

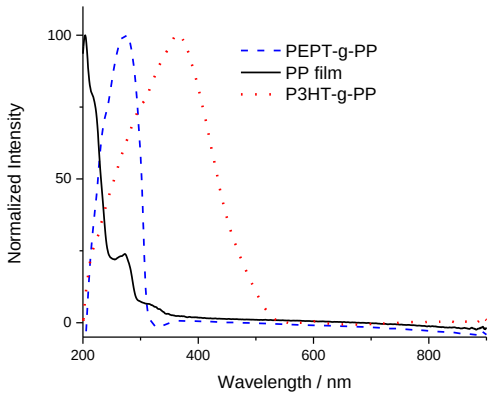


**Figure 4.10. UV-Vis spectra of PP, PEPT-g-PP, and P3HT-g-PP films**

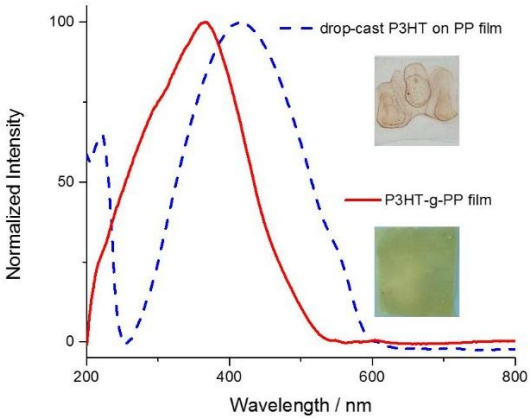


**Figure 4.11: UV-Vis spectra of P3HT-g-PP and drop-casted P3HT on PP films**

Figure 4.10 shows the UV-Vis spectra of the PP, PEPT-g-PP, and P3HT-g-PP films. The spectrum of the PP film (solid line) has a low-intensity peak at around 270 nm that can be attributed to the presence of trace amounts of α,β-unsaturated carbonyl groups.[51-53] There is an intense sharp peak at 268 nm (4.62 eV) in the spectrum of PEPT-g-PP (dashed line) that arises because of $\pi$–$\pi^*$ excitations in the aromatic groups of PEPT. This excitation lies in the ultra-violet range, which explains the colorless transparency of the PEPT-g-PP film in the visible light region (Figure 4.7b). The spectrum of P3HT-g-PP (dotted line) shows an absorption peak maximum at 368 nm, and this may be attributed to the $\pi$-$\pi^*$ transitions in P3HT.[54,55]

A 50-μL chloroform solution of P3HT was drop cast onto the PP film, dried in vacuum for 12 h, and then the UV-Vis spectra were measured. The UV-Vis spectra of the P3HT-g-PP film and film prepared by drop-casting P3HT on the PP film are compared in Figure 4.11.

Figure 4.11 shows that the absorption peak maximum ($\lambda_{max}^{abs}$) of the P3HT-g-PP film is blue-shifted by about 49 nm, compared to that of P3HT drop-cast on the PP film. The connections between the EPT and 3HT units may be responsible for the difference in $\lambda_{max}^{abs}$. The incorporation of aromatic compounds such as benzene, toluene, and xylene into the P3HT main chain has been found to cause a blue-shifted in the absorption peak maximum.[56]

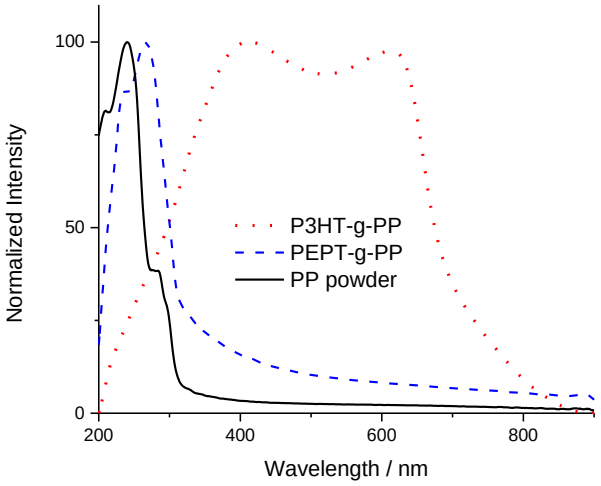


**Figure 4.12. UV-Vis spectra of PP, PEPT-g-PP, and P3HT-g-PP powders**

The UV-Vis spectra of the PP, PEPT-g-PP, and P3HT-g-PP powders are similar to those of the respective films (Figure 4.12). The spectra of PP and PEPT powders are similar to that of the film. However, in the case of P3HT-g-PP, the spectrum of the red powder showed two characteristic peaks at 400 and 619 nm, corresponding to the $\pi$-$\pi^*$ transitions of P3HT. This observation hints at the extended $\pi$-electron delocalization of the conjugated P3HT moiety.[49,55,57] The differences in the UV-Vis spectra of the P3HT-g-PP powder and its film likely arise from the larger surface area of the former. Furthermore, the graft ratio of P3HT on PP powder is higher than that of the PP film, which results in an extended $\pi$-conjugated structure of the P3HT moiety on the surface of the PP powder.

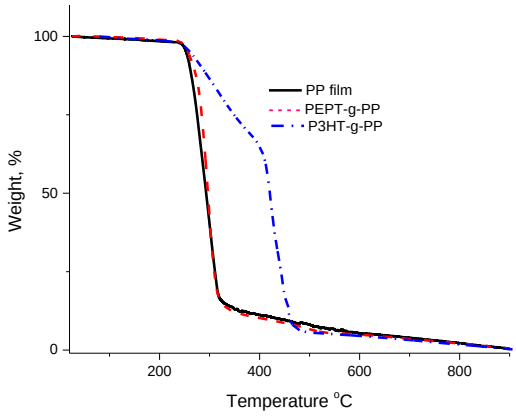


**Figure 4.13. TGA curves of PP, PEPT-g-PP and P3HT-g-PP films**

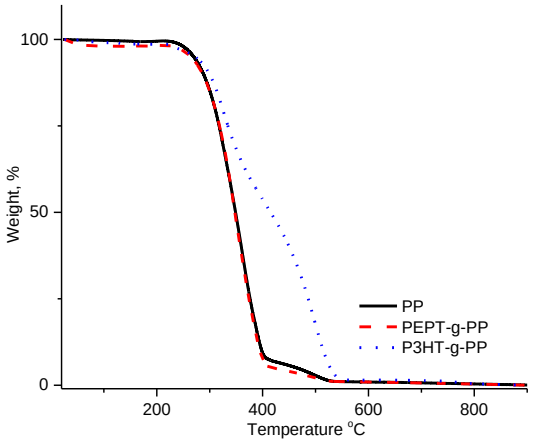


**Figure 4.14. TGA curves of PP, PEPT-g-PP and P3HT-g-PP powders**

The effect of grafting on the thermal stability of PP was studied by TGA. The results for PP, PEPT-g-PP, and P3HT-g-PP films measured in the air are shown in Figure 4.13. Beyler and Hirschler have proposed four mechanisms for the thermal decomposition of polymers: random chain scission, end-chain scission, chain-stripping, and cross-linking.[58] The TG curve of the PP film in air shows a single weight loss step. The thermal degradation starts at 240 °C, and the weight loss of PP film continues up to 85% at 300 °C. This degradation behavior results from random chain scission following the radical transfer process.[59] The TG curve of the PEPT-g-PP film demonstrates its thermal stability, which is similar to that of the PP film. The TG curve of the PEPT-g-PP shows a single degradation stage from 244 to 380 °C, and the weight loss is as high as 83 %

at 300 °C. As shown in Figure 4.13, the P3HT-g-PP film decomposed in two stages. The first stage of degradation occurs from 230 to 330 °C, with a weight loss ranging from 3 to 38 % that corresponds to the thermal decomposition of the PP and PEPT chains. The second stage of degradation of P3HT-g-PP occurs between 330 and 500 °C, and there was a weight loss of between 38 and 95% owing to the presence of P3HT. The thermal stability of P3HT beginning at 350 °C has been previously reported along with the characterization of P3HT and its copolymers.[40,44] These results indicate that the thermal stability of the P3HT-g-PP film is higher than that of the PP and PEPT-g-PP films.

The TGA curves of the PP and PEPT-g-PP powders are also similar (as shown in Figure 4.14). As observed for the PP film, the powder form also shows a single stage thermal decomposition event between 240 and 400 °C, and the weight loss was from 1 to 92%. In contrast, a two-stage decomposition process was observed for the P3HT-g-PP powder. The first decomposition phase lasted from 242 to 370 °C and the second stage occurred between 372 and 555 °C. The first decomposition step can be assigned to the random scission of PP [58,59] and the chain scission of PEPT, while the second degradation step can be attributed to the thermal scission of P3HT.[40,44] The TGA results shown in Figures 4.13 and 4.14 indicate that the thermal stability of PP was significantly improved by the grafting of P3HT onto the PP surface.

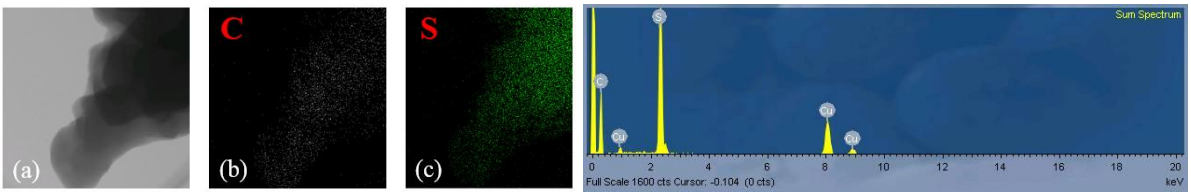


**Figure 4.15. EDX mapping images of P3HT-g-PP**

**Figure 4.16. EDX spectrum of P3HT-g-PP**

To confirm the presence of the sulfur (originating from P3HT) in the grafted PP samples, we carried out TEM-EDX analyses on the P3HT-g-PP samples. The TEM EDX spectra are shown in Figures 4.15 and 4.16, and reveal that the P3HT-g-PP samples contain carbon and sulfur. To distinguish the sulfur (S) contribution from PETP and P3HT grafts on the PP surface, we used quantitative EDX microanalysis and calculated the weight and atomic percentages of the elements, as listed in Table 4.1.

**Table 4.1: The elemental composition of the PEPT-g-PP and P3HT-g-PP samples**

| | | S | C |
|---|---|---|---|
| PEPT-g-PP | Weight % | 14.11 | 85.89 |
| | Atomic % | 5.80 | 94.20 |
| P3HT-g-PP | Weight % | 39.82 | 60.18 |
| | Atomic % | 27.40 | 72.60 |

As shown in Table 4.1, the mass and atomic percentages of S from P3HT-g-PP are higher than those of PEPT-g-PP. The higher mass and atomic percent of S may originate from the P3HT formed during the oxidative polymerization PEPT-g-PP with 3HT. However, EDX techniques only provide information on the chemical composition of elements with atomic numbers greater than three (Z > 3), so hydrogen cannot be detected by EDX. [60] Consequently, these values do not correctly account for the quantity of sulfur on the PP surface; however, they may indicate the difference in the sulfur content of the PEPT-g-PP and P3HT-g-PP samples.

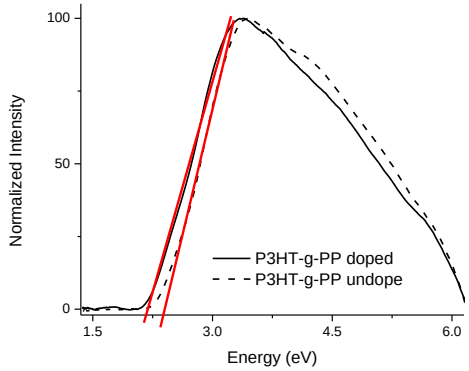


**Figure 4.17. UV-Vis spectra of the undoped and doped P3HT-g-PP films**

UV-Vis spectra of the P3HT-g-PP film were also obtained before and after doping it with iodine at 23 °C (Figure 4.17). The maximum intensity peaks of the undoped and doped samples were observed at 3.4 and 3.3 eV, respectively. The optical band gap energy was calculated indirectly by finding the intersection point between the linear extrapolation (red line in Figure 4.17) and the x-axis. The energy values at 2.16 and 2.40 eV are identical to the energies of the $\pi$-$\pi^*$ transitions of the undoped and doped samples of the P3HT-g-PP samples.[54] These results indicate there is a slight change in the band gap from 2.40 to 2.16 eV on doping with $I_2$. The P3HT-g-PP powder was compressed to form a film, and we measured the electric conductivity using a four-probe method. The conductivity of P3HT-g-PP powder is 0.02 S/cm, indicating that the surface of PP powder was well grafted with P3HT.

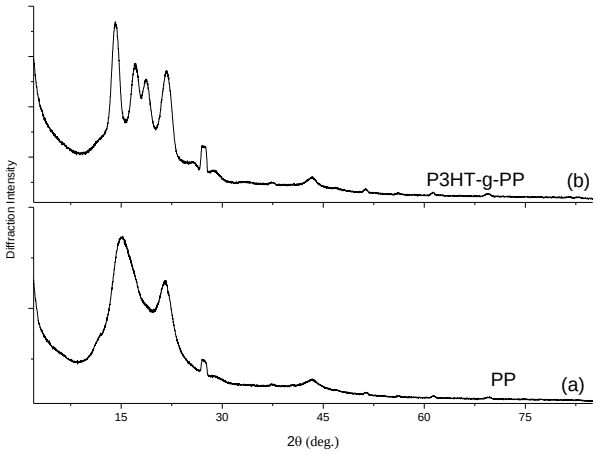


**Figure 4.18. XRD patterns of (a) PP and (b) P3HT-g-PP samples**

The crystal structures of the PP and P3HT-g-PP samples were obtained using X-ray diffraction measurements (as shown in Figure 4.18). Several characteristic peaks that arise from the semi-crystalline structure of PP were observed ranging from 12 to 25°.[61] The influence of grafting on the surface of PP results in a major change in the characteristic peaks in the range 12−25°. Two new peaks at 2θ = 17.1° and 18.7° arise from the crystalline structure of P3HT, as shown in Figure 4.18b.[62-64]

### *4.3.2 Grafting P3HT on PP through $FeCl_3$ oxidative polymerization PS-g-PP and 3HT monomers*

In method described above, 3-(4-ethenylphenyl)thiophene used for the surface-functionalized PP in the first step, need to be synthesized via Suzuki-Miyaura cross-coupling reaction. To simplify the procedure, in this work, 3-(4-ethenylphenyl)thiophene monomer is replaced by styrene monomer. The grafting of P3HT onto the surface of PP was illustrated in Scheme 4.3. In the first step, PP is functionalized with PS to form polystyrene-graft-PP (PS-g-PP) using radicals formed by a mixture of tri-n-butylborane (TBB) and oxygen

molecules in air [36-39]. In the second step, conductive P3HT layer is fabricated on the PP surface by oxidative polymerization 3HT monomers and PS-g-PP.

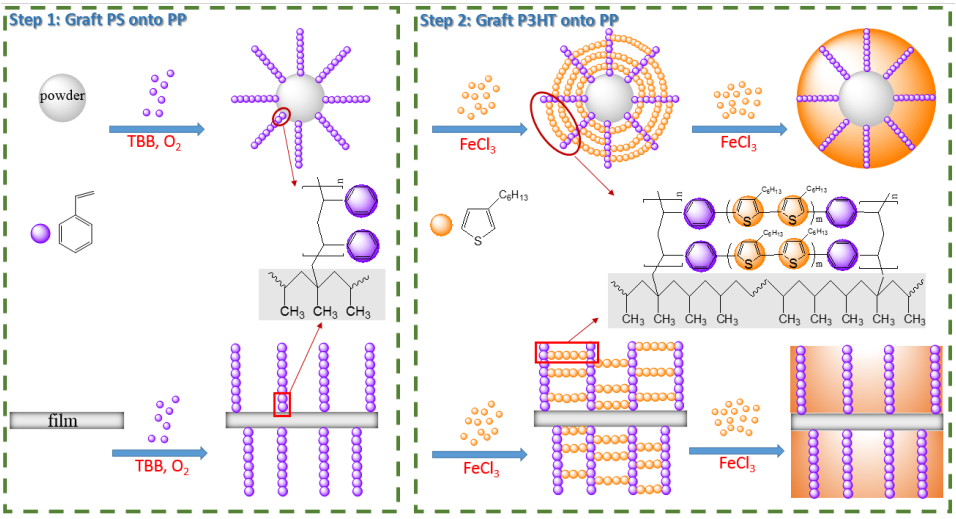


**Scheme 4.3. Grafting of PS and P3HT onto PP film and powder**

The FT-IR (Figure 4.19) and Raman (Figure 4.20) spectra of PP and PS-g-PP were used to confirm the grafting of PS onto the PP surface. The FT-IR spectra of PP and PS-g-PP are shown in Figure 4.19. Compared to the spectrum of PP, Some new bands appear on the spectrum of PS-g-PP (as shown in Figure 4.19b). There are three medium bands in the range of 3100-3000 $cm^{-1}$, belong to the =C–H stretching vibrations from aromatic ring. Another medium band at 1490 $cm^{-1}$ is assigned to the C=C aromatic ring stretching vibration. A strong band observed at 697 $cm^{-1}$ is the characteristic of the ring out of plane deformation. These appeared bands are presented in the polystyrene spectrum.[45] These additional bands indicate that PS was successfully grafted onto the PP surface.

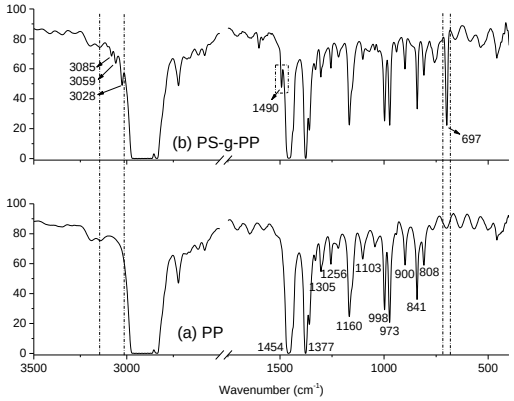


**Figure 4.19. FT-IR spectra of (a) PP and (b) PS-g-PP**

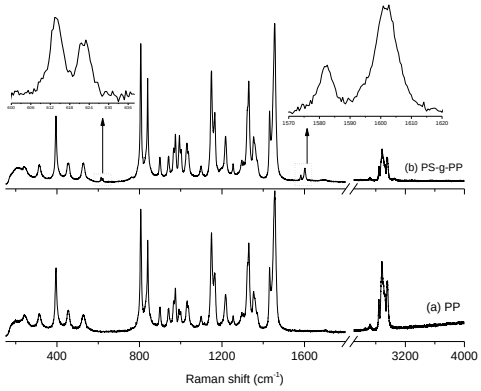


**Figure 4.20. Raman spectra of (a) PP and (b) PS-g-PP**

The Raman spectra of neat PP and PS-g-PP are shown in Figure 4.20. After grafting, some new bands appear on the spectra of PS-g-PP (as shown in Figure 4.20b). A weak band in the range of 1570-1620 $cm^{-1}$ is ascribed to a C=C frequency of aromatic ring chain vibration from styrene [46]. The appeared two bands from 600-636 $cm^{-1}$ verify the presence of CH out of plane vibration in aromatic group [45].

The grafting ratio ($G_r$) of PS onto PP or P3HT onto PP was calculated according to equation $G_r = (m_g - m_o)/m_o \times 100\%$ [37,39] where $G_r$ is the grafting ratio of PS on PP; $m_o$ and $m_g$ are the weights of PP before and after grafting, respectively. In the case of grafting P3HT onto PP, $m_o$ and $m_g$ are the weights of PS-g-PP before and after the grafting with P3HT, respectively.

The graft ratio of PP film was lower than that of PP powder because of the higher surface area of powder compared to the film. In fact, the graft ratio of PS onto the PP film is only 0.4 % while this number is 1.5% in the case of grafting PS onto the PP powder. In this work, when 3HT monomers were oxidative polymerization with PS-g-PP, the 3HT unit would be introduced into the para position of aromatic ring from PS-g-PP (as shown in Scheme 4.3) because the incorporation of 3HT units into the ortho and meta positions may deteriorate the effect conjugation length of the resulting polymer chain and cause the steric repulsion between the incorporated units [65]. In addition, the grafting ratio of 3HT onto the PS-g-PP was also affected significantly by the surface area. In detail, the grafting of P3HT onto the PS-g-PP powder results in a high grafting degree of 3.9 % while this value is just 1.3 % in the case of grafting P3HT onto the PS-g-PP film.

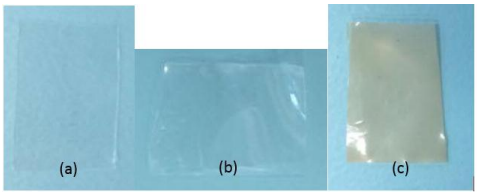


**Figure 4.21. Images of (a) PP, (b) PS-g-PP, and (c) P3HT-g-PP films**

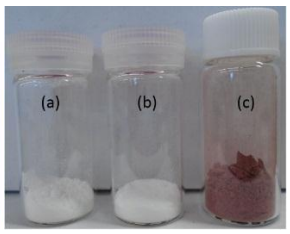


**Figure 4.22. Images of (a) PP, (b) PS-g-PP, and (c) P3HT-g-PP powders**

During the graft reactions of poly(3-hexylthiophene) to PS-g-PP, two reactions occur simultaneously, namely the oxidative self-homopolymerization of 3-hexylthiophene and the graft polymerization of 3-hexylthiophene onto PS-g-PP. The characterization data for the P3HT extracted from the crude grafted product is as same as Figure 4.9. In this case, the number-average molecular weight ($M_n$) and the polydispersity index (PDI) of extracted P3HT are 75 kDa and 3.4, respectively. The color of PS-g-PP film and powder are shown in Figures 4.21b and 4.22b and both film and powder after modifying with P3HT became orange upon immersion in chloroform solution.

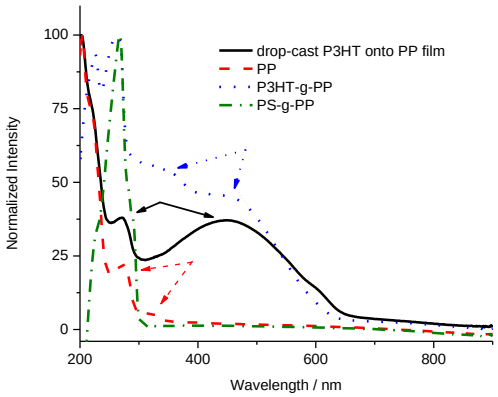


**Figure 4.23. UV-vis spectra of PP, PS-g-PP, P3HT-g-PP, and drop-cast P3HT on the PP films**

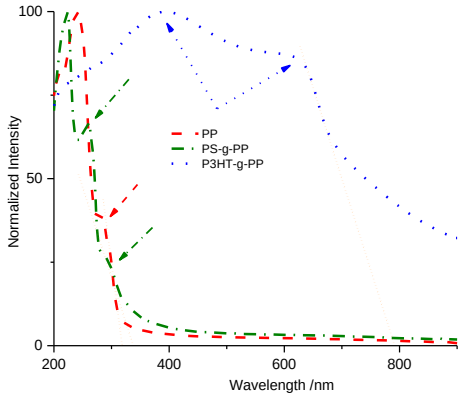


**Figure 4.24. UV-vis spectra of PP, PS-g-PP, and P3HT-g-PP onto the PP powders**

In Figure 4.23, PP film (red dashed line) showed absorption band at around 270 nm and a weak absorption peak at 320 nm. The absorption peak at 270 nm is attributed to a trace of α,β-unsaturated carbonyl groups [51-53]. The weak absorption peak at 320 nm corresponds to a n-$\pi^*$ transition of a trace of conjugated carbonyl group [51]. The spectrum of PS-g-PP (green dashed dotted line) exhibits a strong absorption band at around 270 nm, this sharp absorption peak at 4.6 eV corresponds to the interaction between phenyl groups and the evidence of a $\pi$–$\pi^*$ excitation from aromatic group of polystyrene [66]. The maxima absorption of the spectrum of P3HT-g-PP (blue dotted line) were 268, 333 and 458 nm. A strong peak at 268 nm confirmed the presence

of the interaction of aromatic groups from PS. Two peaks at 333 and 458 nm could be due to a characteristic $\pi$-$\pi^*$ transition of P3HT indicating the $\pi$-electron delocalization of the conjugated P3HT moiety [54,55,57]. A 50 µl chloroform solution of P3HT was drop cast onto the PP film, dried in vacuum for 12h, then the UV-vis spectrum was measured. The result (black solid line) in Figure 4.23 shows two peaks at 276 and 455 nm. The peak at 276 nm is identical to a trace of $\alpha,\beta$-unsaturated carbonyl groups from PP [51-53] while the observed peak at 455 nm indicates a $\pi$-$\pi^*$ transition from the cast P3HT [40,44]. The onset of absorption wavelength considering as the optical band gap energy that is calculated indirectly by finding the intersection point between the tangent line to a curve and the x axis (as shown in Figure 6). The optical band gap energy of PP and PS-g-PP films are 4.09 and 4.03 eV belongs to localized electronic state of PP [67-69] and PS [70,71], respectively. The band gap energy of P3HT-g-PP and drop cast P3HT onto the PP films are 1.92 and 1.79 eV, which are attributed to $\pi$-conjugation from 3HT units [72].

The UV-vis spectra of the PP, PS-g-PP, and P3HT-g-PP powders show similar results to those of the films. The spectrum of the PP powder (red dash line) shows two absorption peaks in the ultra-violet region (241 and 285 nm) that belong to n-$\pi^*$ excitation of a trace of carbonyl group [51-53]. The spectrum of the PS-g-PP (green dashed dotted line) shows the absorption maxima of three peaks at 223, 261, and 299 nm. Two peaks at 223 and 299 nm are identical to the wavelength from the polymer chain of PP film, while a strong peak at 261 nm is associated with the carbon-carbon double bonds from aromatic groups of PS [66]. The P3HT-g-PP (blue dot line) shows two peaks at 392 and 624 nm, which are characteristic $\pi$-$\pi^*$ transition of P3HT, indicating a long $\pi$-electron delocalization of the conjugated P3HT moiety [49,55,57]. The band gap energy also is calculated from the onset wavelength (as shown in Figure 4.24). The energy values at 4.00 and 3.75 eV are obviously identical energy to localized electronic state of PP [67-69], and PS [70,71], respectively. The band gap energy of P3HT-g-PP powder is 1.57 eV, which is lower than that of P3HT-g-PP film of 1.92 eV. The reason could be elucidate from the larger surface area of the powder, so the grafting ratio of P3HT onto the PP powder is higher than that of PP film, resulting in higher content of long $\pi$-conjugation structure of the P3HT moiety on the surface of the PP powder.

**Table 4.2: The absorption wavelength and optical band gap of PP and grafted PP products**

| Samples | | Absorption wavelength onset (nm) | Optical band gap (eV) | Emission wavelength (nm) |
|---|---|---|---|---|
| Film | PP | 303 | 4.09 | - |
| | PS-g-PP | 307 | 4.03 | - |
| | P3HT-g-PP | 644 | 1.92 | 562 |
| Drop-cast P3HT on PP film | | 689 | 1.79 | 627 |
| Powder | PP | 309 | 4.00 | - |
| | PS-g-PP | 330 | 3.75 | - |
| | P3HT-g-PP | 789 | 1.57 | 615 |

The fluorescence spectra of PP, PS-g-PP, P3HT-g-PP in both film and powder are shown in Figure 4.25. In this figure, only P3HT-g-PP displayed strong emission band in the area from 550 to 620 nm. The emission peak of P3HT-g-PP film ($\lambda$ = 562 nm) appeared at the lower wavelength than that of P3HT-g-PP powder ($\lambda$ = 615 nm). The difference in emission peak of film and powder can be elucidated on the different grafting ratio, powder had a higher grafting ratio than film that resulted in longer wavelength absorption and emission (Table 4.2). The emission peak of the P3HT-g-PP film is blue-shifted by about 65 nm, compared to that of P3HT drop-cast on PP film. The connection between the aromatic compound from PS-g-PP and 3HT units may be responsible for the difference in emission wavelength. The incorporation of aromatic compounds such as benzene, toluene, and xylene into the P3HT main chain has been found to cause a blue-shifted in the absorption peak maximum [65].

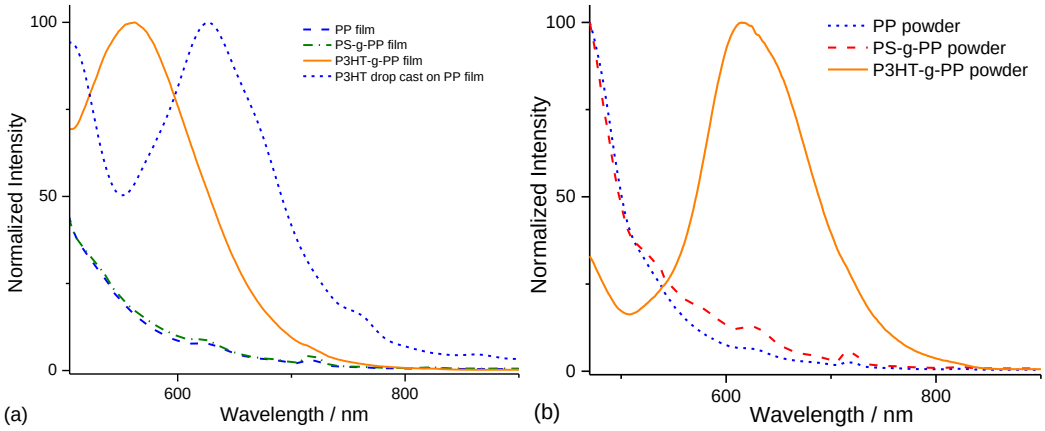


**Figure 4.25: Photoluminescence spectra of PP, PS-g-PP, P3HT-g-PP in film (a) and powder (b)**

TGA was performed to study the effect of grafting on the thermal stability property of PP. As the Figure 4.26 shown, all samples degraded completely and thermally stable without any significant change in weight when the temperature reached over 800ºC. The TG curve of PP film degraded in a single weight loss step in an air atmosphere. The weight loss of PP film underwent thermal degradation beginning at 240ºC and continued up to 85% at 300 °C. The TG curve of PS-g-PP film coincide with that of PP film which shows a single degradation stage that occurred from 244 to 380 °C. The weight loss for PS-g-PP film was up to 83% at 300 °C. The thermal stability of PP is similar to that of PS-g-PP could be elucidate on the analogous degradation properties of PP and PS. The oxidative degradation of PP occurs between 200 and 450 °C while the TG curve of PS starts at 200 °C and ends at 450 °C in the air atmosphere [59]. After grafting P3HT, the TG curve of the P3HT-g-PP showed two stages of degradation as shown in Figure 4.26. The first stage of degradation occurred from 230 °C to 330 °C with weight loss from 3 to 38% corresponding to the thermal decomposition of the PP and PS chain. The second stage of degradation of P3HT-g-PP ranged from 330ºC to 500ºC, where weight loss between 38 and 95% occurred; this weight loss is attributed to the presence of P3HT. The thermal stability of P3HT beginning at 350 °C has been previously reported, along with the characterization of P3HT and its copolymers [40,44]. These results indicate that the thermal stability of the P3HT-g-PP film is higher than that of the PP and PS-g-PP films.

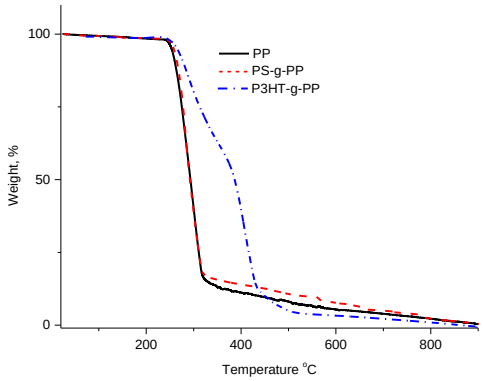


**Figure 4.26. Thermogravimetric (TG) results of PP, PS-g-PP and P3HT-g-PP films**

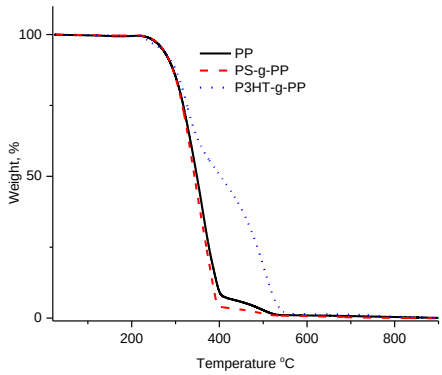


**Figure 4.27. Thermogravimetric (TG) results of PP, PS-g-PP and P3HT-g-PP powders**

The thermal stability of PP, PS-g-PP, and P3HT-g-PP powders show similar results to those of films (Figure 4.27). The TG curve of the PP powder underwent single thermal degradation between 240 and 400 °C, with the weight loss from 1 to 92%. The TG curve of the PS-g-PP powder shows similar thermal decomposition property to that of PP powder. A two stage decomposition was found for the P3HT-g-PP powder. The first decomposition was from 240 to 367 °C and the second step occurred between 368 and 550 °C. The first

decomposition stage is attributed to the random scission of PP and chain scission of PS chain [58,59] while the second degradation step could be due to the thermal scission of P3HT [40,44]. These results reveal that the grafting of P3HT onto the PP surface significantly improved the thermal stability of PP.

The P3HT-g-PP powder was compressed to form a film, and measured the conductivity using a four-probe method. The conductivity of P3HT-g-PP powder is 0.003 S/cm, indicating that the P3HT layer was well built-up on the surface of PP.

The element present in the P3HT-g-PP powder was identified by the EDX microanalysis in TEM. In Figure 4.28, which shows TEM-EDX images, the (a) image shows the STEM of P3HT-g-PP powder. In the (b) image, the green dots represent sulfur elements that were widely distributed throughout the PP powder. This result confirms the presence of sulfur, which originates from the heterocyclic thiophene (3HT) unit grafted to the cellulose. Moreover, as shown in the EDX spectrum, the elemental iron was not detected in P3HT-g-PP powder, which indicated that $Fe^{3+}$ was completely removed by soxhlet extraction with methanol.

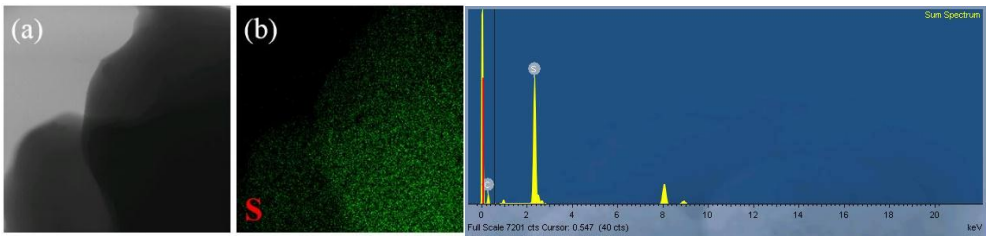


**Figure 4.28: The EDX mapping images (a), (b) and EDX spectrum of P3HT-g-PP powder**

Information concerning the crystal structure of the PP and P3HT-g-PP samples were recorded using X-ray diffraction measurements gave similar results to Figure 4.18

## 4.4 Conclusions

The modification of the PP surface with P3HT was carried out successfully using a simple two-step grafting reaction. In the first step, PP was functionalized with PEPT or PS. In the second step, the build-up of P3HT layer on the PP was made by the oxidative polymerization of 3HT monomers and PS-g-PP or PEPT-g-PP. The incorporation of 3HT units into PS-g-PP results in absorption and emission peaks appeared in UV-vis and photoluminescence spectra. The thermal stability of PP was significantly improved by grafting P3HT onto the PP surface. The doping of the surface with $I_2$ extended the π-conjugation and reduced the band gap energy. The presence of sulfur, originating from the monomeric heterocyclic compound 3HT, was detected by TEM-EDX analysis. The electrical conductivity of the grafted powder indicates that the P3HT layer was well grafted onto the surface of the PP. The grafting of P3HT onto the PP surface also resulted in changes to the crystallinity of the PP.

## 4.5 References


(1) Bhattacharya, A.; Misra, B. N. *Prog. Polym. Sci.* **2004**, *29*, 767-814.

(2) Chen, X.; Wei, S.; Yadav, A.; Patil, R.; Zhu, J.; Ximenes, R.; Sun, L.; Guo, Z. *Macromol. Mater. Eng.* **2011**, *296*, 434−443.

(3) Wanasekara, N.; Chalivendra, V.; Calvert, P. *Polym. Degrad. Stab.* **2011**, *96*, 432−437.

(4) Mazov, I. N.; Ilinykh, I. A.; Kuznetsov, V. L.; Stepashkin, A. A.; Ergin, K. S.; Muratov, D. S.; Tcherdyntsev, V. V.; Kuznetsov, D. V.; Issi, J. P. *J. Alloys Compd.* **2014**, *586*, S440−S442.

(5) Kim, S.-W. *Korean J. of Chem. Eng.* **1996**, *13*, 97-100.

(6) Knaus, S.; Nennadal, A. *Macromol. Symp.* **1998**, *127*, 257-263.

(7) Bettini, S. H. P.; Agnelli, J. A. M. *J. Appl. Polym. Sci* **2002**, *85*, 2706–2717.

(8) Huang, C.-Y.; Chen, C.-L. *Surf. Coat. Technol.* **2002**, *153*, 194–202.

(9) Thakur, V. K.; Vennerberg, D.; Kessler, M. R. *ACS Appl. Mater. Interfaces* **2014**, *6*, 9349−9356.

(10) Balart, J.; Fombuena, V.; Boronat, T.; Reig, M. J.; Balart, R. *J. Mater. Sci.* **2012**, *47*, 2375–2383.

(11) Kostov, K. G.; Nishime, T. M. C.; Hein, L. R. O.; Toth, A. *Surf. Coat. Technol.* **2013**, *234*, 60-66.

(12) Troian-Gautier, L.; Martínez-Tong, D. E.; Hubert, J.; Reniers, F.; Sferrazza, M.; Mattiuzzi, A.; Lagrost, C.; Jabin, I. *J. Phys. Chem. C* **2016**, *120*, 22936–22945.
(13) Nagase, Y.; Naruse, A.; Matsui, K. *Polymer* **1990**, *31*, 121-125.
(14) Dualeh, A. J.; Steiner, C. A. *Macromolecules* **1991**, *24*, 112-116.
(15) Eisenbach, C. D.; Heinemann, T. *Macromol. Chem. Phys.* **1995**, *196*, 2669–2686.
(16) Se¸k, D.; Kaczmarczyk, B. *Polymer* **1997**, *38*, 2925–2931.
(17) Kline, R. J.; Mcgehee, M. D.; Toney, M. F. *Nat. Mater.* **2006**, *5*, 222-228.
(18) MacDiarmid, A. G. *Angew. Chem. Int. Ed.* **2001**, *40*, 2581-2590.
(19) Xin, H.; Ren, G.; Kim, F. S.; Jenekhe, S. A. *Chem. Mater.* **2008**, *20*, 6199-6207.
(20) Xin, H.; Kim, F. S.; Jenekhe, S. A. *J. Am. Chem. Soc.* **2008**, *130*, 5424-5425.
(21) Gunes, S.; Neugebauer, H.; Sariciftci, N. S. *Chem. Rev.* **2007**, *107*, 1324-1338.
(22) Katz, H. E. *J. Mater. Chem.* **1997**, *7*, 369-376.
(23) Burroughes, J. H.; Bradley, D. D. C.; Brown, A. R.; Marks, R. N.; Mackay, K.; Friend, R. H.; Burns, P. L.; Holmes, A. B. *Nature* **1990**, *347*, 539-541.
(24) McQuade, D. T.; Pullen, A. E.; Swager, T. M. *Chem. Rev.* **2000**, *100*, 2537-2574.
(25) Roncali, J. *Chem. Rev.* **1992**, *92*, 711-738.
(26) Jin, M.; Liu, Y.; Li, Y.; Chang, Y.; Fu, D.; Zhao, H.; Han, G. *J. Appl. Polym. Sci.* **2011**, *122*, 3415–3422
(27) Huang, X.; Yu, Y.-H.; Llergo, O. L. d.; Marquez, S. M.; Cheng, Z. *RSC Adv.* **2017**, *7*, 9495-9500.
(28) Kang, G.; Li, L.; Wang, W.; Yu, D. *RSC Adv.* **2016**, *6*, 75038-75044
(29) Wang, X.; Meng, S.; Ma, W.; Pionteck, J.; Gnanaseelan, M.; Zhou, Z.; Sun, B.; Qin, Z.; Zhu, M. *React. Funct. Polym.* **2017**, *112*, 74-80.
(30) Yoshino, K.; Yin, X. H.; Morita, S.; Nakanishi, Y.; Nakagawa, S.; Yamamoto, H.; Watanuki, T.; Isa, I. *Jpn. J. Appl. Phys.* **1993**, *32*, 979-981.
(31) Kurachi, K.; Kise, H. *Polym. J.* **1994**, *26*, 1325-1331.
(32) Yang, J.; Hou, J.; Zhu, W.; Xu, M.; Wan, M. *Synth. Met.* **1996**, *80*, 283-289.
(33) Marcinčin, A.; Jambrich, M. *Springer Netherlands* **1999**, *Polypropylene* 813-820.
(34) Jambrich, M.; Hodul, P. *Springer Netherlands* **1999**, *Polypropylene*, 806-812.
(35) Chanunpanich, N.; Strzhemechny, Y. M.; Schwarz, S. A.; Dormicik, J.; Janke, A.; Braun, H. G.; Kratzmüller, T. *Polym. Int.* **2003**, *52*, 172-178.
(36) Wang, Z. M.; Hong, H.; Chung, T. C. *Macromolecules* **2005**, *38*, 8966-8970.
(37) Okamura, H.; Sudo, A.; Endo, T. *J. Polym. Sci. A. Polym. Chem.* **2009**, *47*, 6163–6167.
(38) Liu, S.; Zheng, Z.; Li, M.; Wang, X. *Res Chem Intermed* **2012**, *38*, 1893–1907.
(39) Liu, S.; Zheng, Z.; Li, M.; Wang, X. *J. Appl. Polym. Sci* **2012**, *125*, 3335–3344.
(40) Hai, T. A. P.; Sugimoto, R. *Synth. Met.* **2016**, *220*, 59-71.
(41) Blangetti, M.; Rosso, H.; Prandi, C.; Deagostino, A.; Venturello, P. *Molecules* **2013**, *18*, 1188-1213.
(42) Miyaura, N.; Suzuki, A. *Chem. Rev.* **1995**, *95*, 2457-2483.
(43) Miyaura, N.; Yanagi, T.; Suzuki, A. *Synth. Commun.* **1981**, *11*, 513-519.
(44) Hai, T. A. P.; Sugimoto, R. *Polym. J.* **2016**, *48*, 1115-1121.
(45) Socrates, G.: Infrared and Raman Characteristic Group Frequencies. *John Wiley & Sons, Ltd* **2001**, *West Sussex, England*, 268-269.
(46) Palm, A.: Raman Spectrum of Polystyrene. *J. Phys. Chem.* **1951**, *55*, 1320–1324.
(47) Báez, M. A. d.; Hendra, P. J.; Judkins, M. *Spectroc. Acta Pt. A-Molec. Biomolec. Spectr.* **1995**, *51*, 2117-2124.
(48) Wang, X.; Michielsen, S. *J. Appl. Polym. Sci.* **2000**, *82*, 1330–1338
(49) Sakakibara, K.; Rosenau, T. *Holzforschung* **2012**, *66*, 9-19.
(50) Sato, M. A.; Morii, H. *Macromolecules* **1991**, *24*, 1196-1200.
(51) Allen, N. S. *Polym. Photochem.* **1981**, *1*, 43-55.
(52) Charlesby, A.; Partridge, R. H. *Proc. Roy. Soc.* **1965**, *A283*, 312-314.
(53) Allen, N. S.; Homer, J.; McKellar, J. F.; Wood, D. G. M. *J. Appl. Polym. Sci* **1977**, *21*, 3147-3152.
(54) Wang, C.; Duong, D. T.; Vandewal, K.; Rivnay, J.; Salleo, A. *Phys. Rev. B* **2015**, *91*, 1-7.
(55) Shrotriya, V.; Ouyang, J.; Tseng, R. J.; Li, G.; Yang, Y. *Chem. Phys. Lett.* **2005**, *411*, 138–143.
(56) Liu, Y.; Nishiwaki, N.; Saigo, K.; Sugimoto, R. *Polymer Bulletin* **2015**, *72*, 1817-1826.
(57) Li, X.-G.; Li, J.; Meng, Q.-K.; Huang, M.-R. *J. Phys. Chem. B* **2009**, *113*, 9718–9727.
(58) C.L., B.; M.M., H.: Thermal Decomposition of Polymers. *SFPE Handbook of Fire Protection Engineering 2* **2002**, *Section 1*, *Chapter 7*, 111-131.
(59) Peterson, J. D.; Vyazovkin, S.; Wight, C. A. *Macromol. Chem. Phys.* **2001**, *202*, 775-784.
(60) Stojilovic, N. *J. Chem. Educ.* **2012**, *89*, 1331−1332.
(61) Nishino, T.; Matsumoto, T.; Nakamae, K. *Polym. Eng. Sci.* **2000**, *40*, 336-343.
(62) Colle, R.; Grosso, G.; Ronzani, A.; Zicovich-Wilson, C. M. *Phys. Status Solidi B* **2011**, *248*, 1360-1368.

(63) Kline, R. J.; McGehee, M. D.; Kadnikova, E. N.; Liu, J.; Fréchet, J. M. J.; Toney, M. F. *Macromolecules* **2005**, *38*, 3312–3319.
(64) Kaniowski, T.; Łużny, W.; Nizioł, S.; Sanetra, J.; Trznadel, M. *Synth. Met.* **1998**, *92*, 7-12.
(65) Liu, Y.; Nishiwaki, N.; Saigo, K.; Sugimoto, R. *Polym. Bull.* **2015**, *72*, 1817–1826.
(66) Li, T.; Zhou, C.; Jiang, M. *Polym. Bull.* **1991**, *25*, 211-216.
(67) Tanaka, T. *J. Appl. Phys.* **1973**, *44*, 2430-2432.
(68) Mishraa, R.; Tripathy, S. P.; Sinha, D.; Dwivedi, K. K.; Ghosh, S.; Khathing, D. T.; Müller, M.; Fink, D.; Chung, W. H. *Nucl. Instrum. Methods Phys. Res. B* **2000**, *168*, 59-64.
(69) Ohki, Y.; Fuse, N.; Arai, T. *IEEE Trans. Dielectr. Electr. Insul.* **2010**, *1*, 1-4.
(70) Al-Ramadin, Y.; Zihlif, A.; Elimat, Z. M. *J. Thermoplast. Compos. Mater.* **2014**, *29*, 1-15.
(71) Rathore, B. S.; Gaur, M. S.; Singh, K. S. *Macromol. Symp.* **2012**, *315*, 169–176.
(72) Yang, Y.-L.; Lee, Y.-H.; Lee, Y.-P.; Chiang, C.-J.; Shen, C.; Wu, C.-C.; Ohta, Y.; Yokozawa, T.; Dai, C.-A. *Polym. Int.* **2014**, *63*, 2068–2075.

# Chapter 5:

# Surface functionalization of biomaterials substrate with poly(3-hexylthiophene)

## 5.1 Introduction

The disadvantage of fossil fuels such as pollution and non-renewable source, which is resulting in increasing attention of renewable resources to replace materials from crude oil. Cellulose, also known as polysaccharide, is a biopolymer found in nature that consists of a long chain with many thousands of glucose unit connected by β-1,4 linkages.[1,2] As sustainable, biodegradable resources having a positive impact on the ecosystem, cellulose and its derivatives have found in widespread applications in the pharmaceutical, fiber, paper, paint and textile industries.[3,4] Chitin and chitosan are crucial biopolymers having special chemical reactivity and physical properties, and found in diverse applications of drug delivery system, antibacterial activity and other systems[5-7]. Surface modification of biomaterials such as cellulose, chitin and chitosan to enhance its physical and chemical properties and improve its functionality has been researched for more than two decades. Three typical techniques for surface modification have been classified as grafting to, grafting from, and grafting through processes.[2,3] Moreover, there are three main methods for grafting vinyl monomers to polysaccharide: (1) free radical polymerization[8-11] , (2) ionic and ring opening polymerization[12-17] and (3) living radical polymerization[18-24].

Recently, advances in the research combining conjugated polymers and biomaterials have driven new interest in enhancing the novel functionalities of materials and further opening the scope of applications such as biosensor, bioelectronics, tissue engineering, and biofuel cell [25-28].

A polythiophene-cellulose composite was synthesized by a two-step reaction in which the thiophene monomer was oxidatively copolymerized with oligothiophene-substituted cellulose derivatives.[29] The fabrication of a thin oriented film of n-butylcinnamoylcellulose and polythiophene simultaneously improve the conductivity and mechanical properties.[30] Composites of cellulose and different conducting polymers (polypyrrole or polyaniline) that utilize the interplay of the two metarials have been produced.[31,32] Composites of cellulose and polyaniline have been applied as the electrodes in fuel cells [33] and energy conversion [34]. A cellulose fiber/graphene oxide material exhibited excellent electromagnetic interference shielding for potential applications in aerospace and wearable electronic devices [35]. The core-sheath structure of a cellulose/polypyrrole composite reinforced with carbon nanofiber resulted in an environmentally friendly electrode material for sodium-ion batteries [36] . The substituted polyaniline/chitosan composites was synthesized using ammonium perdisulfate as an oxidant in an aqueous acid [37]. Grafting of polyaniline onto the radiation crosslinked chitosan has been applied for sensor and electrodes of polymeric batteries [38]. Chitosan-graft-polyaniline based hydrogels was synthesized by simple oxidative method using ammonium persulfate, resulting in high and reversible swelling properties in hydrogel with intrinsic conductivity[39]. Electron beam radiation has been used to synthesize chitin-polyaniline nanocomposite [40]. Polythiophene chitosan magnetic nanocomposite was applied for extraction of triazine herbicides from aquatic media [41]. Grafting polypyrrole onto chitin was accomplished using ammonium peroxy disulphate (APS) as an initiator [42]. However, the main purposes of these works were to make the composite materials due to the insolubility of polythiophene, polypyrrole, and polyaniline. The goal of our research is to graft conjugated polymers such as poly(3-hexylthiophene) directly to chitin/chitosan. Herein, we report a new methodology for directly grafting conjugated polymers to chitin/chitosan by oxidative polymerization using $FeCl_3$.

## 5.2 Experimental section

### *5.2.1 Chemicals*

Cellulose powder was purchased from Wako Pure Chemical Industry Ltd. Cellulose paper was purchased from Toyo Roshi Kaisha, Ltd. 3-Hexylthiophene monomer, chitin, chitosan and anhydrous $FeCl_3$ were from Tokyo Chemical Industry Ltd and used without any further purification. Solvents such as chloroform hexane, acetonitrile and methanol were analytical grade, purchased from Wako Pure Chemical Industry Ltd and used

as a received. All solvents (chloroform, hexane, and acetonitrile), medium for graft reaction were dried by standing over 4A molecular sieves for 8h, and purged with argon gas for 20 minutes before using.

### *5.2.2 Measurement*

UV-vis diffuse reflectance spectroscopy was measured using a Jasco V-650 UV-vis spectrometer. Fluorescence emission spectra were recorded on a Jasco spectrofluorometer FP-8300. Thermo gravimetric analysis (TG) was carried out on a Hitachi Thermal Analysis System STA 7200 RV in air from 20 to 700$^{o}$C at a flow rate of 25 ml min$^{-1}$ and heating rate of 10$^{o}$C min$^{-1}$. $^{1}$H NMR spectra (400MHz) and IR spectra were recorded on a Brucker Acsend 400 spectrometer and a Jasco FT/IR – 480 Plus, respectively. X-ray diffraction patterns were recorded with Cu-Kα radiation (X-ray wavelength: 1.5418 Å) in steps of 0.02$^{o}$ over the 2θ range of 10-70$^{o}$ from a Rigaku Smartlab diffractometer equipped with a D-tex detector. Transmission electron microscopy (TEM) images were observed using a JEOL JEM-2100F microscope. Energy dispersive X-ray (EDX) mappings and line scan spectra were recorded on an Oxford INCA Energy TEM 250. Gel permeation chromatography (GPC) was measured in a system equipped with a Jasco PU-2080 Plus pump and a Jasco RI-2031 plus intelligent RI detector. Electrical conductivity was carried out with an Agilent 34401A 6$^{1/2}$ Digit Multimeter resistometer by a four-probe method. Photoemission Yield spectroscopy (PYS) was measured on PYS machine, produced from Bunkoukeiki Co., Ltd. Contact angle was measured on portable contact angle analyzer PGX.

### *5.2.3 Grafting and sample preparation*

All reactions in this work were carried out in an oven-dried Schlenk flask with a stopcock under an argon atmosphere. An amount of 0.3 g cellulose powder and 0.3 g $FeCl_3$ were dispersed in 7 ml chloroform with a magnetic stirrer. After the mixture was performed ultrasound treatment for 20 minutes, the suspension of cellulose and $FeCl_3$ in chloroform was cooled to 0$^{o}$C in an ice bath. The chloroform (3 ml) solution of 3HT (100 mg, 0.6 mmol) was dropped into a magnetically suspension of cellulose and $FeCl_3$. The reaction was conducted for 2 h at 0$^{o}$C under an argon atmosphere. The stoichiometric ratio of 3HT to $FeCl_3$ was 1:4. The reaction was terminated by adding methanol. The obtained product was washed with methanol to remove any residual $FeCl_3$ by Soxhlet apparatus, and then it was extracted with chloroform to eliminate free poly(3-hexylthiophene) (P3HT) homopolymer using a Soxhlet extractor. Finally, the poly(3-hexylthiophene) grafted to cellulose product was dried under vaccum for 12 h. The grafted celluloses are hereinafter referred as P3HT-g-cellulose.

Grafting of 3-hexylthiophene onto cellulose powder in the different ratio between $FeCl_3$ and cellulose were conducted as above, whereas n is the weight ratio of $FeCl_3$ against cellulose (n = weight of $FeCl_3$/weight of cellulose). A series of grafting reactions of 3-hexylthiophene to cellulose in different solvents such as hexane and acetonitrile were also conducted as above. Similarly, grafting reaction of 3-hexylthiophene to chitin and chitosan were prepared as method described above. The grafted chitin and chitosan are hereinafter referred as P3HT-g-chitin and P3HT-g-chitosan, respectively.

## 5.3 Results and discussion

### *5.3.1 Grafting P3HT to cellulose*

In this work, graft reactions were conducted in three solvents: acetonitrile, chloroform, and hexane. During the graft reactions of poly(3-hexylthiophene) to cellulose, two reactions occur simultaneously, namely the oxidative self-homopolymerization of 3-hexylthiophene and the graft polymerization of 3-hexylthiophene onto cellulose. The ungrided 3-hexylthiophene homopolymer was removed from the grafted cellulose as a a chloroform-soluble fraction by using a Soxhlet extractor, and the final product was dried in vacuo for 12 h. Images of all the P3HT-g-cellulose products are shown in Figure 5.1. As shown in this figures, the color of P3HT-g-cellulose depends on the solvent, used in the graft reaction. These color differences can be clearly identified with the naked eye.

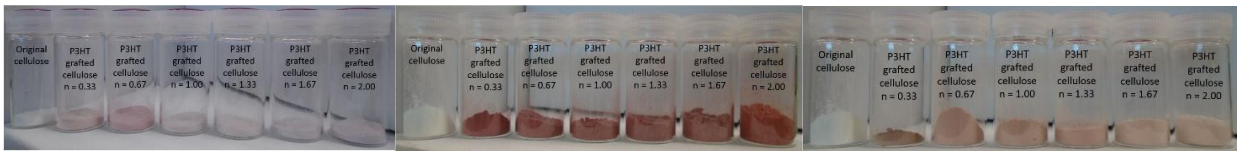


**Figure 5.1: P3HT-g-cellulose product**

**synthesis in chloroform synthesis in hexane synthesis in acetonitrile**

The grafting ratio (Gr) was calculated using the following formula: (A - B - C) / B × 100; where A is the total weight of the cellulose and the crude graft product, B is the weight of the original cellulose, and C is the weight of the extracted homopolymer of 3-hexylthiophene.[43-45] The series of graft reactions was conducted in various solvents to demonstrate the role of the solvent on the process of grafting P3HT to cellulose. Table 5.1 summarizes the results of the grafting ratio and average molecular weight of the grafted product, for reactions conducted in acetonitrile, chloroform, and hexane with different $FeCl_3$/cellulose ratios (wt/wt). In this work, the molecular weight of the extracted homopolymer was used as the molecular weight of the polymer grafted to cellulose.

As shown in Table 5.1, among the three solvents, used for grafting P3HT to cellulose, hexane produced the polymer with the highest molecular weight ($\bar{M}_w$ of around 131 kDa, while the polymer obtained in acetonitrile ($\bar{M}_w$ of around 57 kDa) showed a slightly lower molecular weight than the polymer obtained in chloroform ($\bar{M}_w$ of around 66 kDa). With hexane or chloroform, the graft reaction occurred in a heterogeneous system due to the poor solubility of $FeCl_3$ in these solvents, while acetonitrile provided a homogeneous system for the graft reaction because $FeCl_3$ dissolves completely in this solvent. [46] Moreover, the active sites on the surface of the $FeCl_3$ crystals are the locations where oxidative polymerization occurred with high effectiveness. [47,48] In our previous report, we definitely confirmed that the polymer yield and molecular weight obtained in a heterogeneous system are higher than those obtained in a homogeneous system. [46] In other words, the solubility of $FeCl_3$ in the solvent has an effect on the performance of oxidative polymerization. The effect of the solvent on the grafting ratio (Gr) of P3HT-g-cellulose is shown in Table 5.1. It can be seen that the Gr obtained in hexane (average value of 6.1) is higher than that obtained in chloroform (average value of 4.7), while the graft reaction in acetonitrile resulted in the lowest value (average of 3.6). From Table 5.1 it is seen that the grafting ratio depends slightly on the $FeCl_3$/cellulose weight ratio (wt/wt), regardless of the solvent used. The grafting ratio reached the highest value at n = 1.33 in all solvents used (n = weight of $FeCl_3$/weight of cellulose). The grafting ratio initially increased as n increased, then slightly decreased when n was over 1.33. In these reactions, the stoichiometric ratio of 3HT to $FeCl_3$ was kept constant at 1:4. The competition between self-homopolymerization and the graft reaction in grafting P3HT to cellulose depends on the n value. When n is lower than 1, there are not enough moles of $FeCl_3$ for both the self-homopolymerization and graft polymerizations, which result in a lower grafting ratio. When n is higher than 1.33, the higher number of $FeCl_3$ active sites could accelerate the rate of self-homopolymerization, reducing amount of 3-hexylthiophene grafted to the surface of cellulose. In summary, the optimum n value for grafting is 1.33.

**Table 5.1. The grafting ratio and characterization of extracted P3HT from grafted cellulose**

| Entry | $FeCl_3$/cellulose (wt/wt) | Graft reaction in solvent | Grafting ratio (%) | Molecular weight of extracted P3HT (*) | | |
|---|---|---|---|---|---|---|
| | | | | $M_w$, kDa | PDI | $\bar{M}_w$, kDa |
| 1 | 0.33 | Acetonitrile | 3.6 | 58 | 2.9 | 57.0±1.7 |
| 2 | 0.67 | | 3.7 | 55 | 3.1 | |
| 3 | 1.00 | | 3.7 | 55 | 3.5 | |
| 4 | 1.33 | | 3.8 | 56 | 3.3 | |
| 5 | 1.67 | | 3.6 | 58 | 3.5 | |
| 6 | 2.00 | | 3.5 | 60 | 3.9 | |

| | | | | | | |
|---|---|---|---|---|---|---|
| 7 | 0.33 | Chloroform | 4.7 | 70 | 2.7 | 65.5±2.7 |
| 8 | 0.67 | | 4.7 | 66 | 2.5 | |
| 9 | 1.00 | | 4.8 | 63 | 3.2 | |
| 10 | 1.33 | | 4.9 | 69 | 2.5 | |
| 11 | 1.67 | | 4.7 | 66 | 2.6 | |
| 12 | 2.00 | | 4.5 | 61 | 2.4 | |
| 13 | 0.33 | Hexane | 5.8 | 124 | 3.3 | 131.3±5.8 |
| 14 | 0.67 | | 5.9 | 125 | 3.5 | |
| 15 | 1.00 | | 6.1 | 132 | 3.3 | |
| 16 | 1.33 | | 6.2 | 127 | 3.1 | |
| 17 | 1.67 | | 6.1 | 141 | 3.1 | |
| 18 | 2.00 | | 6.1 | 139 | 3.1 | |

(*) Determined by GPC

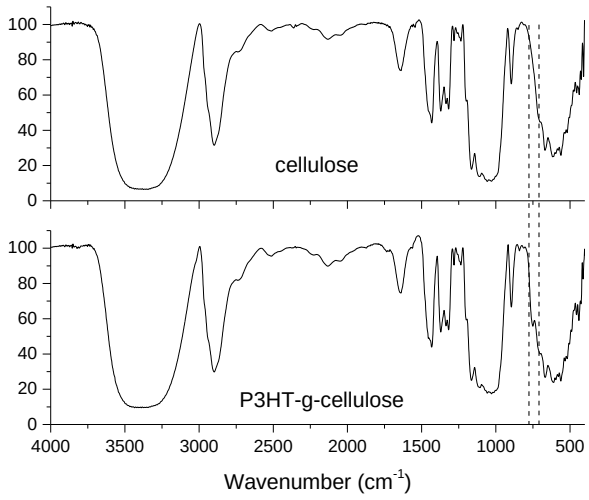


**Figure 5.2. FT-IR spectra of cellulose and P3HT-g-cellulose**

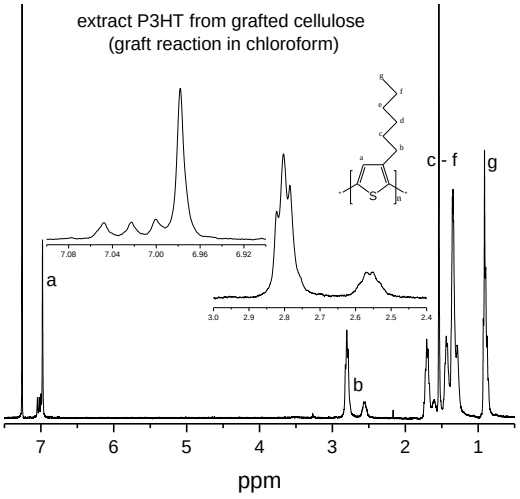


**Figure 5.3. $^{1}$H – NMR spectrum of extracted P3HT from P3HT-g-cellulose**

All P3HT-g-cellulose samples conducted in various solvent (acetonitrile, chloroform, hexane) gave similar spectra. The FT-IR of cellulose and P3HT-g-cellullose are shown in Figure 5.2. Many previous reports have been published on the IR characterization of cellulose.[4,24,32,49-51] The characteristic peaks of cellulose are observed at 2899 cm$^{-1}$ and range from 3250-3500 cm$^{-1}$ which are associated with C-H and O-H stretching vibrations, respectively.[49,50] The prominent peaks attributed to cellulose are observed in the 1314–1372 cm$^{-1}$ range, related to C-H and C-O bending vibrations. [49,50] The characteristic peaks of hexyl group from P3HT including 3000-2800 cm$^{-1}$ region (C-H stretching of the -CH3 and >CH2 groups in the hexyl chain) and 3080-2980 cm-1 range (stretching vibration mode of thiophene at the 4-position Cβ-H) 46 have overlapped with characteristic peaks of cellulose. In the IR spectrum of P3HT-g-cellulose samples, a small additional peak is observed at 748 cm$^{-1}$, attributed to the presence of out-of-plane C-H vibration of the aromatic groups. [52] This aromatic C-H out-of-plane vibration could be associated with the aromatic rings of 3-hexylthiophene.

The characterization data for the homopolymers extracted from the grafted cellulose are shown in Figure 5.3. The signals in the $^{1}$H NMR at δ=0.87 are associated with the methyl proton [46,53] while the peaks observed at δ=2.50 and δ=2.80 belong to the head-to-head (H-H) and head-to-tail (H-T) structure of P3HT, respectively [46,53]. The four triad configurations as follows: HT-HT, TT-HT, HT-HH and TT-HH, respectively [46,53] are observed at δ=6.97, δ=7.00, δ=7.02 and δ=7.05 ppm.

The UV-vis absorption spectra of P3HT-g-cellulose, synthesized in chloroform with different n, are shown in the Figure 5.4. As shown in Figure 5.4, since there is no significant absorption peak for cellulose in the range from 300-800 nm, the maximum peaks at around 514 nm similar to absorption wavelength of the P3HT [54-56], correspond to the $\pi$-$\pi^*$ transitions of 3HT unit in the P3HT-g-cellulose. Although the grafting ratio (Gr) are changed as a result of the difference value of n, the absorption peaks of P3HT-g-cellulose, synthesized in chloroform with various value of n, are not likely to change remarkably. For instance, as shown in Table 5.2, the average number of absorption peak from P3HT-g-cellulose (synthesis in chloroform) is 514$\pm$5 nm. Similar results have also found in the maximum absorption peaks of P3HT-g-cellulose, synthesized in hexane and acetonitrile. In other word, the absorption peak is not depended on the weight ratio of $FeCl_3$/cellulose. All the UV-vis spectra (in Figure 5.4) were characterized by broad absorption peak reflecting the intense $\pi$-conjugated structure of 3HT moieties from the grafted cellulose products. However, a remarkable solvent effect on the shift of the $\boldsymbol{\lambda_{max}^{absorption}}$ could be seen definitely. For instance, as shown in Table 5.2, $\bar{\lambda}_{max}^{abs}$ of P3HT-g-cellulose, synthesized in acetonitrile, chloroform, and hexane are 507, 514, and 543, respectively. The wavelength of the UV-vis absorption in P3HT-g-cellulose, synthesis in hexane, is significantly longer than that of the P3HT-g-cellulose, synthesis in chloroform and acetonitrile (Table 5.2). It is also notice that the molecular weight of P3HT-g-cellulose ($\bar{M}_w$= 131.3), obtained in hexane, is remarkably higher than that of P3HT-g-cellulose, obtained in chloroform ($\bar{M}_w$= 65.5) and acetonitrile ($\bar{M}_w$= 57.0). These indicate that P3HT-g-cellulose, synthesis in hexane, could have higher content of long $\pi$-conjugation structure than P3HT-g-cellulose, synthesis in chloroform and acetonitrile. In addition, the performance of organic field effect transistors and solar cells have been significantly affected by the molecular weight of $\pi$-conjugated polymers. [57-60] In other word, lower molecular weight causes insufficient conjugation length of polymer, results in the shorter absorption wavelength and vice versa.

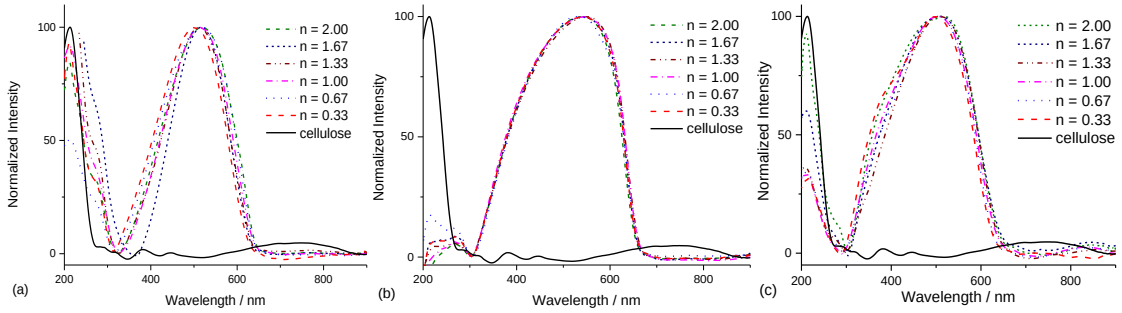


**Figure 5.4. UV-Vis spectra of cellulose and P3HT-g-cellulose**
**(a) synthesis in chloroform (b) synthesis in hexane (c) synthesis in acetonitrile**

Figure 5.5 reveals Fluorescence spectra of P3HT-g-cellulose synthesized in chloroform with different weight ratio of $FeCl_3$/cellulose. In this Figure, all grafted cellulose products display only one strong emission band in the region from 610 to 631 nm. Similar to UV-vis absorption, it can be seen that the emission peaks fluctuate slightly with the average number of 625$\pm$9 since changing the $FeCl_3$/cellulose weight ratio in chloroform. Similarly, the luminescent wavelength of P3HT-g-cellulose, obtained in hexane and acetonitrile, are not affected remarkably by the weight ratio of $FeCl_3$/cellulose. However, the shift of emission peak of P3HT-g-cellulose depended on solvent, used for synthesis. For instance, the fluorescence spectra of P3HT-g-cellulose prepared in hexane ($\bar{\lambda}_{max}^{emis}$ = 662$\pm$2**)** were higher than those in chloform ($\bar{\lambda}_{max}^{emis}$ = 625$\pm$9**)** while P3HT-g-cellulose obtained in acetonitrile gave the shortest wavelength ($\bar{\lambda}_{max}^{emis}$ = 606$\pm$5**)** (as shown in Table 5.2). Higher molecular weight of $\pi$-conjugated polymers, providing sufficient conjugation length, which offers longer wavelength absorption and luminescent than lower molecular weight. [60-62] GPC results in Table 5.1 indicate that P3HT-g-cellulose obtained in hexane gave larger $\bar{M}_w$ than that obtained in acetonitrile and chloroform. Therefore, the shift of emission peak (from 606 to 662), presents that the longer conjugated length makes the absorption peak tend to be shifted toward the longer wavelength region, consequently, the emission spectrum as well. In summary, the optical properties of P3HT-g-cellulose shown in both UV-vis absorption and photoluminescent spectra, reflected that the $\pi$-conjugation structure of P3HT have been successfully

grafted to the surface of cellulose. Moreover, the position of absorption and emission peaks of P3HT-g-cellluose totally depend on the solvent used for graft reaction.

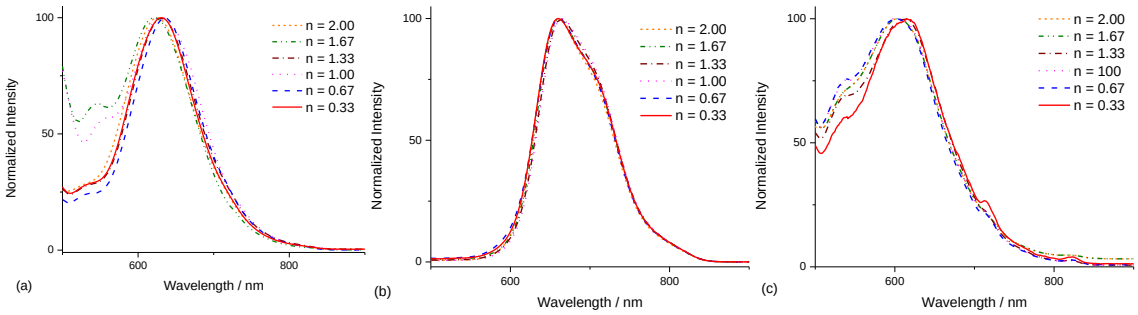


**Figure 5.5. Fluorescence spectra of cellulose and P3HT-g-cellulose**
**(a) synthesis in chloroform (b) synthesis in hexane (c) synthesis in acetonitrile**

**Table 5.2. The optical properties of grafted cellulose**

| Entry | $FeCl_3$/cellulose (wt/wt) | Graft reaction in solvents | $\lambda_{max}^{absorption}$ (nm) | $\bar{\lambda}_{max}^{abs}$ (nm) | $\lambda_{max}^{emission}$ (nm) | $\bar{\lambda}_{max}^{emis}$ (nm) |
|---|---|---|---|---|---|---|
| 1 | 0.33 | Acetonitrile | 499 | 507±4 | 615 | 606±5 |
| 2 | 0.67 | | 507 | | 604 | |
| 3 | 1.00 | | 504 | | 597 | |
| 4 | 1.33 | | 510 | | 613 | |
| 5 | 1.67 | | 510 | | 604 | |
| 6 | 2.00 | | 514 | | 604 | |
| 7 | 0.33 | Chloroform | 502 | 514±5 | 631 | 625±9 |
| 8 | 0.67 | | 518 | | 636 | |
| 9 | 1.00 | | 517 | | 610 | |
| 10 | 1.33 | | 512 | | 631 | |
| 11 | 1.67 | | 517 | | 612 | |
| 12 | 2.00 | | 521 | | 631 | |
| 13 | 0.33 | Hexane | 540 | 543±6 | 660 | 662±2 |
| 14 | 0.67 | | 532 | | 661 | |
| 15 | 1.00 | | 554 | | 665 | |
| 16 | 1.33 | | 549 | | 664 | |
| 17 | 1.67 | | 542 | | 662 | |
| 18 | 2.00 | | 540 | | 660 | |

The thermogravimetric (TG) analysis of cellulose and P3HT-g-cellulose, obtained in different solvents with various weight ratio of $FeCl_3$/cellulose are shown in Figure 5.6. Cellulose is hygroscopic and a slight weight loss of around 5% at 100° C is attributed to the evaporation of water in small quantities. The main loss of cellulose began around 270°C corresponding to cellulose degradation. [63,64] The weight loss from 8 to 75% was found in the decomposition stage of 275-368°C. When the temperature increase further up to 370°C, a loss weight of 25% due to break down of main chain cellulose producing volatile gases[65,66]. The grafted cellulose, synthesis in all solvents (including acetonitrile, hexane and chloroform), are less thermally stable than cellulose although the TG curves of P3HT-g-cellulose coincide with the TG curve of cellulose. The degradation of all grafted celluloses products began at lower temperatures to that of cellulose as shown in Figure 5.6. The slightly difference in TG curves of cellulose and its graft samples indicated the interaction between cellulose and P3HT.

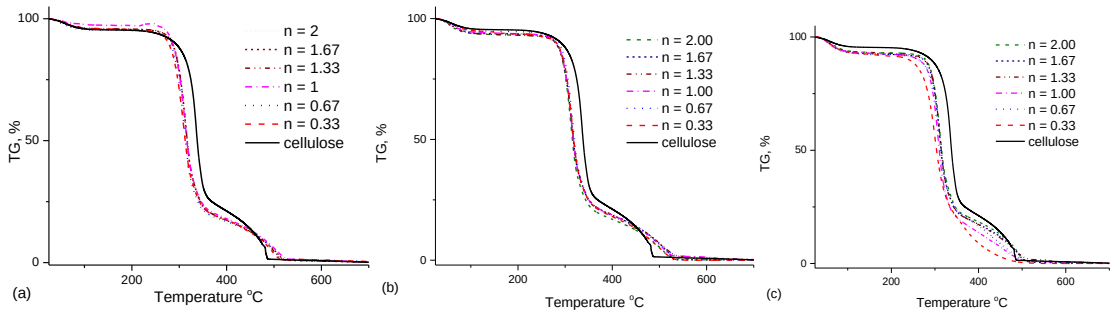


**Figure 5.6. TG curves of cellulose and P3HT-g-cellulose**

**(a) synthesis in chloroform (b) synthesis in hexane (c) synthesis in acetonitrile**

The difference in thermal decomposition behavior of cellulose and grafted cellulose samples can be seen clearly from the derivative thermogravimetric (DTG) curves shown in Figure 5.7. These peaks in DTG curves show the maximum decomposition rate, indicate the completely pyrolysis of cellulose and grafted cellulose. The peaks temperature of grafted cellulose products, obtained in all solvent with different weight ratio, shift toward lower temperature. For instance, as shown in Figure 5.7, the DTG curve of cellulose show a sharp peak at 336ºC while the DTG peak temperature of P3HT-g-cellulose are observed at 312ºC. Therefore, the DTG peak temperature of P3HT-g-cellulose is lower by about 24ºC than that of cellulose itself.

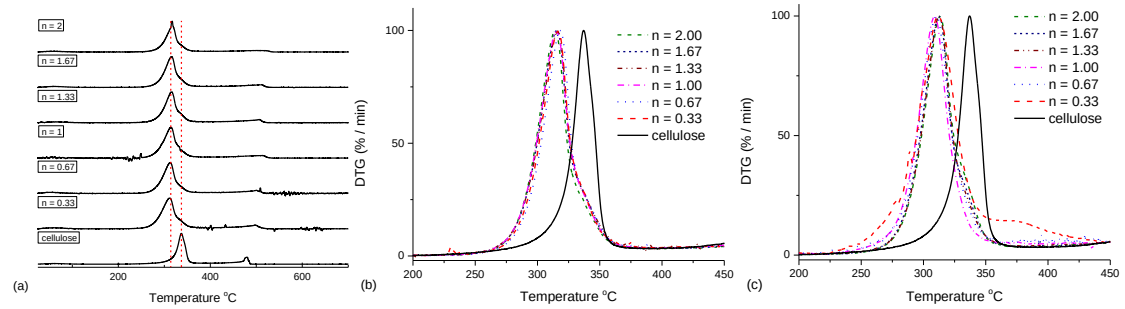


**Figure 5.7. DTG curves of cellulose and P3HT-g-cellulose**

**(a) synthesis in chloroform (b) synthesis in hexane (c) synthesis in acetonitrile**

In summary, the TG and DTG curves show the thermal properties of the grafted P3HT to cellulose had lower stability compared to cellulose itself. In previous reports, grafting vinyl monomer (methyl acrylate, methyl methacrylate, 2-hydroxyethylmethacrylate, and so forth) to polysaccharide product such as cellulose resulted in a decrease in the thermal stability of these polysaccharide [43,44,67-69]. The thermal stability of polymer depends significantly on the crystallinity [70]. Therefore, the grafting P3HT to cellulose could increase the amorphous regions in cellulose resulting in changed in the crystallinity, in turn; the changed crystallinity leads to the decrease of the thermal stability of cellulose.

The thermal stability of P3HT-g-cellulose and the simple mixture of poly(3-hexylthiophene) and cellulose (P3HT/cellulose (30/70) mixture) were compared. As shown in the Figure 5.8, the P3HT homopolymer showed higher thermal stability compared to cellulose itself. The DTG peak temperature is used as a measure of the thermal stability. The DTG peak of cellulose is at 336ºC while the DTG peaks of P3HT is 504 ºC, respectively. The thermal stability of the P3HT-g-cellulose is different from the thermal decomposition property of the P3HT/cellulose (30/70) mixture. The thermal stability of the P3HT-g-cellulose was slightly lower than that of cellulose itself, while the thermal decomposition behavior of the simple mixture of P3HT and cellulose was higher than that of cellulose itself. The results from the TG and DTG curves in Figures 5.8, can be explained based on the incompatible of constituent polymers causes the phase-separation structure in polymer blend. [70,71] When P3HT was mixed with cellulose, there is no connection bond between 3HT unit and cellulose. Therefore, P3HT/cellulose mixture shows separated temperature peaks belong to each constituents of the mixture.

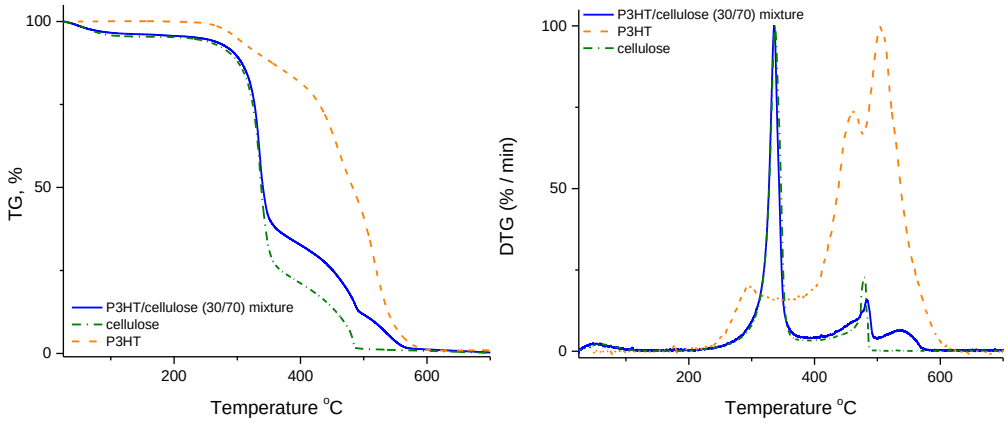


**Figure 5.8: TG and DTG curves of cellulose, P3HT and P3HT/cellulose mixture (30/70)**

The effect of grafting on the crystallinity of cellulose and grafted cellulose has been carried out by XRD analysis. The crystallinity of cellulose is expected to change by the direct grafting of 3HT to the cellulose chain, which may result in reduced thermal stability.[70] Cellulose exists in two crystalline forms: cellulose I and II. [72] The crystallinity index ($I_c$) and percent crystallinity (% $C_r$) of cellulose and the grafted cellulose products were calculated from the XRD patterns using the 2θ peak intensities between 18 and 19° (the diffraction intensity of the amorphous portion) and between 22 to 23° (the intensities of both amorphous and crystalline phases) [2,73] as follows:

$$I_c = \frac{I_{002} - I_{am}}{I_{002}} \qquad \% C_r = \frac{I_{002}}{I_{002} + I_{am}}$$

As shown in Figure 5.9, all diffraction patterns exhibited peaks at 2θ = 17 and 22.5°, which correspond to the amorphous and crystalline phases of cellulose. The data in Table 5.3 reveals that the crystallinity indexes and percentage crystallinities of the various grafted materials decrease slightly upon grafting. The crystallinity index and percent crystallinity of cellulose itself are 0.58 and 72.15%, respectively. After grafting, the crystallinity index varied from 0.53 to 0.57 while percent crystallinity fluctuate from 68 to 71 % as shown in Table 5.3. The grafting of the poly(3-hexylthiophene) to the cellulose backbone increases the amorphous region because of the incorporation of poly(3-hexylthiophen) chains that hinder the crystallization of the cellulose chain. The thermal stability of cellulose depends mainly on its crystallinity.[70,74] These XRD results are in agreement with the TG results; after grafting cellulose crystallinity decreases resulting in a decrease in thermal stability.

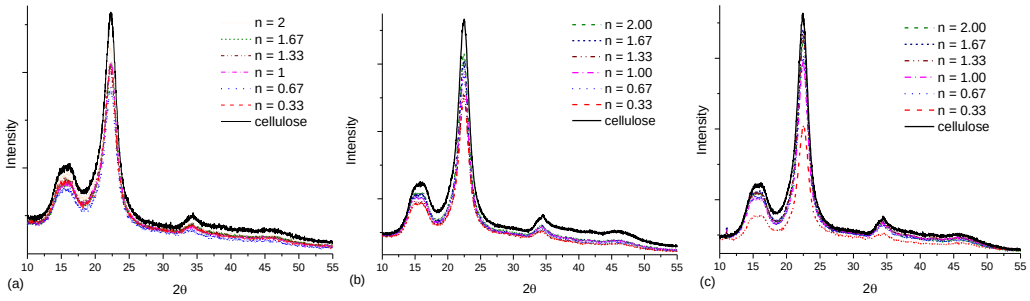


**Figure 5.9. XRD patterns of cellulose and P3HT-g-cellulose**
**(a) synthesis in chloroform (b) synthesis in hexane (c) synthesis in acetonitrile**

**Table 5.3. Crystallinity indexes and % crystallinities of P3HT-g-cellulose**

| Entry | $FeCl_3$/cellulose (wt/wt) | Graft reaction in solvents | Crystallinity index ($I_c$) | % Crystallinity |
|---|---|---|---|---|
| 1 | 0.33 | Acetonitrile | 0.56 | 70.81 |

| | | | | |
|---|---|---|---|---|
| 2 | 0.67 | | 0.53 | 69.38 |
| 3 | 1.00 | | 0.55 | 69.32 |
| 4 | 1.33 | | 0.57 | 70.55 |
| 5 | 1.67 | | 0.54 | 70.11 |
| 6 | 2.00 | | 0.55 | 69.29 |
| 7 | 0.33 | Chloroform | 0.55 | 70.72 |
| 8 | 0.67 | | 0.57 | 71.29 |
| 9 | 1.00 | | 0.56 | 70.11 |
| 10 | 1.33 | | 0.55 | 69.32 |
| 11 | 1.67 | | 0.56 | 69.12 |
| 12 | 2.00 | | 0.55 | 71.75 |
| 13 | 0.33 | Hexane | 0.56 | 71.38 |
| 14 | 0.67 | | 0.57 | 70.83 |
| 15 | 1.00 | | 0.55 | 70.94 |
| 16 | 1.33 | | 0.56 | 68.85 |
| 17 | 1.67 | | 0.57 | 70.45 |
| 18 | 2.00 | | 0.57 | 71.27 |

The elements present in the P3HT-g-cellulose sample (entry 16 in Table 5.1) was identified by the EDX microanalysis in TEM. In Figure 5.10, which show TEM-EDX images, the white and red dots represent the carbon and oxygen elements, respectively while the sulfur and chlorine elements are marked by the green and cyan dots, respectively. This is vital to confirm the presence of sulfur, which originates from the heterocyclic thiophene (3HT) unit grafted to the cellulose.

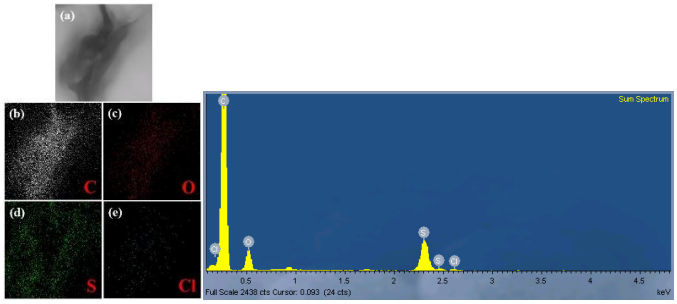


**Figure 5.10. EDX maps and spectrum of P3HT-g-cellulose**

To determine the role of P3HT grafted to the surface of cellulose, photoemission yield spectroscopy (PYS) has been applied to evaluate the ionization energy of cellulose and P3HT-g-cellulose. [75,76] Figure 5.11 shows the PYS spectra of cellulose and P3HT-g-cellulose (obtained in acetonitrile and hexane). The ionization energy were determined from the linear plot and the cubic root plot for the yield spectra, as shown in Figures 16-18 in supplementary. From the linear extrapolation, the ionization energy was determined. In detail, ionization energy of cellulose is 4.83 eV while these values of P3HT-g-cellulose, synthesis in acetonitrile and hexane, are 4.74 and 4.67, respectively. In comparison to the cellulose itself, the ionization of P3HT-g-cellulose is reduced by 0.09 and 0.16 eV, depend on solvent (acetonitrile or hexane) used for synthesis. With the presence of P3HT on the surface of cellulose, the ionization energy appeared on the lower energy side, which correspond to the ionization potential of P3HT. [77,78] Moreover, P3HT-g-cellulose, obtained in hexane, with longer π-conjugated structure due to higher molecular weight, gave a lower ionization energy than P3HT-g-cellulose, synthesis in acetonitrile. Furthermore, the conductivity of P3HT-g-cellulose ($5.7 \times 10^{-6}$ S/cm) is found to be higher than that of cellulose ($10^{-9}$ S/cm).

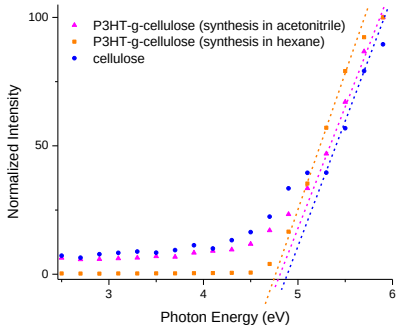


**Figure 5.11. PYS spectra of cellulose, P3HT-g-cellulose**

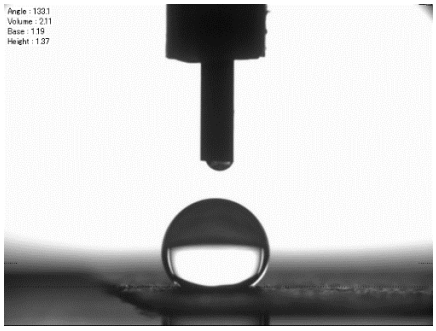

**Figure 5.12. Illustration of contact angle formed by water drop on a surface of P3HT-g-cellulose paper**

The highly polar surface of cellulose, which is related to its OH-rich structure, creates a major problem for the application of cellulose due to its poor compatibility with non-polar materials. Some reports have been published that studied the wettability of cellulose surface [79] or searched for strategies to reduce the polar character of cellulose [80]. In this work, the effect of grafting P3HT to the surface of cellulose was also tested by contact angle measurement (as shown in Figure 5.12), which is a measure of the wettability of a solid by a liquid. In our results, cellulose and P3HT-g-celluloce obtained in acetonitrile were completely wettable by water, with a contact angle of 0 °. The OH groups at the cellulose surface are subjected to interactions with water at a high speed. However, P3HT-g-cellulose obtained in hexane exhibited a contact angle of 133.1°, indicating a substantial decrease in its attraction to water due to the presence of heterocyclic thiophene groups from P3HT layer on the surface of cellulose. The contact angle of 0° of the P3HT-g-celluloce obtained in acetonitrile can be explained by the lower grafting ratio and molecular weight of P3HT on the cellulose surface.

Figures 5.13 provides an overview of the grafting of poly(3-hexylthiophene) to cellulose. Although cellulose grafted with P3HT was successfully synthesized and confirmed by FT-IR, XRD, TG, UV-vis, fluorescence, PYS, contact angle, conductivity and TEM EDX techniques, the mechanisms of the grafting reactions involving cellulose and 3-hexylthiophene in the presence of anhydrous $FeCl_3$ remains unclear. The $Fe^{2+}$–$H_2O_2$ system (Fenton reagent) has been used to graft vinyl monomers to cellulose for over two decades.[2] In most previous research, it was supposed that the presence of $Fe^{3+}$ had a negative effect on grafting and led to termination of the growing grafted chain.[10,11] However, some complex reagents composed of $Fe^{3+}$, ascorbic acid, potassium fluoride, and ethylenediaminetetraacetic acid have been used in grafting reactions.[10,81] In our method, anhydrous $FeCl_3$ is well dispersed in chloroform by ultrasonic treatment; the reaction of $FeCl_3$ takes place heterogeneously because of its insolubility in this solvent. In the solid state, the $Fe^{3+}$ ion at the surface of the crystal has one unshared chloride ion and one empty orbital, leading to strong Lewis acidity and high hygroscopicity.[82] Furthermore, in the solid state the oxidant activity of $FeCl_3$ is high.[48] The following reaction steps are proposed for the grafting reaction of 3HT to cellulose. In the first step, radical formation on the cellulose backbone may occur on the oxygen atom of the (-$CH_2OH$) group. At the same time, 3HT monomers are oxidized to the corresponding radical cations by $FeCl_3$.[82] Initially, the oxidized 3HT monomer may couple with the free radical on the oxygen atom of the (-$CH_2OH$) group. In the propagation step, $FeCl_3$ continues to oxidize the 3HT molecules on the surface of cellulose to their radical cations; this surface radical cation is then thought to couple with another 3HT radical cation in solution. Repetition of this process is thought to bind the P3HT to the surface of the cellulose. Termination may result from the substitution of the hydrogen atom of a 3HT molecule with a chlorine end group[83,84].

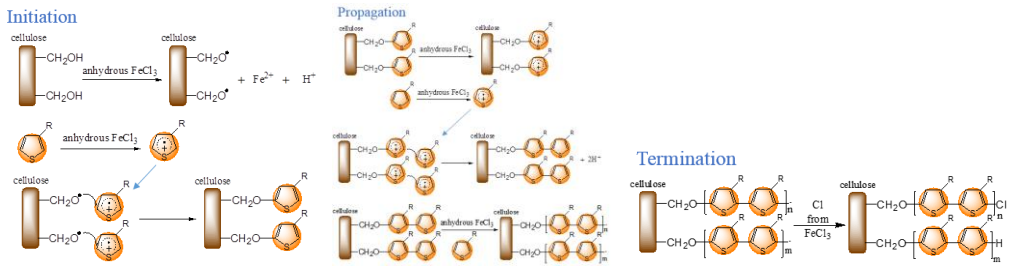


**Figure 5.13. Grafting of P3HT onto cellulose**

### *5.3.2 Grafting P3HT to chitin and chitosan*

In previous results, hexane is the best medium for grafting P3HT to cellulose. Therefore, this solvent is chosen for graftting P3HT to chitin and chitosan. As a result, the different color of chitin and chitosan before and after grafting with P3HT can be clearly observed with the naked eye.


**Figure 5.14. Images of chitin and P3HT-g-chitin (left); chitosan and P3HT-g-chitosan (right)**

All FT-IR investigation related to chitin characterization have been discussed in previous reports [85-88]. a very small peak appeared as a shoulder on a peak at 752 $cm^{-1}$ correspond to CH out-of-plane vibration from the aromatic rings of 3HT unit [52,89] after grafting P3HT. For the P3HT-g-chitosan, the appearance of shoulder at 1457 and 1588 $cm^{-1}$ could from the C=C and C─C stretching mode from the aromatic of 3HT unit and the CH out-of-plane vibration from the aromatic rings of 3HT [52,89] make the peak at 891 $cm^{-1}$ sharper after grafting P3HT to chitosan.

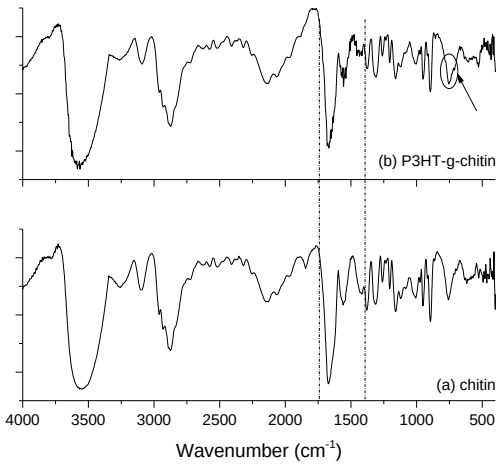


**Figure 5.15: FT-IR curves of chitin (a) and P3HT-g-chitin (b)**

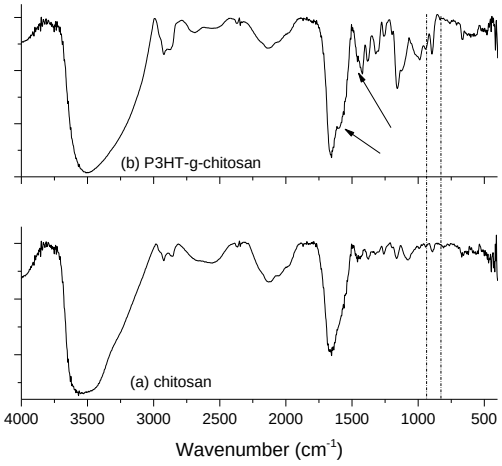


**Figure 5.16. FT-IR of (a) chitosan and (b) P3HT-g-chitosan**

As shown in Table 5.4, the grafting ratio reached the highest value at n = 1.33 of both grafted chitin and chitosan. These results are simliar to those of garfting P3HT to cellulose.

**Table 5.4. The grafting ratio and characterization of extracted P3HT from grafted cellulose**

| Entry | Samples | $FeCl_3$/chitin or chitosan (wt/wt) | Grafting ratio (%) | Molecular weight of extracted P3HT (*) | |
|---|---|---|---|---|---|
| | | | | $M_w$, kDa | PDI |

| | | | | | |
|---|---|---|---|---|---|
| 1 | P3HT-g-chitin | 0.33 | 3.2 | 98 | 2.7 |
| 2 | | 0.67 | 3.2 | 95 | 3.3 |
| 3 | | 1.00 | 3.3 | 95 | 3.8 |
| 4 | | 1.33 | 3.4 | 86 | 3.4 |
| 5 | | 1.67 | 3.3 | 88 | 3.3 |
| 6 | | 2.00 | 3.3 | 90 | 3.6 |
| 7 | P3HT-g-chiosan | 0.33 | 3.2 | 87 | 2.9 |
| 8 | | 0.67 | 3.4 | 95 | 3.5 |
| 9 | | 1.00 | 3.6 | 86 | 3.2 |
| 10 | | 1.33 | 3.5 | 99 | 3.7 |
| 11 | | 1.67 | 3.3 | 93 | 3.6 |
| 12 | | 2.00 | 3.4 | 84 | 3.8 |

As shown in Figures 5.17 and 5.18, the optical properties of P3HT-g-chitin and P3HT-g-chitosan including both UV-vis absorption and photoluminescence emission spectra reflected that the π-conjugation structure of P3HT have been successfully grafted to the surface of chitin and chitosan. In addition, weight ratio of $FeCl_3$/chitin or chitosan does not significantly influence on the maximum absorption peaks as well as the photoluminescence emission peaks.

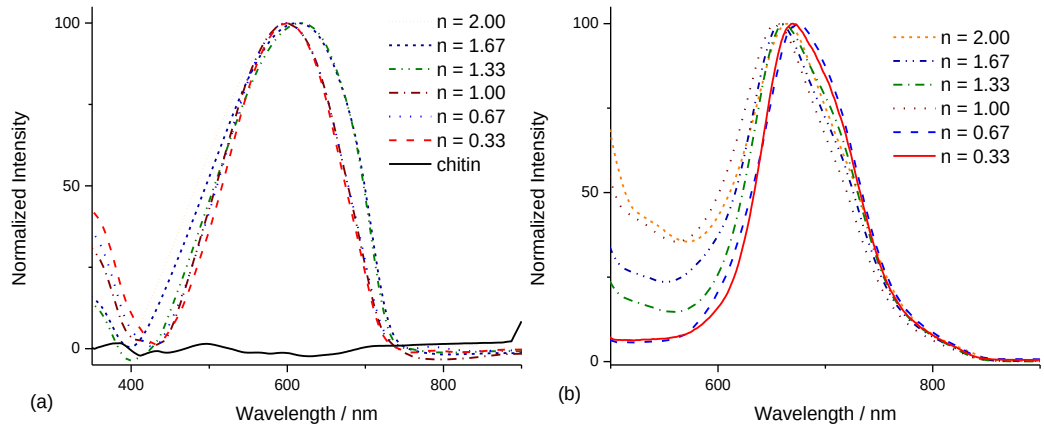


**Figure 5.17. UV-vis spectra (a) and Fluorescence spectra (b) of P3HT-g-chitin**

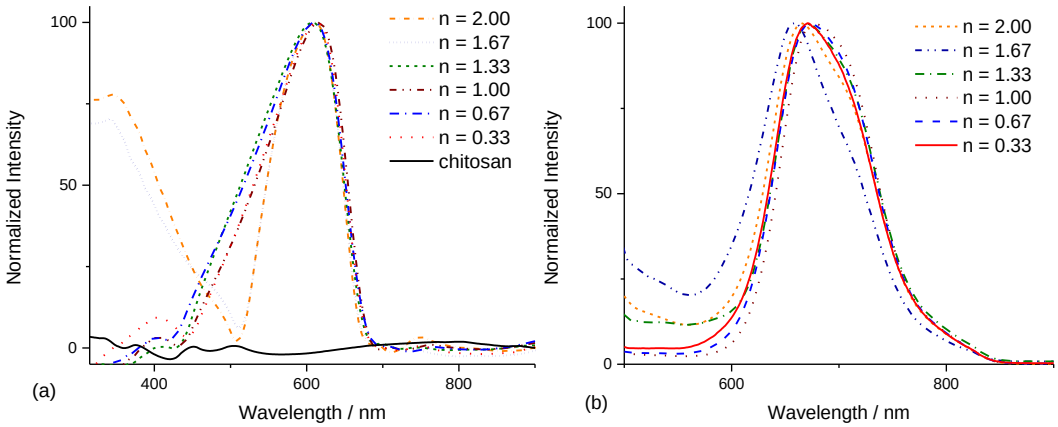


**Figure 5.18. UV-vis spectra (a) and Fluorescence spectra (b) of chitosan and P3HT-g-chitosan**

Similar to the TG and DTG of P3HT-g-cellulose, the TG and DTG curves (in Figures 5.19 and 5.20) show the lower thermal stability of the grafted chitin/chitosan compared to chitin/chitosan. In previous publications, grafting vinyl monomers (methyl acrylate, methyl methacrylate, 2-hydroxyethylmethacrylate, and so forth) to

polysaccharide products have been found to cause a decrease in the thermal stability of these polysaccharide [43,44,67-69]. In addition, the thermal stability of polymer depends significantly on the crystallinity [70]. Therefore, the decreased in thermal decomposition of grafted chitin/chitosan could be associated to the degree of crystallinity of chitin/chitosan. In other words, the grafting P3HT to chitin/chitosan could increase the amorphous regions in chitin/chitosan resulting in changed in the crystallinity, in turn; the changed crystallinity leads to the decrease of the thermal stability of chitin/chitosan.

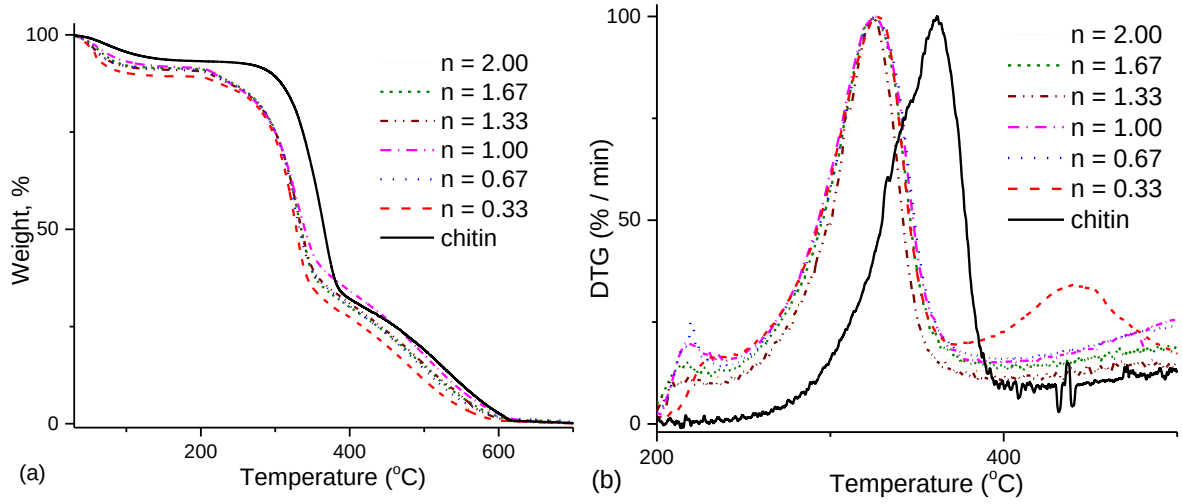


**Figure 5.19: TG (a) and DTG (b) of chitin and P3HT-g-chitin**

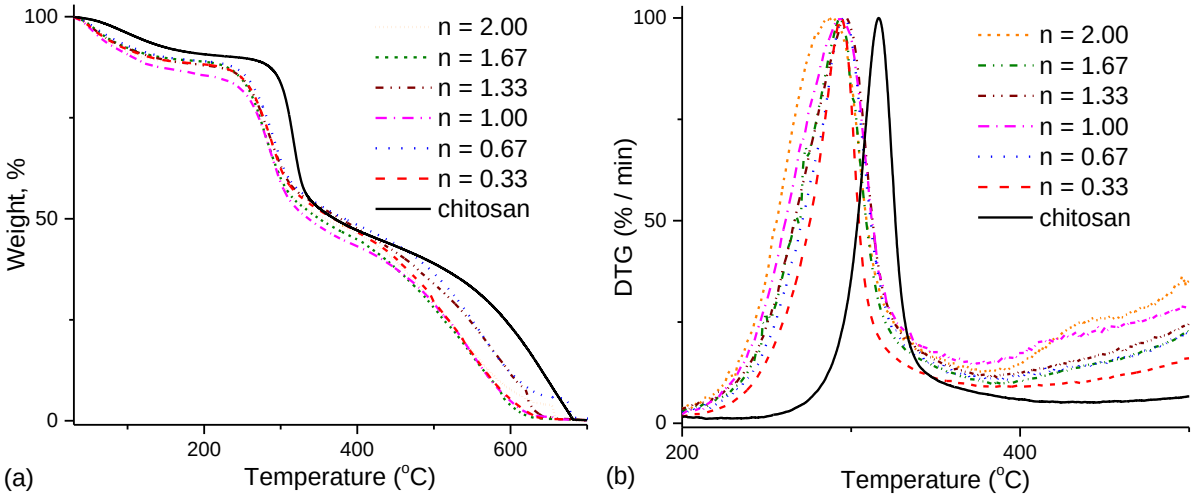


**Figure 5.20: TG (a) and DTG (b) of chitosan and P3HT-g-chitosan**

After grafting, the crystallinity index of chitin and chitosan are also lower than that of original chitin and chitosan (as shown in Figures 5.21 and 5.22). The grafting (3HT/F) copolymer to chitin/chitosan cause the disorder of the crystalline structure, resulted in the increase of amorphous region. Furthermore, the thermal stability of polymer depends mainly on the crystallinity[70]. These XRD results are in agreement with the TG results. Therefore, grafting (3HT/F) copolymer to chitin/chitosan lead to less thermal stability of chitin and chitosan.

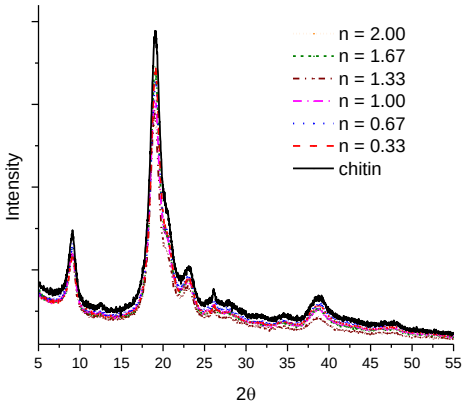


**Figure 5.21. XRD pattern of chitin and P3HT-g-chitin**

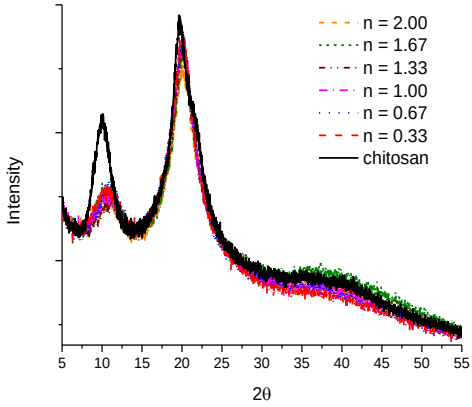


**Figure 5.22. XRD pattern of chitosan and P3HT-g-chitosan**

The elements present in the P3HT-g-chitin and P3HT-g-chitosan samples were detected by the EDX microanalysis in TEM. In the TEM-EDX images of Figure 5.23, all elements include carbon, oxygen, nitrogen, sulfur and chlorine were represented. These results confirmed the presence of sulfur, which originates from the heterocyclic thiophene (3HT) unit grafted to the cellulose.

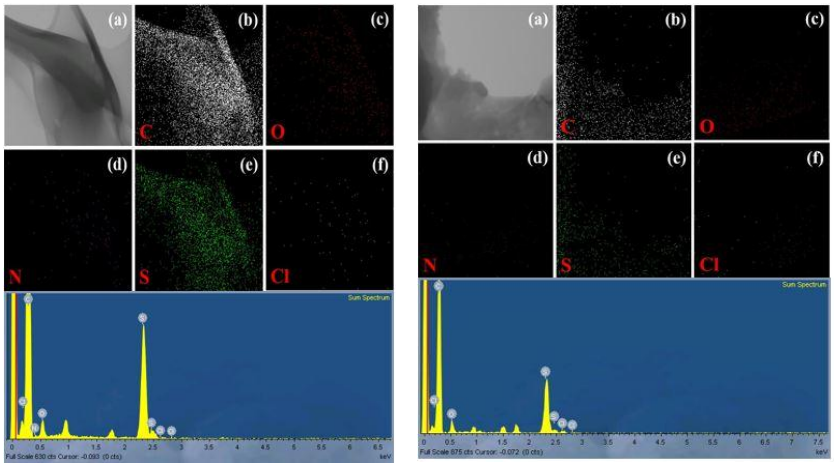


**Figure 5.23. The EDX mapping and spectrum images of P3HT-g-chitin (left) and P3HT-g-chitosan (right)**

The conductivity of chitin/chitosan and grafted chitin/chitosan were measured by using four-probe method. As a result, the conductivity of chitin/chitosan were improved significant from $10^{-9}$ S/sm (for chitin/chitosan) to 3.5 x $10^{-7}$ and 7.6 x $10^{-7}$ S/cm (for P3HT-g-chitin and P3HT-g-chitosan, respectively).

In addition, the contact angle measurements are used to determine the effect of P3HT on the wettability property of chitin and chitosan before and after grafting. In this measurement, two samples P3HT-g-chitin and P3HT-g-chitosan with the highest grafting ratio were selected for measurement. The chitin and chitosan have very low hydrophobicity, in detail, the water droplet was absorbed completely by the surface of chitin and chitosan within 20 s. As a result, the contact angle is almost 0$^o$, indicated the hydrophilic surface of chitin and chitosan. In contrast, the presence of P3HT on the surface of chitin/chitosan significantly increased hydrophobicity of chitin/chitosan with higher water contact angles. As shown in Figure 11 and supplementary-Figure 10, the water droplet remain on the surface of grafted chitin/chitosan without seeping deeper. The P3HT-g-chitin and P3HT-g-chitosan displayed a water contact angles of 97.7$^o$ and 107.0$^o$, respectively. The results imply that the poly(3-hexylthiophene) grafted to the surface of chitin and chitosan resulted in the improvement of the hydrophobicity.

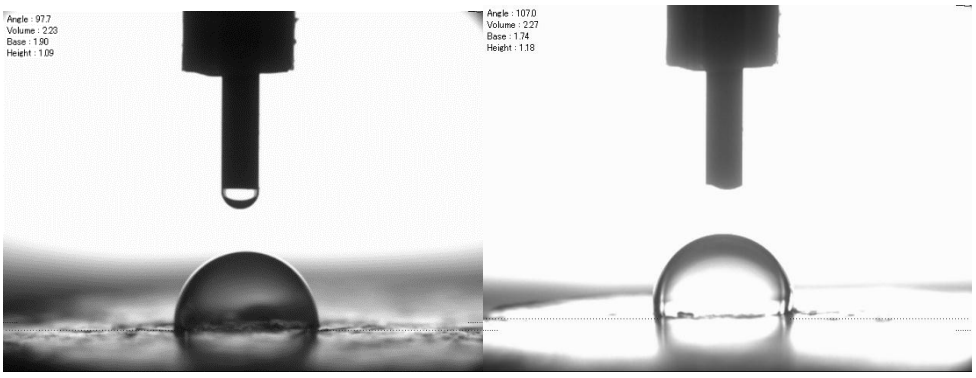


**Figure 5.24. Images for contact angle of P3HT-g-chitin (left) and P3HT-g-chitosan (right)**

## 5.4 Conclusions

Surface functionalization of cellulose with poly(3-hexylthiophene) (P3HT) was conducted with $FeCl_3$ as an oxidant in three different solvents: acetonitrile, chloroform, and hexane. Of these three solvents, hexane best promoted the grafting P3HT to cellulose with a high grafting ratio and molecular weight. The maxima of the UV-vis absorption and fluorescent spectra, observed at around 500 and 600 nm, respectively, represented the build-up of the conjugated chain length formed by the grafting of P3HT onto the cellulose surface. The HOMO level of cellulose as determined by photoemission yield spectroscopy decreased from 4.83 to 4.67 eV after modification with P3HT. Grafting P3HT onto the surface of cellulose provided super-hydrophobic property with a lotus effect. The conductivity of cellulose also improved significantly, from $10^{-9}$ to $10^{-6}$ S/cm when P3HT was present on the surface. The thermal stability and crystallinity of cellulose decreased slightly upon graft polymerization with P3HT. The modification of the surface of chitin and chitosan have been grafted successfully with P3HT, using same method. Introducing the P3HT layer in the surface helped to enhance the conductivity of chitin and chitosan. The S element from 3HT unit was detected by TEM-EDX. The absorption and emission peaks in the range from 500 to 600 nm is an evidence of $\pi$- $\pi^*$ conjugation from 3HT unit, grafted to chitin and chitosan. The modified chitin and chitosan display high water contact angles imply that the hydrophilic nature of chitin and chitosan turned to hydrophobicity after the grafting with P3HT. The thermal stability of grafted cellulose was found to depend on its crystallinity. The thermal stabilities of the P3HT-g-chitin and P3HT-g-chitosan were slightly lower than that of chitin and chitosan themself, while the thermal decomposition behavior of a simple mixture of a P3HT with chitin and chitosan were superior to that of chitin/chitosan alone.

## 5.5 References

(1) Qin, C.; Soykeabkaew, N.; Xiuyuan, N.; Peijs, T. *Carbohydr. Polym.* **2008**, *71*, 458-467.

(2) Gürdağ, G.; Sarmad, S.: Polysaccharide Based Graft Copolymers. *Springer-Verlag Berlin Heidelberg* **2013**, 15-57.

(3) Roy, D.; Semsarilar, M.; Guthriea, J. T.; Perrier, S. b. *Chem. Soc. Rev.* **2009**, *38*, 2046–2064.

(4) Gupta, K. C.; Khandekar, K. *Biomacromolecules* **2003**, *4*, 758-765.

(5) Pillai, C. K. S.; Paul, W.; Sharma, C. P. **2009**, *34*, 641–678.

(6) Rinaudo, M. *Prog. Polym. Sci.* **2006**, *31*, 603–632.

(7) Sashiwa, H.; Aiba, S.-i. *Prog. Polym. Sci.* **2004**, *29*, 887-908.

(8) Biçak, N.; Sherrington, D. C.; Senkal, B. F. *React. Funct. Polym.* **1999**, *41*, 69–76.

(9) Ibrahim, M. M.; Flefel, E. M.; El-Zawawy, W. K. *Polym. Adv. Technol.* **2002**, *13*, 548-557.

(10) Misra, B. N.; Dogra, R.; Mehta, I. K. *J. Polym. Sci. Pol. Chem.* **1980**, *18*, 749-752.

(11) Ogiwara, Y.; Kubota, H. *J. Appl. Polym. Sci.* **1969**, *13*, 1613–1620.

(12) Feit, B.-A.; Bar-Nun, A.; Lahav, M.; Zilkha, A. *J. Appl. Polym. Sci.* **1964**, *8*, 1869–1888.

(13) Ikeda, I.; Kurushima, Y.; Takashima, H.; Suzuki, K. *Polym. J.* **1988**, *20*, 243-250.

(14) John, G.; Pillai, C. K. S. *Polym. Bull.* **1989**, *22*, 89-94.

(15) Hafrén, J.; Córdova, A. *Macromol. Rapid Commun.* **2005**, *26*, 82-86.

(16) Lönnberg, H.; Zhou, Q.; Brumer, H.; Teeri, T. T.; Malmström, E.; Hult, A. *Biomacromolecules* **2006**, *7*, 2178–2185.
(17) Carlmark, A.; Larsson, E.; Malmström, E. *Eur. Polym. J.* **2012**, *48*, 1646–1659.
(18) Daly, W. H.; Evenson, T. S.; Iacono, S. T.; Jones, R. W. *Macromol. Symp.* **2001**, *174*, 155-163.
(19) Carlmark, A.; Malmström, E. *J. Am. Chem. Soc.* **2002**, *124*, 900–901.
(20) Carlmark, A.; Malmström, E. E. *Biomacromolecules* **2003**, *4*, 1740–1745.
(21) Stenzel, M. H.; Davis, T. P.; Fane, A. G. *J. Mater. Chem.* **2003**, *13*, 2090-2097.
(22) Hernández-Guerrero, M.; Davis, T. P.; Barner-Kowollik, C.; Stenzel, M. H. *Eur. Polym. J.* **2005**, *41*, 2264–2277.
(23) Moreira, G.; Fedeli, E.; Ziarelli, F.; Capitani, D.; Mannina, L.; Charles, L.; Viel, S.; Gigmes, D.; Lefay, C. *Polym. Chem.* **2015**, *6*, 5244-5253.
(24) Roy, D.; Guthrie, J. T.; Perrier, S. *Macromolecules* **2005**, *38*, 10363-10372.
(25) Irimia-Vladu, M. *Chem. Soc. Rev* **2014**, *43*, 588-610.
(26) Chen, Z.; Wu, P.; Cong, R.; Xu, N.; Tan, Y.; Tan, C.; Jiang, Y. *ACS Appl. Mater. Interfaces* **2016**, *8*, 3567–3574.
(27) Suginta, W.; Khunkaewla, P.; Schulte, A. *Chem. Rev.* **2013**, *113*, 5458–5479.
(28) Dash, M.; Chiellini, F.; Ottenbrite, R. M.; Chiellini, E. *Prog. Polym. Sci.* **2011**, *36*, 981–1014.
(29) Sakakibara, K.; Rosenau, T. *Holzforschung* **2012**, *66*, 9-19.
(30) Henry, C.; Armand, F.; Araspin, O.; Bourgoin, J. P.; Wegner, G. *Chemistry of Materials* **1999**, *11*, 1024-1029.
(31) Rußler, A.; Sakakibara, K.; Rosenau, T. *Cellulose* **2011**, *18*, 937-944.
(32) Beneventi, D.; Alila, S.; Boufi, S.; Chaussy, D.; Nortier, P. *Cellulose* **2006**, *13*, 725 –734.
(33) Wang, C. H.; Chen, C. C.; Hsu, H. C.; Du, H. Y.; Chen, C. P.; Hwang, J. Y.; Chen, L. C.; Shih, H. C.; Stejskal, J.; Chen, K. H. *J. Power Sources* **2009**, *190*, 279-284.
(34) Bober, P.; Kovářová, J.; Pfleger, J.; Stejskal, J.; MiroslavaTrchová; Novák, I.; Berek, D. *Carbon* **2016**, *109*, 836-842.
(35) Wan, Y.-J.; Zhu, P.-L.; Yu, S.-H.; Sun, R.; Wong, C.-P.; Liao, W.-H. *Carbon* **2017**, *115*, 629–639.
(36) Zhang, Z.; JuanZhang; XingxingZhao; FuhuaYang. *Carbon* **2015**, *95*, 552-559.
(37) Yavuz, A. G.; Uygun, A.; Bhethanabotla, V. R. *Carbohydr. Polym.* **2009**, *75*, 448–453.
(38) Ramaprasad, A. T.; Rao, V.; Sanjeev, G.; Ramanani, S. P.; Sabharwal, S. *Synth. Met.* **2009**, *159*, 1983–1990.
(39) Marcasuzaa, P.; Reynaud, S.; Ehrenfeld, F.; Khoukh, A.; Desbrieres, J. *Biomacromolecules* **2010**, *11*, 1684–1691.
(40) Ramaprasad, A. T.; Rao, V.; Sanjeev, G. *J. Appl. Polym. Sci.* **2011**, *121*, 623–633.
(41) Feizbakhsh, A.; Ehteshami, S. *Chromatographia* **2016**, *79*, 1177-1185.
(42) Ramaprasad, A. T.; Latha, D.; Rao, V. *J. Phys. Chem. Solids* **2017**, *104*, 169–174.
(43) Nishioka, N.; Yoshida, N. *Polym. J.* **1992**, *24*, 1009-1015.
(44) Nishioka, N.; Yamaoka, M.; Haneda, H.; Kawakami, K.; Uno, M. *Macromolecules* **1993**, *26*, 4694-469.
(45) Nishioka, N.; Kosai, K. *Polym. J.* **1981**, *13*, 1125-1133.
(46) Hai, T. A. P.; Sugimoto, R. *J. Mol. Struct.* **2017**, *1146*, 660–668.
(47) Niemi, V. M.; Knuuttila, P.; 0sterholm, J. E.; Korvola, J. *Polym. Rep.* **1992**, *33*, 1559-1562.
(48) Hai, T. A. P.; Sugimoto, R. *Synth. Met.* **2016**, *220*, 59-71.
(49) Vieira, J. G.; Oliveira, G. d. C.; Filho, G. R.; Assunção, R. M. N. d.; Meireles, C. d. S.; Cerqueira, D. A.; Silva, W. G.; Motta, L. A. d. C. *Carbohydr. Polym.* **2009**, *78*, 779–783.
(50) Khalil, H. P. S. A.; Ismail, H.; Rozman, H. D.; Ahmad, M. N. *Eur. Polym. J.* **2001**, *37*, 1037–1045.
(51) Higgins, H. G.; Stewart, C. M.; Harrington, K. J. *J. Polym. Sci. Pol. Chem.* **1961**, *51*, 59-84.
(52) Socrates, G.: Infrared and Raman Characteristic Group Frequencies. *John Wiley & Sons, Ltd* **2001**, *West Sussex, England*, 268-269.
(53) Sato, M. A.; Morii, H. *Macromolecules* **1991**, *24*, 1196-1200.
(54) Hai, T. A. P.; Sugimoto, R. *Catal. Lett.* **2017**, *147*, 1955-1965.
(55) Li, X.-G.; Li, J.; Meng, Q.-K.; Huang, M.-R. *J. Phys. Chem. B* **2009**, *113*, 9718–9727.
(56) Hai, T. A. P.; Matsukuma, H.; Sugimoto, R. *Polymer* **2017**, *121*, 247–255.

(57) Kline, R. J.; McGehee, M. D.; Kadnikova, E. N.; Liu, J.; Fréchet, J. M. J.; Toney, M. F. *Macromolecules* **2005**, *38*, 3312–3319.

(58) Jen-HsienHuang; Fang-ChungChen; Chen, C.-L.; Huang, A. T.; Hsiao, Y.-S.; Teng, C.-M.; Yen, F.-W.; Chen, P.; Chu, C.-W. *Org. Electron.* **2011**, *12*, 1755–1762.

(59) Kingsley, J. W.; Marchisio, P. P.; Yi, H.; Iraqi, A.; Kinane, C. J.; Langridge, S.; Thompson, R. L.; Cadby, A. J.; Pearson, A. J.; Lidzey, D. G.; Jones, R. A. L.; Parnell, A. J. *Sci. Rep.* **2014**, *4*, 1-7.

(60) Hayashi, S.; Shin-ichiYamamoto; Koizumi, T. *Sci. Rep.* **2017**, *7*, 1-8.

(61) Meier, H.; Stalmach, U.; Kolshorn, H. *Acta Polymerica* **1997**, *48*, 379–384.

(62) Kishino, S.; Ueno, Y.; Ochiai, K.; Rikukawa, M.; Sanui, K.; Kobayashi, T.; Kunugita, H.; Ema, K. *Phys. Rev. B* **1998**, *58*, R13430-13433.

(63) Shurong, W.; Qian, L.; Zhongyang, L.; Lihua, W.; Kefa, C. *Front. Energy Power Eng. China* **2007**, *1*, 413–419.

(64) Bradbury, A. G. W.; Sakai, Y.; Shafizadeh, F. *J. Appl. Polym. Sci.* **1979**, *23*, 3271–3280.

(65) Bassilakis, R.; Carangelo, R. M.; AWójtowicz, M. *Fuel* **2001**, *80*, 1765-1786.

(66) Fisher, T.; Hajaligol, M.; Waymack, B.; Kellogg, D. *J. Anal. Appl. Pyrolysis* **2002**, *62*, 331-349.

(67) Nishioka, N.; Funakoshi, M.; Inamoto, K.; Uno, M.; Ueda, A. *J. Appl. Polym. Sci.* **2010**, *118*, 2482–2487.

(68) Fernández, M. J.; Fernández, M. D.; Casinos, I.; Guzmán, G. M. *J. Appl. Polym. Sci.* **1990**, *39*, 2219-2235.

(69) Fernández, M. J.; Fernández, M. D.; Casinos, I.; Guzmán, G. M. *J. Appl. Polym. Sci.* **1990**, *39*, 1101-1119.

(70) Reich, L.; Stivala, S. S.: Elements of Polymer Degradation. *McGraw-Hill* **1971**, *New York*.

(71) Isayev, A. I.: Encyclopedia of Polymer Blends - Structure V3. *Wiley VCH* **2016**.

(72) Kamide, K.: Cellulose and cellulose derivatives molecular characterization and its applications. *Elsevier Science* **2005**.

(73) Park, S.; Baker, J. O.; Himmel, M. E.; Parilla, P. A.; Johnson, D. K. *Biotechnol. Biofuels* **2010**, *3*, 1-10.

(74) Calahorra, M. E.; Cortázar, M.; Eguiazábal, J. I.; Guzmán, G. M. *J. Appl. Polym. Sci.* **1989**, *37*, 3305–3314.

(75) Miyazaki, S.; Maruyama, T.; Kohno, A.; Hirose, M. *Microelectron. Eng.* **1999**, *48*, 63-66.

(76) Ishii, H.; Kinjo, H.; Sato, T.; Machida, S.-i.; Nakayama, Y. *Electronic Processes in Organic Electronics* **2014**, *8*, 131-155.

(77) Sohn, Y.; Richter, J.; Ament, J.; Stuckless, J. T. *Appl. Phys. Lett.* **2004**, *84*, 76-78.

(78) Onoda, M.; Tada, K.; Nakayama, H. *Appl. Phys. Lett.* **1999**, *86*, 2110-2115.

(79) Bartel, F. E.; Ray, B. R. *J. Am. Chem. Soc.* **1952**, *74*, 778–783.

(80) Freire, C. S. R.; Silvestre, A. J. D.; Neto, C. P.; Gandini, A.; Fardim, P.; Holmbom, B. *J. Colloid Interface Sci.* **2006**, *301*, 205-209.

(81) Misra, B. N.; Dogra, R.; Mehta, I. K. *J. Polym. Sci., Polym. Chem. Ed.* **1980**, *18*, 749-752.

(82) Niemi, V. M.; Knuuttila, P.; 0sterholm, J.-E.; Korvola, J. *Polym. Rep.* **1992**, *33*, 1559-1562.

(83) Liu, Y.; Nishiwaki, N.; Saigo, K.; Sugimoto, R. *Bull. Chem. Soc. Jpn.* **2013**, *86*, 1076-1078.

(84) McCarley, T. D.; Noble, C. O.; IV; DuBois, C. J.; Jr.; McCarley, R. L. *Macromolecules* **2001**, *34*, 7999-8004.

(85) Focher, B.; Beltrame, P. L.; Naggi, A.; Torri, G. *Carbohydr. Polym.* **1990**, *12*, 405-418.

(86) Ren, L.; Tokura, S. *Carbohydr. Polym.* **1994**, *23*, 19-25.

(87) Chen, X.; Chew, S. L.; Kerton, F. M.; Yan, N. *Green Chem.* **2014**, *16*, 2204-2212.

(88) Chen, X.; Liu, Y.; Kerton, F. M.; Yan, N. *RSC Adv* **2015**, *5*, 20073–20080.

(89) Hai, T. A. P.; Sugimoto, R. *Polym. J.* **2016**, *48*, 1115–1121.

# Chapter 6:

# Photoluminescent control of biomaterials through novel oxidative polymerization

## 6.1 Introduction

In chapter 6, we successfully surface functionalization of polysaccharide including chitin, chitosan, and cellulose with poly(3-hexylthiophene). In this chapter, the surface of those polysaccharides were chemically modified to control its photoluminescence with a series of conducting polymers, including fluorene (F) and 3-hexylthiophene (3HT), through oxidative polymerization with $FeCl_3$. In this report, P3HT and PF are used as conjugated polymers because of their unique properties, including high solubility, high efficiency emission in a wide variety of colors, low operating voltage,[1] performance enhancement of organic light-emitting diode (OLEDS),[2] high photoluminescence quantum efficiencies, and thermal stability.[3,4,5]

## 6.2 Experimental section

### *6.2.1 Materials*

Cellulose powder was purchased from Wako Pure Chemical Industries Ltd. 3-Hexylthiophene (3HT), fluorene (F) monomer, anhydrous $FeCl_3$, chitin and chitosan were obtained from Tokyo Chemical Industry Co. Ltd. and used without further purification. Analytical grade solvents such as chloroform and methanol were purchased from Wako Pure Chemical Industries Ltd and used as received. Chloroform was dried over a 4 Å molecular sieves for 8 h, and purged with argon gas for 20 min before use.

### *6.2.2 Equipment*

UV-Vis spectra were obtained by diffuse reflectance measurements with a Jasco V-650 UV-Vis spectrometer, set in absorbance photometric mode, with a UV-Vis bandwidth of 2.0 nm, data interval of 1.0 nm, and a scan rate of 400 nm $min^{-1}$. Thermogravimetric (TG) analyses were conducted in air on a Hitachi STA 7200 RV thermal analysis system, from 20 to 700 °C at a flow rate of 25 ml $min^{-1}$, and a heating rate of 10 °C $min^{-1}$. $^1H$ NMR spectra (400 MHz) and IR spectra were recorded on a Bruker Ascend 400 NMR spectrometer and a Jasco 480 Plus FT-IR spectrometer, respectively. X-ray diffraction patterns were recorded with Cu-Kα radiation (X-ray wavelength: 1.5418 Å) in steps of 0.02° over the 10–70° 2θ range on a Rigaku Smartlab diffractometer equipped with a D-tex detector. Transmission electron microscopy (TEM) images were acquired with a JEOL JEM-2100F microscope. Energy dispersive X-ray (EDX) maps and line scan spectra were recorded on an Oxford INCA Energy TEM 250. Gel permeation chromatography (GPC) was performed on a system equipped with a Jasco PU-2080 Plus pump and a Jasco RI-2031 plus intelligent RI detector. Fluorescence spectra were recorded at room temperature on a Jasco spectrofluorometer FP-8300. Quantum yields were measured on Hamamatsu UV-NIR absolute PL quantum yield spectrometer.

### *6.2.3 Grafting and sample preparation*

All reactions in this work were carried out in an oven-dried Schlenk flask with a stopcock under an argon atmosphere. Cellulose powder (0.4 g) and $FeCl_3$ (0.4 g) were dispersed in chloroform (7 ml) with a magnetic stirrer. The mixture was ultrasonicated for 20 min and cooled to 0 °C in an ice bath. A solution of 3HT (100 mg, 0.6 mmol) in chloroform (3 ml) was dropped into the suspension of cellulose and $FeCl_3$, with stirring, and the reaction mixture was stirred under argon for 2 h at 0 °C. The stoichiometric ratio of 3HT to $FeCl_3$ was 1:4. The reaction was terminated by the addition of methanol. The product was washed with methanol to remove any residual $FeCl_3$, followed by extraction with chloroform to eliminate free poly(3-hexylthiophene) (P3HT) homopolymer using a Soxhlet extractor. Finally, the cellulose grafted with 3-hexylthiophene was dried under vacuum for 12 h. Grafting of fluorene and the copolymer of fluorene and 3-hexylthiophene to cellulose powder was conducted using a similar procedure to that described above. The grafted celluloses are hereinafter referred as (3HT/F-a/b)-g-cellulose, where a/b is the ratio of 3HT and F used during the polymerization conditions. The grafting of the copolymer of fluorene and 3-hexylthiophene to chitin and chitosan were conducted using a similar procedure to that described above. The grafted chitin/chitosan are hereinafter referred as (3HT/F-a/b)-g-chitin and (3HT/F-a/b)-g-chitosan, where a/b represents the monomer ratio of 3HT and F during polymerization conditions.

## 6.3 Results and discussion

During the grafting reactions of poly(3-hexylthiophene) (P3HT), polyfluorene (PF), and their copolymers to cellulose, chitin, and chitosan. The self-polymerizations of 3-hexylthiophene and fluorene occurred

concurrently with graft polymerization to cellulose. The ungrafted 3-hexylthiophene (3HT) and fluorene(F) polymers were extracted from the grafted products with chloroform. Graft ratio (Gr) was calculated by the following formula: (A - B - C) / B × 100; where A is the total weight of cellulose (or chitin or chitosan) and crude graft product, B is the weight of original cellulose (or chitin or chitosan), and C is the weight of extracted homopolymer or copolymer of fluorene and 3-hexylthiophene. [6-8] In this paper, the molecular weight of the extracted copolymer was used as the molecular weight of the copolymer grafted to cellulose (or chitin or chitosan). As shown in Table 6.1, (3HT/F-0/100)-g-cellulose (entry 1) had the lowest molecular weight while (3HT/F-100/0)-g-cellulose (entry 5) had the highest molecular weight. In addition, decreasing fluorene (F) monomer content, the molecular weight of the grafted (3HT/F)-cellulose copolymer increased ( from entry 2 to entry 4). These results can be explained on the basis of the difference in oxidation potential between 3-hexylthiophene (3HT) and fluorene (F).[9] The characterization of 3HT/F copolymer on chitin and chitosan showed similar results to that on cellulose (entries 6-15 in Table 1)

Figure 6.1 displays the $^1$H NMR spectra of the (3HT/F-100/0), (3HT/F-0/100), and (3HT/F-34/66) copolymers extracted with chloroform. The two peaks between δ 2.0 and 3.0 in Figure 1a correspond to the α-methylene protons of poly(3-hexylthiophene) (P3HT), while the signal at δ 4.0–4.2 in Figure 1b is assigned to the methylene groups of polyfluorene (PF). The 3HT/F copolymer (Figure 1c) is identified by the two groups of signal at δ 2.0–3.0 (α-methylenes of the 3HT unit) and δ 4.0–4.2 (methylene groups of the F unit). The F content in the copolymer can be calculated from the areas of the peaks in these two ranges.[10] The $^1$H NMR spectra of the (3HT/F-20/80) and (3HT/F-58/42) copolymers extracted with chloroform are similar to Figure 1c, although the F contents of these copolymers depend on the 3HT/F molar feed ratio. The $^1$H NMR spectra of the (3HT/F-100/0), (3HT/F-0/100), and (3HT/F-34/66) copolymers extracted from grafted chitin and grafted chitosan also present as same results as Figure 6.1

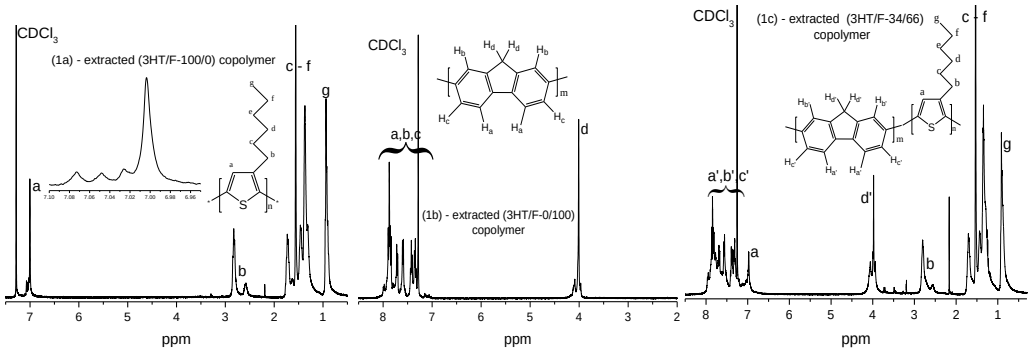


**Figure 6.1. $^1$H NMR spectra of: (1a) extracted (3HT/F-100/0) copolymer (entry 5, Table 1); (1b) extracted (3HT/F-0/100) copolymer (entry 1, Table 1); and (1c) extracted (3HT/F-34/66) copolymer (entry 3, Table 1)**

As shown in Figures 6.2, 6.3 and 6.4, the color of the (3-hexylthiophene and fluorene) copolymers grafted to cellulose, chitin, and chitosan depends on the fluorene content of copolymer. These color differences can be clearly identified with the naked eye.


**Figure 6.2. Images of the (3-hexylthiophene and fluorene) copolymers grafted**
**(a) cellulose (b) chitin (c) chitosan**

**Table 6.1: Characterization of grafted and extracted polymers**

| Samples | Entry | 3HT/F | Gr % | Fluorene content in copolymer (**) | Molecular weight of graft copolymer (*) | |
|---|---|---|---|---|---|---|
| | | | | | $M_w$ ,kDa | PDI |

| | | | | | | |
|---|---|---|---|---|---|---|
| (3HT/F) -g- cellulose | 1 | 0/100 | 6.2 | 100 | 0.9 | 1.4 |
| | 2 | 20/80 | 6.7 | 75 | 2.5 | 1.9 |
| | 3 | 34/66 | 5.8 | 60 | 4.1 | 2.6 |
| | 4 | 58/42 | 6.1 | 35 | 4.9 | 2.7 |
| | 5 | 100/0 | 7.2 | 0 | 115 | 2.8 |
| (3HT/F) -g- chitin | 6 | 0/100 | 5.7 | 100 | 1.1 | 1.7 |
| | 7 | 25/75 | 4.7 | 69 | 3.0 | 1.9 |
| | 8 | 50/50 | 4.6 | 42 | 13.9 | 2.3 |
| | 9 | 75/25 | 5.1 | 18 | 25.1 | 3.0 |
| | 10 | 100/0 | 4.4 | 0 | 93.1 | 3.1 |
| (3HT/F) -g- chitosan | 11 | 0/100 | 5.4 | 100 | 0.8 | 1.4 |
| | 12 | 25/75 | 4.1 | 70 | 2.8 | 1.6 |
| | 13 | 50/50 | 5.5 | 40 | 11.5 | 2.9 |
| | 14 | 75/25 | 5.6 | 20 | 27.9 | 3.5 |
| | 15 | 100/0 | 5.8 | 0 | 86.1 | 3.3 |

(*) Determined by GPC; (**) Determined by $^{1}$H NMR

The FT-IR spectra of cellulose and the grafted (3HT/F)-g-celluloses are shown in Figure 6.3. The IR spectrum of cellulose has been reported on many previous occasions.[11-16] A broad peak in the 3250–3500 $cm^{-1}$ region is associated with O-H stretching vibrations. A sharp peak at 2899 $cm^{-1}$ corresponds to C-H stretching vibrations.[11,12] A number of peaks assigned to C-H and C-O bending vibrations of cellulose are observed in the 1314–1372 $cm^{-1}$ range. A small additional peak at 748 $cm^{-1}$ is observed in the IR spectrum of the grafted cellulose powder that is attributed to the presence of out-of-plane C-H vibration of the aromatic groups. [17] This aromatic C-H out-of-plane vibration is associated with the aromatic rings of 3-hexylthiophene and fluorene. Previously, many investigations concerning the IR spectra of chitin characterization have been reported [18-21]. As shown in Figure 6.3, virgin chitin show the peak at 3561 $cm^{-1}$ represents the stretch of the OH group, and the bands at 3260 and 3097 $cm^{-1}$ are attributed to the vibration of NH group [20]. These peaks are seen at 2959, 2934, and 2880 $cm^{-1}$ belong to the asymmetric $CH_2$ stretching, $CH_3$ stretching, and CH symmetric [21]. These peaks at 1315 and 1375 $cm^{-1}$ belong to the $CH_2$ wagging, CH bending and $CH_3$ symmetric deformation. The amide I (inter-hydrogen bond between C=O with the N-H group and with the side chain group $CH_2OH$) and amide II (in-plane N-H bending and C-N stretching) bands are observed at 1660 and 1556 $cm^{-1}$, respectively [19-21]. The several peaks in the range of 1114 ─ 1216 $cm^{-1}$ correspond to C-O stretching and asymmetric bridge oxygen [22]. In grafted chitin samples, the bands at 3000─2800 $cm^{-1}$ from the characteristic of the hexyl group of 3HT unit could overlap with broad bands of various vibrations from the asymmetric $CH_2$ stretching, $CH_3$ stretching, and CH symmetric of chitin. Similarly, the C=C and C─C stretching mode from the aromatic of F and 3HT unit in the range of 1500 and 1450 $cm^{-1}$ are thought to overlap with amide II from chitin. However, a peak at 752 $cm^{-1}$ correspond to CH out-of-plane vibration from the aromatic rings of 3HT and fluorene unit [10,17], become intense since grafting (3HT/F) copolymer to chitin. As shown in the FT-IR spectra of pure chitosan from Figure 6.3, the band from 3200-3600 $cm^{-1}$ belongs to the OH and NH stretching vibrations, the band observed from 2820 to 2950 corresponds to C─H stretching mode and the peak at 1660 $cm^{-1}$ is attributed to C=O stretching [18,23-25]. The band at 3090-3030 $cm^{-1}$ from the υ ($C_\beta$─H) at the 4 position of 3HT unit [26] could be overlapped by the stretching vibration of OH and NH groups. The $CH_3$ and $CH_2$ stretching vibrations from the hexyl group of 3HT unit at 3000-2800 $cm^{-1}$ may be also overlapped by the C─H stretching mode of chitosan. However, the CH out-of-plane vibration from the aromatic rings of 3HT and fluorene unit [10,17] appeared at 790 $cm^{-1}$, become sharper after grafting (3HT/F) to chitosan.

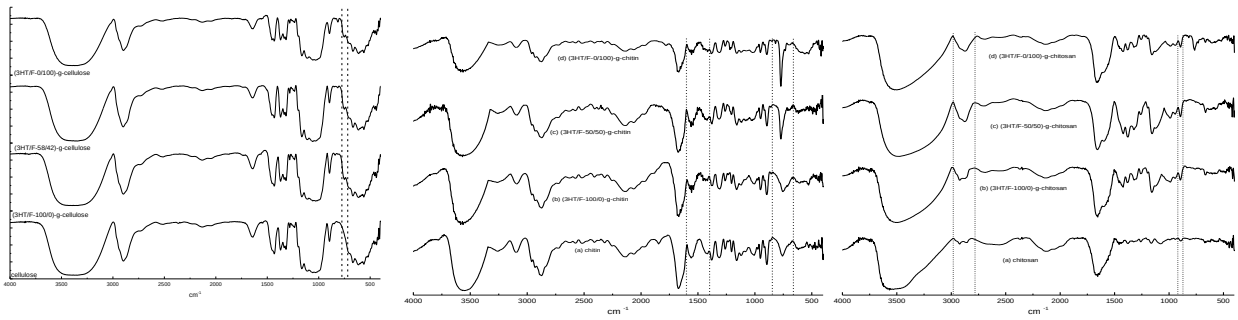

**Figure 6.3. FT-IR spectra of the (3-hexylthiophene and fluorene) copolymers grafted to cellulose (left), chitin (middle), and chitosan (right)**

Figure 6.4a depicts the UV-Vis spectra of cellulose paper grafted with the (3HT/F) copolymers. The ungrafted cellulose paper exhibits no absorption peak; however, all of the (3HT/F)-g-cellulose materials show strong absorption bands between 250 and 650 nm, which are assigned to the $\pi$-$\pi^*$ transitions of P3HT, PF, and the P3HT/PF copolymer. The absorption maximum of (3HT/F-0/100)-g-cellulose is located at 371 nm, which is attributed to PF, while the absorption maximum of (3HT/F-100/0)-g-cellulose is seen at 509 nm, which is associated with P3HT.[10] When the F content in the grafted cellulose copolymer was increased from 42 to 80%, the absorption maximum shifted to shorter wavelengths. As shown in Figures 6.4b and 6.4c, there are no absorption peak in the range from 240-880 nm on the neat chitin and chitosan, respectively. In contrast, the strong absorption bands round 250-650 nm appeared on the (3HT/F)-g-chitin and (3HT/F)-g-chitosan samples, these peaks can be assigned to the $\pi$- $\pi^*$ transition from P3HT, PF and copolymer of P3HT and PF. The maximum absorption peaks of (3HT/F-0/100)-g-chitin and (3HT/F-0/100)-g-chitosan are located at 379 and 372 nm, respectively which are attributed to PF, while the maximum absorption peaks of (3HT/F-100/0)-g-chitin and (3HT/F-100/0)-g-chitosan are seen at 553 and 565 nm, respectively which belong to P3HT.[10] When the F content increased from 25 to 75 in both grafted chitin and chitosan samples, the absorption maximum peaks shifted to shorter wavelengths. The optical band gap of the grafted chitin/chitosan products were determined from the onset of absorption by finding the intersection point between the tangent line to a curve and the x-axis (as shown in Figure 6.4). The maximum absorption wavelength, the onset absorption wavelength, and optical band gap are summarized in Table 6.2. The band gap energy of chitin and chitosan are 4.66 and 4.45 eV, respectively. The presence of conjugated copolymer of 3HT and F causes a decrease in the bandgap energy of the chitin and chitosan, resulting $E_g^{op}$ (optical bandgap) varied between 1.8 and 2.7 eV. The change in the band gap could be from the F unit, in conjunction with the 3HT unit in the copolymers, resulted in the extended conjugation length of the copolymer backbone on chitin/chitosan.

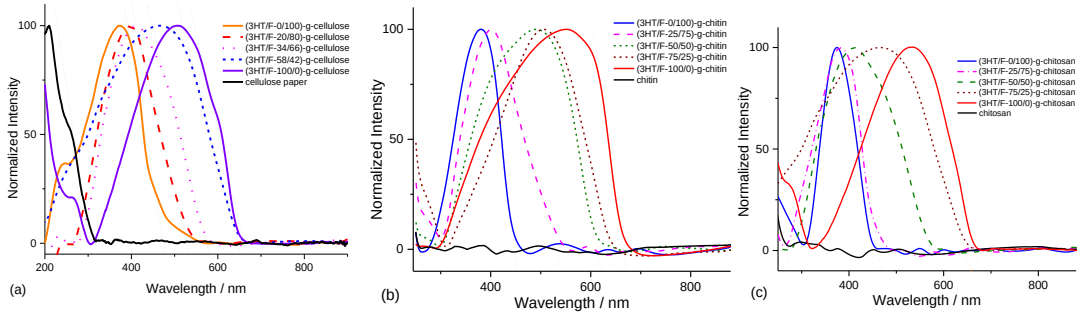


**Figure 6.4. UV-Vis spectra of (a) cellulose and grafted cellulose, (b) chitin and grafted chitin; (c) chitosan and grafted chitosan**

The emission maximum of (3HT/F)-g-cellulose are also shown in Figure 6.5a and summarized in Table 6.2. The optical band gap of cellulose is 4.03 eV, while the band gap energy of the cellulose grafted with the copolymer of PF and P3HT, varied between 1.86 and 2.59 eV. The emission spectra of (3HT/F)-g-

chitin/chitosan samples were recorded and shown in Figure 6.5. All samples show single emission in the wavelength range from 500 to 700 nm. The maximum emission peaks of all grafted products are summarized in Table 6.2. The $\lambda_{max}^{emission}$ of (3HT/F-100/0)-g-chitin and (3HT/F-100/0)-g-chitosan are 672 and 653 nm, respectively. The presence of F unit in (3HT/F) copolymer grafted to chitin and chitosan lead to the blue-shift of emission peak from about 650 nm to 550 nm. The blue shift of the luminescence spectra obtained from (3HT/F)-g-chitin/chitosan could be ascribed to rigid biphenyl unit of PF, which cause efficient blue emission. [1] In summary, the fluorescence of grafted cellulose, chitin, and chitosan could response to the change of the feeding ratio between 3HT and F unit.

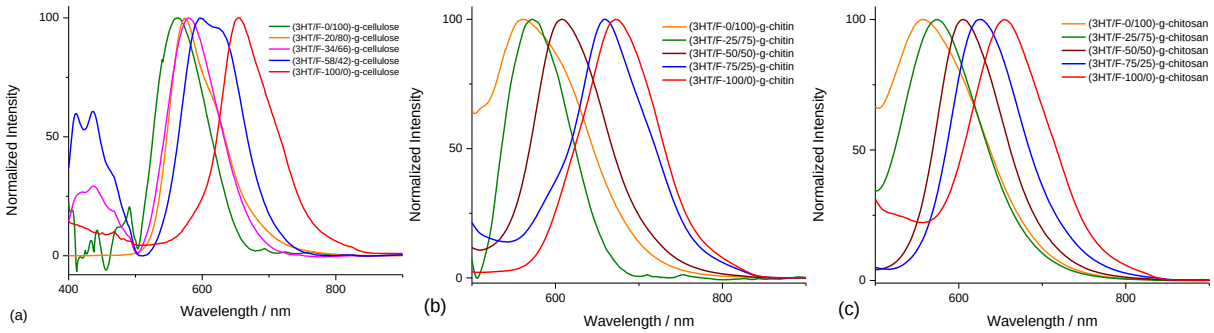


**Figure 6.5. Fluorescence spectra of (3HT/F) copolymer grafted to cellulose (a), chitin (b) and chitosan (c)**

**Table 6.2. The optical properties and band gap data of grafted cellulose, chitin, and chitosan**

| Samples | $\lambda_{max}^{absorption}$ (nm) | $\lambda_{onset}$ (nm) | $E_g^{op}$ (eV) | $\lambda_{max}^{emission}$(nm) |
|---|---|---|---|---|
| Cellulose | 206 | 307 | 4.03 | - |
| (3HT/F-0/100)-g-cellulose | 371 | 478 | 2.59 | 563 |
| (3HT/F-20/80)-g-cellulose | 392 | 531 | 2.33 | 574 |
| (3HT/F-34/66)-g-cellulose | 412 | 580 | 2.13 | 580 |
| (3HT/F-58/42)-g-cellulose | 468 | 651 | 1.90 | 597 |
| (3HT/F-100/0)-g-cellulose | 509 | 666 | 1.86 | 655 |
| chitin | - | 266 | 4.66 | - |
| (3HT/F-0/100)-g- chitin | 379 | 452 | 2.74 | 560 |
| (3HT/F-25/75)-g- chitin | 402 | 541 | 2.29 | 572 |
| (3HT/F-50/50)-g- chitin | 490 | 621 | 1.99 | 608 |
| (3HT/F-75/25)-g- chitin | 509 | 652 | 1.90 | 659 |
| (3HT/F-100/0)-g- chitin | 553 | 670 | 1.85 | 672 |
| chitosan | - | 278 | 4.45 | - |
| (3HT/F-0/100)-g- chitosan | 372 | 454 | 2.73 | 556 |
| (3HT/F-25/75)-g- chitosan | 383 | 469 | 2.64 | 574 |
| (3HT/F-50/50)-g- chitosan | 413 | 584 | 2.12 | 605 |
| (3HT/F-75/25)-g- chitosan | 468 | 657 | 1.88 | 627 |
| (3HT/F-100/0)-g- chitosan | 565 | 676 | 1.83 | 653 |

Absolute determination method [27,28] was used to record the fluorescence quantum yield of cellulose/chitin/chitosan and grafted cellulose/chitin/chitosan with (3HT/F) copolymers. As shown in Figure 6.6, the quantum yields of cellulose and (3HT/F-100/0)-g-cellulose sample were the lowest, while (3HT/F-0/100)-g-cellulose exhibited the highest quantum yield. In addition, the quantum yield of chitin/chitosan and grafted (3HT/F-100/0) to chitin/chitosan are the lowest values, while grafted (3HT/F-0/100) to chitin/chitosan have the highest quantum yields. The quantum yield increased with increasing F content. The raise of fluorene content in (3HT/F) copolymer grafted to cellulose/chitin/chitosan, resulted in an increase in the quantum yield values of grafted cellulose/chitin/chitosan products. These data agree very well with our previous report [10], in the characterization of P3HT and PF copolymer, the quantum yield determined using the relative method also

increase with an increase in the fluorene content. The presence of F unit helps to tune the emission and results in a high quantum yield.

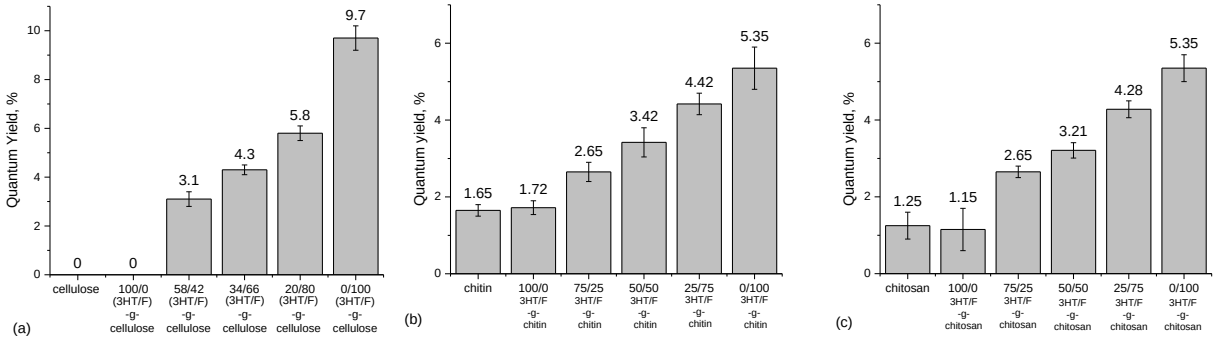


**Figure 6.6. Quantum yields of (a) cellulose and grafted cellulose, (b) chitin and grafted chitin; (c) chitosan and grafted chitosan**

Figure 6.7a shows the TG curves of cellulose paper and (3HT/F) copolymers grafted on cellulose paper. As shown in the Figure 6.7a, the TG curve of cellulose shows two stages of degradation in air. The first stage of degradation occurs from 270 to 345 °C, with a weight loss from 6 to 72%. The second stage of degradation ranges from 347 to 525 °C, with a weight loss between 72 and 98%. The decompositions of the (3HT/F)-g-cellulose paper samples also proceeded in two steps; however, the degradation of the grafted celluloses began at lower temperatures to that of cellulose. For instance, the (3HT/F-20/80)-g-cellulose sample started to degrade at 230 °C, while (3HT/F-58/42)-g-cellulose began to decompose at 247 °C.

TG curves of chitin show two stages of decomposition in an air atmosphere (Figure 6.7b). The first stage of degradation of chitin started from 245 to 389 °C with weight loss from 7 to 67%. The second stage of decomposition of chitin occurred from 389 to 624 °C where weight loss between 67 and 99%. The (3HT/F) copolymers grafted to chitin also showed the two steps in the decomposition. However, all grafted chitin began the decomposition at lower temperature than that of chitin. In detail, all grafted chitins show the initial decomposition temperature of 206 °C.

The decomposition behavior of chitosan and grafting (3HT/F) copolymers to chitosan gave similar results to those of chitin. As shown in the Figure 6.7c, the two stages of decomposition in an air atmosphere were shown in TG curves of chitosan. The first stage of decomposition of chitosan occurred from 253 to 339 °C with weight loss from 11 to 46%. The second stage of degradation of chitosan started from 339 to 686 °C where weight loss between 46 and 99%. After grafting with conjugated copolymers, all (3HT/F)-g-chitosan samples also showed the two steps in the decomposition. However, all grafted chitosan samples began the decomposition at lower temperature than that of chitosan. For instance, (3HT/F-25/75)-g-chitosan showed the first degradation from 224 to 325°C and the second decomposition was in the range from 326 to 640°C

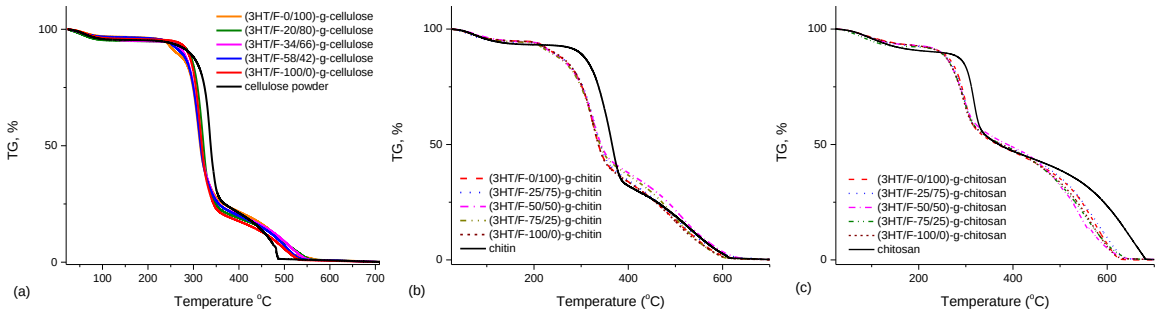


**Figure 6.7. Thermogravimetric (TG) of (a) cellulose and grafted cellulose, (b) chitin and grafted chitin, and (c) chitosan and grafted chitosan**

The differences in the thermal decomposition properties of these samples can be observed clearly from the first-derivative thermogravimetric (DTG) curves shown in Figure 6.8a, where the temperature peak is used as a measure of thermal stability. The temperature peak of cellulose paper is observed at 344 °C, indicating that

the decomposition rate of the cellulose is highest at 344 °C. The DTG curves for the (3HT/F)-g-cellulose samples show sharp peaks at lower temperatures than cellulose.

The difference in the thermal decomposition properties of these samples can be observed obviously from the DTG curves (Figure 6.8b). In DTG curves, there are two temperature peaks belong to two step degradations. The high temperature peak is used as a measure of the thermal stability. In detail, the temperature peak of chitin is 363ºC while they are 324ºC for (3HT/F)-g-chitin samples. As result, the thermal stability of (3HT/F)-g-chitin are lower by 39ºC than that of chitin.

For grafted chitosan, there are also two temperature peaks correspond to two step decompositions (as shown in Figure 6.8c. The initial peak temperature is used as a measure of the thermal stability. The peak temperature of chitosan is 318ºC while these values are 294ºC for (3HT/F)-g-chitosan samples. Therefore, the thermal stability of chitosan samples are higher by 24ºC than that of (3HT/F)-g-chitosan.

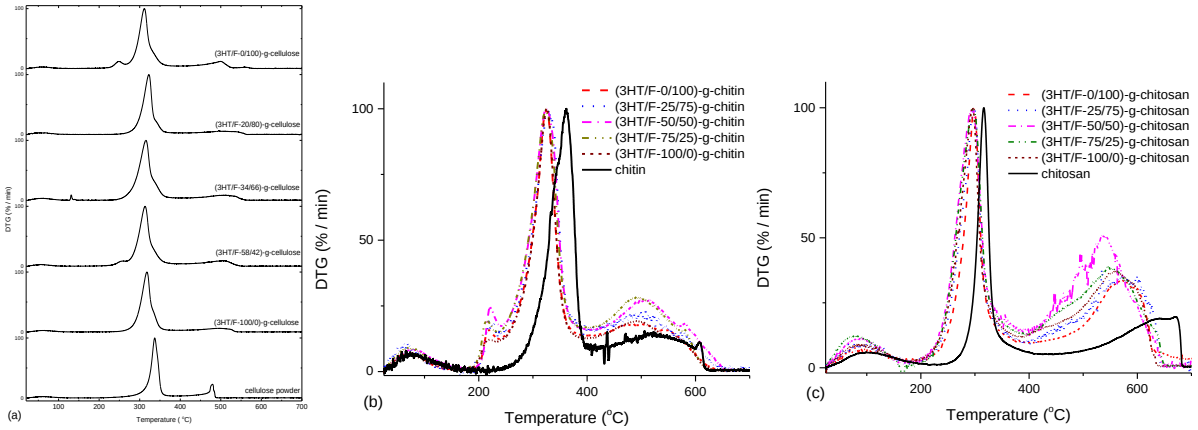


**Figure 6.8. Derivative thermogravimetric (DTG) of (a) cellulose and grafted cellulose, (b) chitin and grafted chitin, and (c) chitosan and grafted chitosan**

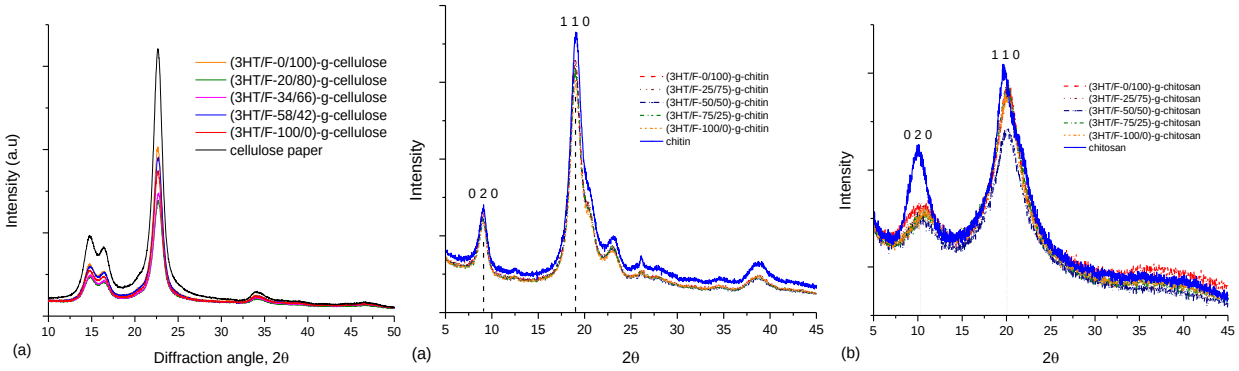


**Figure 6.9. XRD pattern of (a) cellulose and (3HT/F)-g-cellulose, (b) chitin and (3HT/F)-g-chitin; (c) chitosan and (3HT/F)-g-chitosan**

The crystallinity of cellulose is expected to change by the direct grafting of 3HT or F to the cellulose chain, which may result in reduced thermal stability.[29]

Cellulose exists in two crystalline forms, cellulose I and II. [30] The crystallinity index ($I_c$) and percent crystallinity (% $C_r$) of cellulose and the grafted cellulose products were calculated from the XRD patterns using the 2θ peak intensities between 18 and 19° (the diffraction intensity of the amorphous portion) and between 22 to 23° (the intensities of both amorphous and crystalline phases) [31] as follows:

$$I_c = \frac{I_{002} - I_{am}}{I_{002}} \quad ; \quad \% C_r = \frac{I_{002}}{I_{002} + I_{am}}$$

Varieties of reports have been studied for calculation the degree of crystallinity of chitin and chitosan using X-ray measurement.[18,32-35] There are two equations for determination the crystallinity index:

$CrI_{020} = (I_{020} - I_{am})/ I_{020} \times 100$ and $CrI_{110} = (I_{110} - I_{am})/ I_{110} \times 100$; where $I_{020}$ is the maximum intensity of the crystalline peak from the (020) lattice diffraction, $I_{110}$ is the maximum intensity of the crystalline peak from the (110) lattice diffraction and $I_{am}$ is the intensity of amorphous diffraction at $2\theta=12.6^{o}$ [18,32-35]

**Table 6.3: Crystallinity index of chitin/chitosan and grafted (3HT/F) to chitin/chitosan**

| Sample | Crystallinity Index ($CrI_{020}$) % | Crystallinity Index ($CrI_{110}$)% |
|---|---|---|
| chitin | 63.1 | 85.6 |
| (3HT/F-100/0)-g-chitin | 59.5 | 83.4 |
| (3HT/F-75/25)-g-chitin | 60.8 | 84.1 |
| (3HT/F-50/50)-g-chitin | 61.5 | 84.8 |
| (3HT/F-25/75)-g-chitin | 61.4 | 84.2 |
| (3HT/F-0/100)-g-chitin | 59.3 | 83.8 |
| chitosan | 40.1 | 56.1 |
| (3HT/F-100/0)-g-chitosan | 16.7 | 52.7 |
| (3HT/F-75/25)-g-chitosan | 15.8 | 52.1 |
| (3HT/F-50/50)-g-chitosan | 16.3 | 44.3 |
| (3HT/F-25/75)-g-chitosan | 17.5 | 51.8 |
| (3HT/F-0/100)-g-chitosan | 18.1 | 51.9 |

As shown in Figure 6.9a, all diffraction patterns of cellulose and grafted cellulose exhibited peaks at $2\theta = 17$ and 22.5°, which correspond to the amorphous and crystalline phases of cellulose. The data in Table 6.3 reveal that the crystallinity indexes and percentage crystallinities of the various grafted materials decrease slightly upon grafting. After grafting, the crystallinity index varied from 0.53 to 0.56. The percent crystallinities of cellulose is 70.05. These values also decrease upon grafting, to 68.24%.

The neat chitin (Figure 6.9b) shows three characteristic diffraction peaks at 9.1°, 19.1°, and 23.1°, that corresponding to 020, 110, 120 planes, respectively.[18,32-35] After grafting (3HT/F) copolymer to chitin, all diffraction patterns coincided with those of neat chitin. However, the crystallinity index of all grafted chitin samples decreased slightly compared to original chitin as shown in Table 6.4. The $CrI_{020}$ and $CrI_{110}$ are 63.1 and 85.6, respectively. After grafting (3HT/F) copolymer to chitin, these values varied from 59 to 61% ($CrI_{020}$) and from 83 to 84% ($CrI_{110}$), respectively. The two characteristic diffraction peaks of origin chitosan were observed at 10.3° and 20.0° that belong to 020 and 110 planes, respectively (Figure 6.9c). [18,32-35] The diffraction patterns of (3HT/F)-g-chitosan samples also show two diffraction peaks of 020 and 110 planes. As shown in Table 6.4, the $CrI_{020}$ of (3HT/F)-g-chitosan samples decline significantly compared to neat chitosan, while the $CrI_{110}$ of (3HT/F)-g-chitosan samples decrease slightly. In summary, the grafting of the (3HT/F) copolymer to the cellulose backbone increases the amorphous region because of the incorporation of (3HT/F) copolymer chains that hinder the crystallization of the cellulose chain. Therefore, the thermal stability of cellulose depends mainly on its crystallinity.[29] Similarly, after grafting, the crystallinity index of chitin and chitosan are also lower than that of original chitin and chitosan. The grafting (3HT/F) copolymer to chitin/chitosan cause the disorder of the crystalline structure, resulted in the increase of amorphous region. Furthermore, the thermal stability of polymer depends mainly on the crystallinity[29]. These XRD results are in agreement with the TG results. Therefore, grafting (3HT/F) copolymer to chitin/chitosan lead to less thermal stability of chitin and chitosan.

**Table 6.4: Crystallinity indexes and % crystallinities of cellulose and (3HT/F)-g-cellulose**

| Sample | Crystallinity index | % Crystallinity |
|---|---|---|
| cellulose powder | 0.57 | 70.05 |
| (3HT/F-100/0)-g-cellulose | 0.56 | 69.96 |
| (3HT/F-58/42)-g-cellulose | 0.56 | 69.76 |
| (3HT/F-34/66)-g-cellulose | 0.52 | 67.52 |
| (3HT/F-20/80)-g-cellulose | 0.53 | 68.40 |
| (3HT/F-0/100)-g-cellulose | 0.53 | 68.24 |

## 6.4 Conclusions

In this chapter, a novel, easy, and simple oxidative procedure is reported for the fabrication of conjugated copolymer layer of P3HT and PF on the surface of cellulose, chitin, and chitosan. This approach is an interesting method to create a biomaterial with innovative optical properties. The desired blue-/red-shifted absorption and emission of grafted cellulose/chitin/chitosan can be manipulated by different feeding ratios of the 3HT/F units. The quantum yield of (3HT/F)-g-cellulose/chitin/chitosan increased with an increase in the fluorene unit. The crystallinity of cellulose, chitin, and chitosan decreased slightly after graft polymerization of PF and P3HT. The thermal stability of the (3HT/F)-g-cellulose/chitin/chitosan was slightly lower than that of cellulose/chitin/chitosan. The bonding between chitin/chitosan and the (3HT/F) copolymer changed the degree of crystallinity in chitin/chitosan, thereby decreasing their thermal stability.

## 6.5 References


(1) Leclerc, M. *J. Polym. Sci. Pol. Chem.* **2001**, *39*, 2867–2873.

(2) Schelkle, K. M.; Bender, M.; Jeltsch, K.; Buckup, T.; Mullen, K.; Hamburger, M.; Bunz, U. H. F. *Angew. Chem. Int. Ed.* **2015**, *54*, 1-5.

(3) Chou, C.-H.; Hsu, S.-L.; Dinakaran, K.; Chiu, M.-Y.; Wei, K.-H. *Macromolecules* **2005**, *38*, 745-751.

(4) Kreyenschmidt, M.; Klaerner, G.; Fuhrer, T.; Ashenhurst, J.; Karg, S.; Chen, W. D.; Lee, V. Y.; Scott, J. C.; Miller, R. D. *Macromolecules* **1998**, *31*, 1099-1103.

(5) Wan, Y.-J.; Zhu, P.-L.; Yu, S.-H.; Sun, R.; Wong, C.-P.; Liao, W.-H. *Carbon* **2017**, *115*, 629–639.

(6) Nishioka, N.; Yoshida, N. *Polym. J.* **1992**, *24*, 1009-1015.

(7) Nishioka, N.; Yamaoka, M.; Haneda, H.; Kawakami, K.; Uno, M. *Macromolecules* **1993**, *26*, 4694-469.

(8) Nishioka, N.; Kosai, K. *Polym. J.* **1981**, *13*, 1125-1133.

(9) Wang, X.; Chen, B.; Xu, J.; Zhou, W.; Pu, S. *J. Appl. Polym. Sci.* **2008**, *108*, 1924–1933.

(10) Hai, T. A. P.; Sugimoto, R. *Polym. J.* **2016**, *48*, 1115–1121.

(11) Vieira, J. G.; Oliveira, G. d. C.; Filho, G. R.; Assunção, R. M. N. d.; Meireles, C. d. S.; Cerqueira, D. A.; Silva, W. G.; Motta, L. A. d. C. *Carbohydr. Polym.* **2009**, *78*, 779–783.

(12) Khalil, H. P. S. A.; Ismail, H.; Rozman, H. D.; Ahmad, M. N. *Eur. Polym. J.* **2001**, *37*, 1037–1045.

(13) Higgins, H. G.; Stewart, C. M.; Harrington, K. J. *J. Polym. Sci. Pol. Chem.* **1961**, *51*, 59-84.

(14) Beneventi, D.; Alila, S.; Boufi, S.; Chaussy, D.; Nortier, P. *Cellulose* **2006**, *13*, 725 –734.

(15) Roy, D.; Guthrie, J. T.; Perrier, S. *Macromolecules* **2005**, *38*, 10363-10372.

(16) Gupta, K. C.; Khandekar, K. *Biomacromolecules* **2003**, *4*, 758-765.

(17) Socrates, G.: Infrared and Raman Characteristic Group Frequencies. *John Wiley & Sons, Ltd* **2001**, *West Sussex, England*, 268-269.

(18) Focher, B.; Beltrame, P. L.; Naggi, A.; Torri, G. *Carbohydr. Polym.* **1990**, *12*, 405-418.

(19) Ren, L.; Tokura, S. *Carbohydr. Polym.* **1994**, *23*, 19-25.

(20) Chen, X.; Chew, S. L.; Kerton, F. M.; Yan, N. *Green Chem.* **2014**, *16*, 2204-2212.

(21) Chen, X.; Liu, Y.; Kerton, F. M.; Yan, N. *RSC Adv* **2015**, *5*, 20073–20080.

(22) Osada, M.; Miura, C.; Nakagawa, Y. S.; Kaihara, M.; Nikaido, M.; Totani, K. *Carbohydr. Polym.* **2013**, *92*, 1573–1578.

(23) Umar, A.; Naim, A. A.; Sanagi, M. M. *Mater. Lett.* **2014**, *124*, 12–14.

(24) Negrea, P.; Caunii, A.; Sarac, I.; Butnariu, M. *Dig. J. Nanomater. Biostruct.* **2015**, *10*, 1129 - 1138.

(25) Yavuz, A. G.; Uygun, A.; Bhethanabotla, V. R. *Carbohydr. Polym.* **2009**, *75*, 448–453.

(26) Hirai, T.; Nagae, Y.; White, K. L.; Kamitani, K.; Kido, M.; Uchiyama, T.; Nishibori, M.; Konishi, Y.; Yokomachi, K.; Sugimoto, R.; Saigo, K.; Ohishi, T.; Higaki, Y.; Kojio, K.; Takahara, A. *RSC Adv* **2016**, *6*, 111993-111996

(27) Würth, C.; González, M. G.; Niessner, R.; Panne, U.; Haisch, C.; Genger, U. R. *Talanta* **2012**, *90*, 30–37.

(28) Würth, C.; Grabolle, M.; Pauli, J.; Spieles, M.; Resch-Genger, U. *Nat. Protoc.* **2013**, *8*, 1535–1550.

(29) Reich, L.; Stivala, S. S.: Elements of Polymer Degradation. *McGraw-Hill* **1971**, *New York*.

(30) Kamide, K.: Cellulose and cellulose derivatives molecular characterization and its applications. *Elsevier Science* **2005**.

(31) Gürdağ, G.; Sarmad, S.: Polysaccharide Based Graft Copolymers. *Springer-Verlag Berlin Heidelberg* **2013**, 15-57.

(32) Kumirska, J.; Czerwicka, M.; Kaczyński, Z.; Bychowska, A.; Brzozowski, K.; Thöming, J.; Stepnowski, P. *Mar. Drugs.* **2010**, *8*, 1567-1636.

(33) Zhang, Y.; Xue, C.; Xue, Y.; Gao, R.; Zhang, X. *Carbohydr. Res.* **2005**, *340*, 1914–1917.

(34) Ioelovich, M. *J. Chem.* **2014**, *3*, 7-14.

(35) Kumar, A. B. V.; Varadaraj, M. C.; Lalitha, R. G.; Tharanathan, R. N. *Biochim. Biophys. Acta*. **2004**, *1670*, 137–146.